UNIVERSITÀ DEGLI STUDI DI MILANO

DIPARTIMENTO

Biotecnologie Mediche e Medicina Traslazionale

SCUOLA DI DOTTORATO

Medicina Sperimentale e Biotecnologie Mediche

XXX Ciclo

Novel approaches of "personalised medicine" as proof-of-principle for *CDKL5*-related pathologies

Dottorando: ***MARIA FAZZARI***

Supervisore: ***Prof.ssa NICOLETTA LANDSBERGER***

Coordinatore: ***Prof. MASSIMO LOCATI***

ANNO ACCADEMICO: 2016-2017

To Martina and her big green eyes…

INDEX

1. ABSTRACT

Alterations of *CDKL5* give rise to several forms of neurological disorders generally characterised by epileptic encephalopathy, severe developmental delay, hypotonia and RTT-like features. To date no cure exists and only secondary symptoms can be treated.
About 15% of *CDKL5* patients carry a nonsense mutation and might benefit of a read-through strategy as "personalised" medicine approach. The read-through process occurs when a near-cognate aminoacyl-tRNA binds a premature stop codon (PTC), allowing its suppression and the subsequent protein elongation. This mispairing event can rarely occur, but can be facilitated using a wide range of drugs. In order to test PTC suppression, we have chosen some human pathogenic *CDKL5* nonsense mutations located in the two main domains of the protein: the catalytic N-terminus (R59X, R134X) or the C-terminal tail (Q347X, E364X, R550X, S855X). We then evaluated the read-through process using aminoglycoside and non-aminoglycoside drugs in cells transfected with the mutagenized constructs. In this study, we have demonstrated that tested *CDKL5* PTCs can be suppressed by gentamicin and geneticin (G418) in a dose-dependent manner and that PTC position can be critical for read-through. In particular, G418 was found to be more effective than gentamicin. Considering the known aminoglycosides toxicity, we evaluated the activity of PTC124 and GJ072 but no PTC suppression was detectable in our experimental conditions. Finally, in order to understand whether the full-length derivatives may maintain the proper function of WT CDKL5, we analysed some features of read-through products compared to the WT protein. In particular, while premature truncated proteins showed an altered subcellular localisation, read-through products demonstrated a nucleo-cytoplasmic distribution more similar to the WT one. Moreover, by evaluating the auto-phosphorylation of the TEY motif, the read-through derivatives demonstrated to recover some catalytic activity, although remaining highly hypomorphic. Nevertheless, preliminary studies on *Cdkl5*-null neurons transfected with R134X construct suggested that G418 treatment can ameliorate impaired neuronal morphology. Collectively, our results indicate that: (i) aminoglycosides are able to induce read-through of different *CDKL5* PTCs; (ii) the read-through derivatives recover some features characterizing the WT protein; (iii) PTC position can be crucial for read-though and for rescue of a proper function and (iv) neuronal morphological defects might be rescued by small amount of a possible hypomorphic CDKL5, therefore supporting the potential validity of a read-through therapy.

2. INTRODUCTION

2.1 Rett syndrome

Rett syndrome (RTT OMIM 312750) is a severe childhood neurological disorder affecting principally girls. The disease has an incidence of 1:10000 [1] girls born alive, thus representing one of the main causes of severe intellectual disability in girls.
First cases of girls affected by this syndrome were reported in German about fifty years ago (1966) by the physician Andreas Rett [2]. However, seventeen years later, RTT was recognized by the medical community thanks to the English work of Dr. Hagberg and his colleagues who described patients with a clinical phenotype well overlapping to the one described by Rett [3].
In 1999, Huha Zhogbi's laboratory identified *MECP2* (*Methyl-CpG binding Protein 2*) as the main genetic cause of classical RTT, thus reporting the first neurodevelopmental disorder related to epigenetics [4].

2.1.1 Clinical features of RTT

Girls affected by typical RTT appear to be healthy until the first six-eighteen months of life, when a developmental arrest followed by a regression phase occurs.
Consensus criteria for correct diagnosis of RTT were developed by Hagberg and collaborators [5] [6] and then revised in 2010 by the RettSearch Consortium, constituted by a group of physicians [7]. Revised diagnostic criteria include the core features which are fundamental to simplify the diagnosis of RTT or its variants (Table 1) [7].
The progression of clinical phenotypes can be divided in different phases.
The *stagnation phase* is characterized by growth arrest, hypotonia, and in some case deceleration of head growth leading to microcephaly. During *rapid regression* phase, patients lose hands skills, ability to speech and autistic phenotypes appear, such as hand stereotypes, mental retardation together with motor abnormalities and seizures. With *stationary phase*, the loss of skills stops and patients may be subjected to scoliosis. The *late motor deterioration* is characterized by decrease or complete loss of mobility and the appearance of Parkinsonian features [6] [1]. In addition to the described clinical features,

RTT patients suffer of autonomic perturbation, including respiratory and gastrointestinal problems, cardiac abnormalities such as long Q-T intervals, tachycardia and sinus bradycardia.

RTT Diagnostic Criteria
Main Criteria 1. Partial or complete loss of acquired purposeful hand skills. 2. Partial or complete loss of acquired spoken language 3. Gait abnormalities: Impaired (dyspraxic) or absence of ability. 4. Stereotypic hand movements such as hand wringing/squeezing, clapping/tapping, mouthing and washing/rubbing automatisms
Supportive Criteria for atypical RTT 1. Breathing disturbances when awake 2. Bruxism when awake 3. Impaired sleep pattern 4. Abnormal muscle tone 5. Peripheral vasomotor disturbances 6. Scoliosis/kyphosis 7. Growth retardation 8. Small cold hands and feet 9. Inappropriate laughing/screaming spells 10. Diminished response to pain 11. Intense eye communication - “eye pointing”
Exclusion Criteria for typical RTT 1. Brain injury secondary to trauma (peri- or postnatally), neurometabolic disease, or severe infection that causes neurological problems 2. Grossly abnormal psychomotor development in first 6 months of life
Required for typical or classic RTT 1. A period of regression followed by recovery or stabilization 2. All main criteria and all exclusion criteria 3. Supportive criteria are not required, although often present in typical RTT
Required for atypical or variant RTT 1. A period of regression followed by recovery or stabilization 2. At least 2 out of the 4 main criteria 3. 5 out of 11 supportive criteria

Table 1. Consensus criteria for RTT diagnosis (adapted from Neul *et al.*, 2010 [7])

As the patients get older, their conditions reach a plateau and some of them survive up to sixty-seventy years of age [1].

Beyond classical RTT, atypical patients have been described, having milder or more severe phenotypes. Atypical variants of RTT can be organised in three main classes: the *preserved speech variant* (a.k.a Zappella variant), the *early seizure variant* (a.k.a Hanefeld variant), the *congenital variant* (a.k.a Rolando variant). The Zappella variant is characterized by moderate intellectual disability, milder reduction of hand skills, the capability to say single words or phrases while epilepsy is a rare event. More severe are the Hanefeld and the Rolando variants; the former entails often intractable seizures before the first sixth month of age, while the second implies grossly abnormal initial development including severe psychomotor delay and inability to walk together with the lack of the typical intense RTT eye gaze [7].

Whereas more than 95% of patients affected by classical RTT presents alterations in the *MECP2* gene [1], only 30-40% of variant patients exhibits mutation in this locus. In particular, such mutations are mainly found in the *preserved speech variant*, while different causative genes are often associated with other variants: *CDKL5* with the *early seizure variant*, and *FOXG1* with the *congenital form* [7].

2.1.2 MeCP2 structure and functions

MECP2 is a complex gene located at X chromosome (Xq28) consisting of four exons that can be alternatively spliced in two isoforms: MeCP2-e1 and MeCP2-e2. Moreover, the presence of a 3'-untraslated region containing multiple polyadenylation sites permits the generation of four different transcripts [1] [8].

MeCP2 is a nuclear protein isolated in 1992 by Adrian Bird's laboratory for its capability to bind methylated DNA [9]. It is composed by five main structural domains: the N-terminal domain (NTD), the methyl-binding domain (MBD), the intervening domain (ID), the transcriptional repression domain (TRD), and the C-terminal domain (CTD, Fig. 1) [8]. Although all domains with the exception of the N-terminal have crucial roles for MeCP2 functions, only the MBD and TRD functions have been clearly elucidated. In particular, the MBD is necessary for specific binding to methylated DNA, while the TRD is crucial for the recruitment on methylated DNA of transcriptional corepressors such as Sin3A, NCoR and ATRX.

MeCP2 is a multifunctional protein involved mainly in transcription regulation. Although it is still under discussion its capacity to activate transcription and the possible relevance of this activity in *MECP2*-related disorders, in well accordance with its capability to bind methylated DNA, MeCP2 is mainly considered a transcriptional repressor [8].

Additional studies have identified MeCP2 as a *global regulator* of chromatin. It has in fact been demonstrated that in mature neurons, where the protein reaches its maximal abundance, there is one molecule of Mecp2 every two nucleosomes. In these cells, Mecp2 is proposed to substitute itself to histone H1, therefore functioning as a linker histone [10]. According to this structural role, it has been demonstrated that the absence of Mecp2 leads to an increase of H3 acetylation and H1 levels [11].

Beyond regulation of gene expression and influence on chromatin structure roles, additional functions of MeCP2 have been demonstrated. In particular, different studies have proposed a direct or indirect effect on protein synthesis; indeed, a reduction in the AKT/mTOR signalling pathway in the absence of Mecp2 has been found in mouse brain and human cells [12] [13]. Furthermore, a role of MeCP2 in mRNA splicing [14] and miRNA maturation [15] has been proposed. Whereas all these studies suggest an involvement of this protein in gene expression, a recent publication suggests that a subfraction of MeCP2 colocalises with the centrosome where it affects cell proliferation and microtubule nucleation [16].

Figure 1. MeCP2 protein structure.
Schematic representation of MeCP2 protein illustrating the different domains. Adapted from Bellini *et al.*, 2014 [8].

Alterations of *MECP2* are in most cases *de novo* and comprise missense, nonsense and frameshift mutations. Among them, eight hot-spot mutations exist accounting for 65% of all *MECP2* mutations and consisting in C to T transitions (R106W, R133C, T158M, R168X, R255X, R270X, R294X, R306C). Moreover, although missense mutations can be distributed along the whole open reading frame, most of them falls in the MBD, while deletions/insertions occur mostly in the CTD [17]. Alterations of *MECP2* have also been associated with other forms of intellectual disability, including autism, mental retardation, schizophrenia and Angelman-like syndrome; moreover duplication of Xq28 region gives rise to *MECP2* duplication syndrome in males [18]. These observations indicate the

crucial role of MeCP2 in the brain. Indeed, while MeCP2 is a ubiquitously expressed protein, its highest levels are reached in the Central Nervous System (CNS, MeCP2 e-1 isoform) and, particularly, in neurons. MeCP2 expression is low in immature neurons but it increases during maturation reaching the maximal abundance in mature neurons [19] [20]. Such expression profile suggests MeCP2 involvement in neuronal maturation and dendritic arborisation [21]. Indeed, the overall structure of RTT brains is generally maintained but they are characterized by a reduction in size and weight, with smaller, less arborized and more compacted neurons. Furthermore, *Mecp2*-mutant mouse models exhibit evident defects in dendritic spines and morphology [22] and such observations have been confirmed by studies in post-mortem RTT brains [23]. Morphological impairments are also associated with defects in synaptic connectivity due to decrease of excitatory synapse number [23] [24] and imbalance between excitation and inhibition [25]. Moreover, Mecp2 loss of function causes alterations in spontaneous synaptic transmission and short- and long-term synaptic plasticity, such as LTP and LTD that are well correlated with learning and memory deficits of RTT patients [26] [27] [28].

2.2 *CDKL5*-related pathologies

As already mentioned, beside classic RTT, atypical variants lacking *MECP2* mutations exist.

The first case of atypical early-onset seizure variant of RTT was identified in 1985 by Hanefeld who described a girl with infantile spasms and hypsarrhythmia sharing clinical characteristics with RTT patients [29]. This RTT variant, also known as *Hanefeld variant*, presents a phenotype overlapping to West syndrome (or Infantile Spasm Syndrome, X-linked, ISSX, OMIM: 308350) whose clinical outcomes comprise the triad of infantile spasms, hypsarrhythmia and variable mental retardation [30]. In 2003, two cases of unrelated female patients sharing a similar epileptic phenotype and hypsarrhythmia were reported by Kalscheuer *et al*. These patients presented an apparently balanced translocation where the X-chromosomal breakpoints disrupted *CDKL5* [31].

Since then mutations in *CDKL5* have generally been associated with early infantile epileptic encephalopathy, ISSX, early onset seizures variant of RTT, West syndrome, Angelman or Angelman-like syndrome [32] [33].

2.2.1 Clinical features of *CDKL5*-related pathologies

The central clinical feature of *CDKL5*-related pathologies is epileptic encephalopathy, often characterized by intractable seizures starting within the fifth month of life. Epilepsy is in general polymorphic and various types of seizures could affect the same patient in different period of its life.

In 2008, Bahi-Buisson *et al.* described three stages of *CDKL5*-related epileptic encephalopathy, consisting in early epilepsy (stage 1), infantile spasms (stage 2) and multifocal and refractory epilepsy (stage 3) [34].

Early epilepsy (stage 1) is characterized by tonic-clonic seizures, lasting less then 1 minute but very frequent and occurring usually 2-5 times per day. Stage 2 consists of infantile spasms and atypical hypsarrhytmia. It affects about 75% of *CDKL5* patients, showing profound mental retardation, massive hypotonia and no language or visual interactions; such patients could face a honey-moon period (decrease or absence of seizures) when treated with anti-epileptic drugs during the progression into this stage. At last, stage 3 is shared by almost 71% of *CDKL5* patients and presents multifocal and drug-resistant seizures, including tonic spasms and myoclonia [34].

Despite these evidence, to date no EEG data or MRI analysis identified an exact pattern or specific abnormalities in *CDKL5* patients [31] [35] [36] [37].

Moreover, almost 55% of patients carrying genomic deletions or point mutations in *CDKL5* acquire progressive microcephaly, while the few described patients with *CDKL5* duplications appear to exhibit macrocephaly [38]. Interestingly, in contrast with CDKL5 deficiency, none of these patients showed epilepsy while learning impairment, autistic and hyperactive behaviours have been reported [38].

CDKL5 patients share some clinical features with RTT syndrome including hand stereotypes, severe hypotonia and altered psychomotor development but they do not exhibit the regression period that is considered one of the main criteria for RTT diagnosis [7]. In addition, different studies described cortical visual loss [37] [39] [40] [41], while intense eye gaze or neurovegetative functions including breathing abnormalities, cold extremities, gastrointestinal disturbances typical of classic RTT patients are not, or only occasionally, observed in *CDKL5* patients [37] [42]. Moreover, about 30% of patients could be able to walk [37].

Finally, contrarily to classic RTT, CDKL5 syndrome cannot be considered gender-related. Indeed *MECP2* mutations have been rarely found in males and generally give rise to a more severe encephalopathy leading to death within the first years of life [42]. On the contrary, Liang *et al.*, analysing a cohort of patients affected by epileptic encephalopathy, observed a *CDKL5* mutations frequency of 5% in males and 14% in females [35]. Furthermore, clinical severity seems to be similar in *CDKL5* patients of both genders [35] [43] [44] even if Fehr *et al.* have observed in males a more severe phenotype characterized by slightly earlier seizures, inability to walk, impairments in spoken communication and hand functions [32]. Sartori *et al.* described a male affected by Klinefelter syndrome (47, XXY) and a large C-terminal CDKL5 truncation showing a similar phenotype to other *CDKL5*-mutated boys; such observation suggests that the presence of a wild-type *CDKL5* allele and a balanced X inactivation pattern does not reduce the severity of disease [45] [42].

Altogether these studies highlight that, although mutations in *CDKL5* have been originally associated with the early-onset variant of RTT, the gene is actually cause of a large spectrum of neurodevelopmental disorders that can be considered clinically separated from RTT.

2.2.2 *CDKL5* structure: from gene to protein

The *CDKL5* gene was identified analysing the Xp22 region through a positional cloning study aimed at isolating disease genes in this portion. Sequence analysis showed homologies to a subgroup of kinases, the serine-threonine kinases, and for this reason *CDKL5* was firstly named STK9 (Serine-Threonine Kinase 9) [46]. Then, observing its similarity to some kinases involved in cell division [31], the protein was renamed as CDKL5/STK9 and finally CDKL5 (Cyclin-Dependent Kinase-Like 5).

The mammalian *CDKL5* gene structure and the related transcripts were studied in different species: human, mouse, rat.

The human *CDKL5* gene is composed of twenty-seven exons and can be alternatively spliced in five major transcript isoforms, which are named *hCDKL5_1* to *hCDKL5_5* (Fig. 2) [47].

hCDKL5_1 isoform is highly expressed in CNS, but can be detected in kidney, testis, prostate glands, thymus and thyroid gland; this transcript encodes the protein weighting

107 kDa that is the most abundant isoform in CNS. The *hCDKL5_2* sequence is similar to the first one isoform but includes 123 bases (41 a.a.) from exon 17 lacking in *hCDKL5_1*. *hCDKL5_3* and *hCDKL5_4* share the same sequence of *hCDKL5_1* and *hCDKL5_2*, respectively, but the utilisation of a cryptic splice donor site gives rise to a coding sequence lacking 51 bases at 3' end of exon 11 codifying therefore for a shorter protein. *hCDKL5_2*, *hCDKL5_3* and *hCDKL5_4* are widely expressed but with lower abundance than *hCDKL5_1*. The last isoform, *hCDKL5_5*, is similar to *hCDKL5_1* and *hCDKL5_3* but is characterized by a different 3' sequence due to the use of a cryptic splice site in exon 19 and the inclusion of exons 20, 21, 22; in addition such isoform was found to be less stable if compared to h*CDKL5*_1 [48]. In adult, h*CDKL5*_5 transcript is only expressed in testis and codify for a protein weighting 115 kDa [47].

The murine *Cdkl5* gene comprises a total of twenty-three exons giving rise to five major transcript isoforms [47]. The first two isoforms are orthologous to *hCDKL5_1* and *hCDKL5_2* and have thus been named *mCdkl5_1* and *mCdkl5_2*. Contrarily, the remaining isoforms do not have full orthology and are thus named *mCdkl5_6*, *mCdkl5_7* and *mCdkl5_8*.

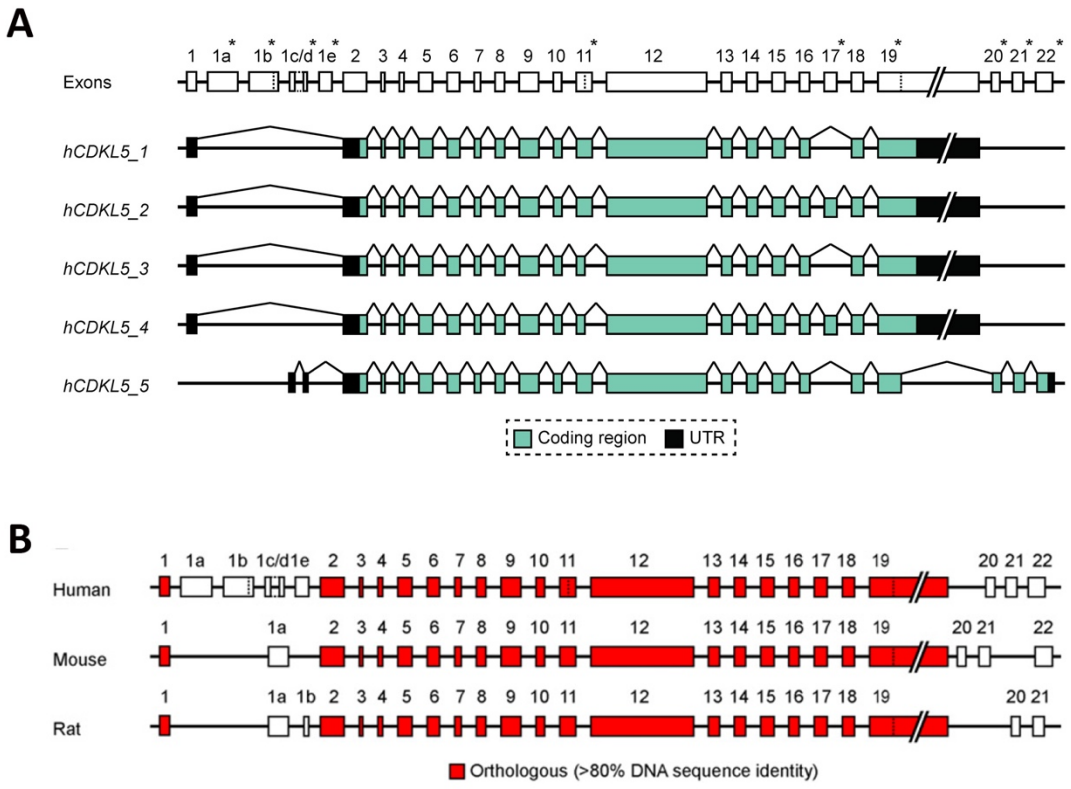

Figure 2. Graphical representation of *CDKL5/Cdkl5* gene structures.

A) Schematic illustration of the human *CDKL5* gene and its five different splicing isoforms (h*CDKL5*_1 to h*CDKL5*_5). Splicing events are indicated as angled lines linking exons while dotted lines within

exons show alternative splice sites. Asterisks indicate where differences between isoforms have been found [47].

B) Schematic correlation between human, mouse and rat *CDKL5* gene structures [49].

Concordantly with its human orthologous, *mCDKL5_1* is the most abundant isoform in CNS, while the expression of *mCdkl5_6* and *mCdkl5_7* is confined to adult murine testis; *mCdkl5_8* is transcribed in spleen and, at lower levels, in brain, heart, liver, lung and testis [47].

Recently, the rat *Cdkl5* was also characterised by Hector *et al.*; the gene is organized in twenty-three discrete exons codifying for four distinct transcript isoforms: r*Cdkl5*_1, r*Cdkl5*_2, r*Cdkl5*_9 and r*Cdkl5*_10 [49]. The first two isoforms are the most abundant in rat brain and share a similar expression pattern of their orthologous h/m*CDKL5*_1 and h/m*CDKL5*_2. r*Cdkl5*_9 and r*Cdkl5*_10 are predominantly expressed in testis.

The analysis of the 5' and 3' ends of *CDKL5* transcripts has identified multiple Transcription Start Sites (TSS) and polyadenylation signals. In particular, in the first two isoforms the major 5' TSS and canonical 3' polyadenylation signal are maintained between the three species [47] [49].

Cdkl5-mRNA is highly expressed in brain and mainly in adult forebrain reaching a peak in more superficial cortical layers. In particular, a strong expression was detected in specific cortical area, including frontal cortex, motor cortex and cingulate gyrus, suggesting a region specific role for CDKL5 [42]. Importantly, high levels of *Cdkl5*-mRNA have been also detected in hippocampus and entorhinal cortex, two areas important for memory and learning, and in several thalamic nuclei. In cerebellum, *Cdkl5*-mRNA is expressed in all lobules but its level seems to be lower if compared to the other brain areas [42].

Considering the different neuronal sub-populations, *Cdkl5*-mRNA appears predominately expressed in glutamatergic and GABAergic neurons, while at very low levels in dopaminergic areas (*substantia nigra* or ventral tegmental area) or in noradrenergic areas (*locus coeruleus*) [42]. Interestingly, *Cdkl5*-mRNA is localised in the entire neuronal cell body, from soma to dendritic spines where the protein is locally synthetized after stimuli [50].

The protein expression mainly coincides with the described mRNA expression levels [51]. Considering the different neural populations, the kinase is highly expressed in virtually all NeuN-positive neurons while very low expression is detectable in glia [51].

Moreover, CDKL5 expression is modulated during development and it is characterized by low expression during embryogenesis, with a strong increase during postnatal period reaching a plateau at P14 [52].

CDKL5 is a serine-threonine kinase belonging to CMGC family which includes the cyclin-dependent kinases (CDK), the mitogen-activated protein kinases (MAP kinases or ERKs, extracellular-signal-regulated kinases), the glycogen synthase kinases (GSK) and the CDK-like kinases. It is characterized by an N-terminal catalytic domain sharing homology with the other members of CDKL-family and a long C-terminal tail unique for CDKL5.

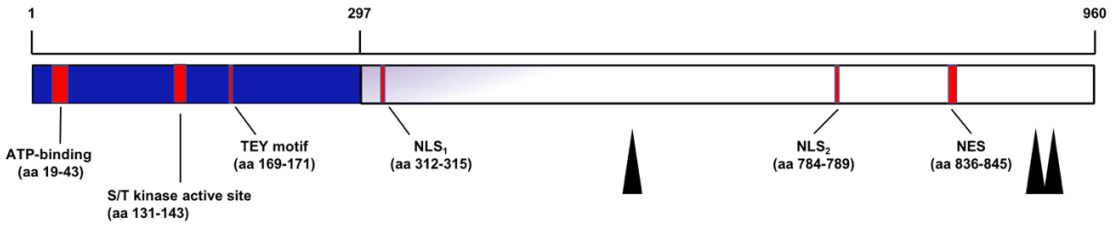

Figure 3. Schematic illustration of CDKL5$_{107}$ structure.
Representation of different functional domains and signatures distributed along the protein. In blue is represented the N-terminal catalytic domain containing the ATP-binding site, the serine/threonine active site and the TEY motif. In white is shown the C-terminal tail carrying two nuclear localisation signals (NLS_1 and NLS_2) and three PxxP sites (arrowheads). Adapted from Kilstrup-Nielsen *et al.*, 2012 [42].

In the catalytic domain (a.a. 13-297, Fig. 3) specific signatures of serine-threonine kinase group have been identified, which includes (i) an ATP-binding motif (a.a. 19-43) composed by a glycine-rich stretch close to a lysine residue (K42) involved in ATP binding [53]; (ii) a serine-threonine active site (a.a. 131-143) including a conserved aspartic acid (D135) crucial for catalytic activity [53]; (iii) an "activation loop" with a DFG domain and a TEY motif (DFGFARNLSEGNNANYTEY; a.a. 153-171). As for other members of the CMGC family, during activation, the TEY motif (a.a. 169-171) is dually phosphorylated through an auto- or hetero-phosphorylation process, while the conserved DFG motif stabilizes the active conformation forming polar contacts with other regions of the kinase [54] [55] [42].

On the other hand, the C-terminal tail, that is not homologous to regions of other human proteins, appears to function as a regulatory portion of the protein. In fact, it has been proved to negatively regulate the catalytic activity of the kinase and to modulate its stability [55]. Moreover, the C-terminal tail of CDKL5 regulates its capability to shuttle

between nucleus and cytoplasm [52]; in this region are indeed present two putative nuclear localisation signals (NLS_1, a.a. 312-315, NLS_2 a.a. 784-789) and a putative nuclear export signal (NES, a.a. 836-845). Finally, in the C-terminal portion of CDKL5 can be identified three PxxP sites constituting putative binding site for Src homology 3-domain proteins, including Proto-oncogene tyrosine-protein kinase Src and Growth factor receptor-bound protein 2 (Grb2) [55].

2.2.3 *CDKL5* mutations

The analysis of a database collecting genetic alterations (http://mecp2.chw.edu.au) in *CDKL5* permitted to identify 498 variants of which 178 are pathogenic mutations and can be divided into missense, nonsense, frameshift, splice-site mutations and more complex rearrangements [56].

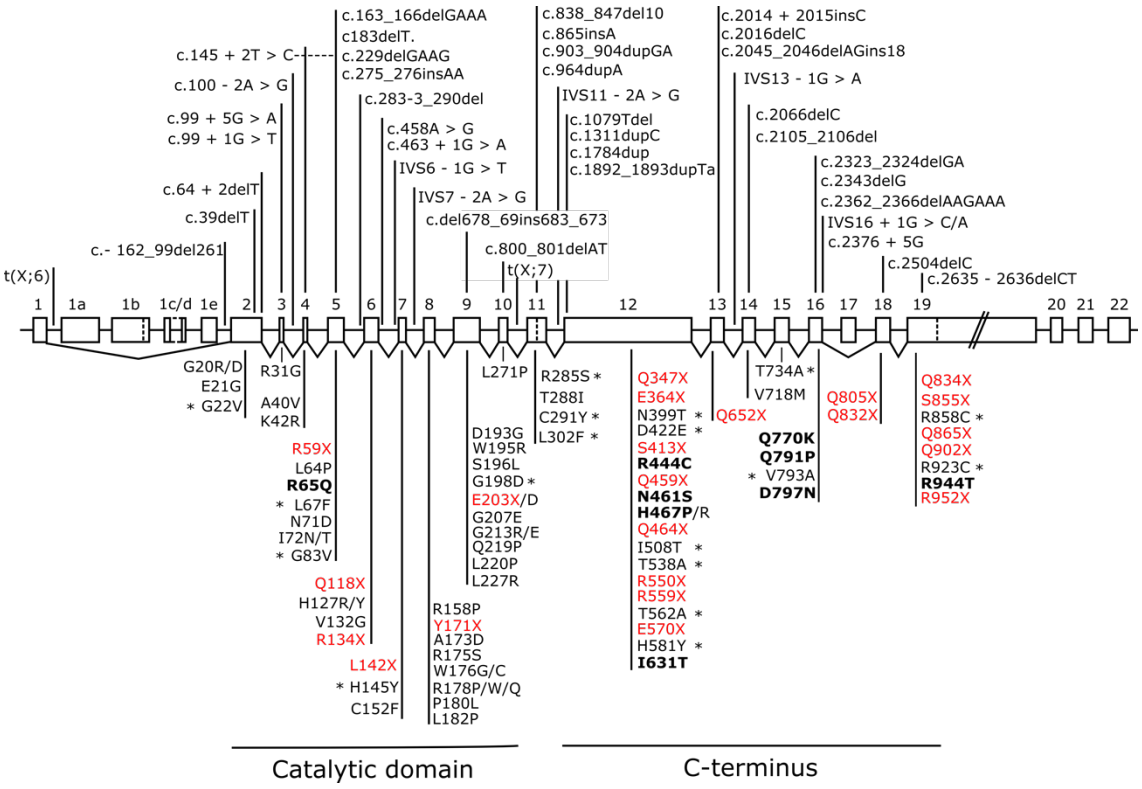

Figure 4. Graphical representation of *CDKL5* mutations.
Illustration of *CDKL5* mutations according to Kilstrup *et al.*, 2012 [42] and Hector *et al.*, 2016 [47]. Mutations above the gene are indicated using cDNA nomenclature and they consist in splice variants, deletions and frameshift mutations as described in Kilstrup *et al.*, 2012 [42]. Below the gene missense (black) and nonsense (red) mutations were integrated with RettBASE database (http://mecp2.chw.edu.au) and they are represented with amino acid nomenclature. *: uncertain pathogenicity; bold text: benign or likely benign variants.

Pathogenic missense mutations are almost exclusively localised in the kinase domain suggesting the crucial role of this region for maintaining CDKL5 proper function (Fig. 4). Indeed, C152F and R175S, mutations that falls in the catalytic domain, have been correlated to altered phosphotransfer activity and impaired kinase activation or substrate specificity, respectively [54].

On the contrary, nonsense mutations are equally distributed along the entire open reading frame (Fig. 4 in red). In particular, nonsense mutations located in the last portion of the C-terminal tail cause a mis-localisation of the kinase leading to its accumulation in the nucleus [52]. Although we are still lacking extensive genotype-phenotype studies, some evidence suggested that alterations in the C-terminal tail give rise to milder phenotypes [42].
Duplications of *CDKL5* were also reported indicating that a tight regulation of the kinase expression level is crucial for the CNS [38].

2.2.4 CDKL5 functions

Functions of a protein are strictly correlated with its localisation and its specific, and often regulated, protein-protein interactions.
In both proliferating cells and neurons, CDKL5 can be identified into the nucleus and cytoplasm [54] [52] [57] (Table 2). In nuclear compartment of hippocampal neurons and in mouse brain, the kinase shows a diffuse staining with brilliant dots not overlapping with the heterochromatic DAPI-positive DNA, while finely dotted CDKL5-positive puncta can be identified in soma, neurites and in dendritic spines [57] [58].
Subcellular localisation of CDKL5 is influenced by several factors including the cellular maturation stage and activity, and the protein phosphorylation state.
Indeed, in neurons CDKL5 is mainly cytoplasmic during embryogenesis while the nuclear fraction increases in postnatal stages until adulthood [52]. Moreover, the phosphorylation by dual specificity tyrosine-phosphorylation-regulated kinase 1a (DYRK1A) leads to an increase of cytoplasmic CDKL5 when the two kinases are co-expressed in mouse neuroblastoma Neuro2a cells [59].

Stimulation is one more factor that influence CDKL5 localisation. In particular, glutamate stimulation determines to a rapid exit of CDKL5 from the nucleus followed by massive proteasome-dependent degradation in hippocampal neurons [57].
Furthermore, localised synthesis of CDKL5 in dendrites and in dendritic spines is activated by neuronal activity; this induction occurs at all stages of neuronal maturation but it is prolonged in young neurons, while in mature neurons the activation of NMDA receptor induces a protein phosphatase 1-dependent dephosphorylation and a subsequent proteasome-dependent degradation of CDKL5 [50].

2.2.4.1 Nuclear functions of CDKL5: regulation of gene expression

In the nucleus CDKL5 was found to associate with different proteins including MeCP2, DNA (cytosine-5)-methyltransferare 1 (DMNT1) and SR-family splicing factor 35 (SC35) (Table 2); such interactions suggest a role in the regulation of gene expression.
In vitro biochemical data indicate that CDKL5 can associate with and phosphorylate MeCP2 supporting the hypothesis that such proteins belong to the same pathway; these data might be sustained by the partial overlapping clinical phenotype [60] [54]. Of note the C-terminal domain (precisely a.a. 450-550) seems to be required for the interaction with the methyl-binding protein [60].
Moreover, Kameshita *et al.* have demonstrated the capability of CDKL5 to bind and phosphorylate the N-terminal region of DNMT1 *in vitro* using a truncated derivative of CDKL5 containing only the catalytic domain. Nevertheless, additional studies are required to confirm this capability *in vivo* and in the presence of a full-length CDKL5 [61]. Finally, Ricciardi *et al.* have shown that CDKL5 co-localises with and co-immunoprecitates SC35 in nuclear speckles *in vivo* and *in vitro*. In addition, the authors have demonstrated that CDKL5 mis-expression is able to alter nuclear speckles and this is mostly dependent on the catalytic activity. Interestingly, using minigene-based splicing assays, it has been verified that loss of CDKL5 causes splicing defects [62].

2.2.4.2 Cytoplasmic functions of CDKL5: regulation of neuronal morphogenesis and dendritic spines development

In cytoplasmic compartment, CDKL5 has crucial roles in the regulation of neuronal morphogenesis and excitatory spine development.

Deregulated expression of CDKL5 severely alters different aspects of neuronal morphology including dendritic arborisation, polarisation and dendritic spine shape. Indeed, *CDKL5* silencing in cortical neurons resulted in a reduction of dendrites and axons total length together with a delayed neuronal migration [51]. Likewise, *CDKL5* knockdown gave rise to a polarisation defect exhibited by the presence of several neurons displaying no axon or the presence of multiple axons; this defect is at least in part mediated by the association of CDKL5 with shootin1, a key brain protein in axonal formation and neuronal polarisation [63]. Moreover, *CDKL5* silencing has determined an increase in dendritic protrusion density and the generation of thinner and filopodia-like spines together with a reduction of number of excitatory synapses and synaptophysin puncta. Such defects in spine structure are correlated to impaired synaptic activity: *CDKL5* knockdown neurons have shown reduction in mEPSCs [58].

The morphological abnormalities observed *in vitro* in silenced neurons have been confirmed also *in vivo* using *Cdkl5* mouse models [64] [65] [66].

The capability to modulate neuronal morphology is also highlighted by CDKL5 interaction with proteins involved in the regulation of microtubule [67] or actin cytoskeleton (Table 2) [51] [58].

Barbiero *et al.* have described a novel role of CDKL5 in the regulation of microtubule dynamics through the interaction with IQGAP1 (IQ domain-containing GTPase-activating protein 1), an important modulator of cell migration and polarity [67]. In this work, the authors have evidenced that the absence of CDKL5 leads to an altered cell migration together with the displacement of IQGAP1 from cellular leading edge and the reduction of its capability to interact with Rac1 and CLIP170 (+TIP cytoplasmic linker protein 170). Interestingly, the altered capability of CLIP170 to bind microtubules and morphological neuronal defects due to *CDKL5* silencing was rescued using the neurosteroid pregnenolone, a ligand of CLIP170 receptor [67].

CDKL5 involvement in the regulation of actin cytoskeleton was also suggested by its association with an important regulator of actin cytoskeleton, Rac1 (Ras-related C3 botulinum toxin substrate 1), and by its co-localisation with F-actin in the peripheral domain of growth cones in neurons (Table 2) [51]. Interestingly, BDNF stimulation enhances the CDKL5-Rac1 interaction and leads to a transient increase of CDKL5 phosphorylation suggesting a role of CDKL5 in BDNF-induced activation of Rac1 [51].

The regulation of spine development and synaptic activity is also mediated by the association of CDKL5 with NGL-1, a lipid anchored protein structurally related to netrin

family of axon guidance molecules [68]. CDKL5 binding leads to NGL1 phosphorylation strengthening its interaction with PSD95, a transmembrane protein localised in the Post Synaptic Density (PSD). Beyond NGL-1, CDKL5 interacts in PSD with the other two members of the NGL-family (NGL-2, NGL-3) and co-localises *in vivo* and *in vitro* with excitatory synaptic markers including PSD95, Shank (SH3 and multiple ankyrin repeat domains), NR2 (NMDA Receptor subunit 2) and VGLUT1 (Vescicular Glutamate Transporter 1; Table 2) [58].

Two more cytoplasmic CDKL5 substrate are amphiphysin 1 (Amph1) and Histone Deacetylase 4 (HDAC4, Table 2). The first one is a protein involved in synaptic vesicles recycling through clathrin-mediated endocytosis whose phosphorylation by CDKL5 negatively influences its binding to endophilin, an important factor in synaptic vesicle endocytosis [69]. The second one is a class II histone deacetylase expressed at high level in neurons and normally retained in cytoplasm in a phosphorylated state; the loss of CDKL5 determines a decrease of HDAC4 phosphorylation leading to its the nuclear translocation [70].

Interactors	Subcellular domain	CDKL5 region	References
DYRK1A	Nucleus	(Possibly) aa 1-352	Oi *et al.*, 2017
MeCP2	Nucleus	a.a. 450-550	Mari *et al.*, 2005
DNMT1	Nucleus	a.a. 650-850	Kameshita *et al.*, 2008
SC35	Nucleus	nd	Ricciardi *et al.*, 2009
Shootin1	Cytoplam	a.a. 299-1030	Nawaz *et al.*, 2016
IQGAP1	Cytoplasm	a.a. 299-1030	Barbiero *et al.*, 2017
Rac1	Cytoplasm	a.a. 670-934	Chen *et al.*, 2010
F-actin	Cytoplasm	nd	Chen *et al.*, 2010
NGL-1/2/3	Cytoplasm	nd	Ricciardi *et al.*, 2012
PSD95	Cytoplasm	nd	Ricciardi *et al.*, 2012
Shank	Cytoplasm	nd	Ricciardi *et al.*, 2012
NR2	Cytoplasm	nd	Ricciardi *et al.*, 2012
VGLUT1	Cytoplasm	nd	Ricciardi *et al.*, 2012
Amph1	Cytoplasm	(Possibly) a.a. 1-352	Sekiguchi *et al.*, 2013
HDAC4	Cytoplasm	(Possibly) a.a. 339-1030	Trazzi *et al.*, 2016

Table 2. Representation of CDKL5 interactors identified to date.
For each protein is indicated the subcellular compartment where the interaction occurs and, if available, the region of CDKL5 involved in the association. nd: not determined. DYRK1A [59]; MeCP2 [60]; DNMT1 [61]; SC35 [62]; Shootin1 [63]; IQGAP1 [67], Rac1, F-actin [51]; NGL-1/2/3, PSD95, Shank, NR2, VGLUT1 [58]; Amph1 [69]; HDAC4 [70].

To conclude Livide *et al.*, have recently identified a deregulation of *GRID1* (encoding for glutamate D1 receptor 1, GluD1) in *CDKL5* patients' derived cells [71]. GluD1 functions as an adhesion molecule binding presynaptic neurexin through cerebellin and inducing presynaptic differentiation. The authors have found that *GRID1* expression is downregulated in iPS (induced Pluripotent Stem) cells, while it is upregulated in NPCs (Neural Precursors Cells) and in mature neurons. Interestingly, the same *GRID1* expression profile was found in *MECP2* patients' derived cells, while chromatin immunoprecipitation (ChIP) analysis in SHSY-5Y cells indicated the capability of MeCP2 to bind the *GRID1* promoter. These data support the already mentioned possible molecular link between MeCP2 and CDKL5 [71].

2.2.4.3 Mouse models: recapitulating pathophysiology of *CDKL5*-related pathologies

To better understand the different functions and roles of CDKL5 and to improve the knowledge of the pathophysiology of *CDKL5*-related diseases, three different mouse models have been generated.

The first *Cdkl5* knockout mouse model was described by Wang *et al.* in 2012 (C57BL/6 background); it was generated by deleting exon 6 via homologous recombination in Embryonic Stem (ES) cells, therefore causing a premature truncation in the N-terminal catalytic domain [64].

Cdkl5$^{-/Y}$ mice exhibit subtle but consistent hyperactivity, motor defects, including hindlimb and forelimb clasping, and reduced anxiety; these phenotypes have already been described in mouse models of RTT and autism spectrum disorder (ASD) [1] [72]. Additional behavioural tests evidenced deficits in social interactions, learning and memory.

Although seizures are a hallmark of *CDKL5*-diseases, EEG recordings in the generated *Cdkl5*-null mouse evidenced a normal EEG pattern with the absence of spontaneous seizures, therefore posing some concerns on the face validity of this animal model that is generally characterized by very mild symptoms. However, the analysis of event-related potential (ERP), as a measure of cognitive processes, showed delayed ERP polarity suggesting impaired neuronal connectivity.

Amendola *et al.* described a second conditional mouse model generated through the deletion of *Cdkl5* exon 4 (C57BL/6 background) [65]. Concordantly with Wang's mouse model, knockout mice do not show spontaneous epileptic activity and abnormal EEG can be recorded only after convulsant treatment. Moreover, monitoring the responses to a moving visual stimulus in visual drum test, the authors have verified a reduction in the number of head tracks in knockout compared to wild type mice together with a decrease of visual evoked responses (VEPs).

Different behavioural analyses of this line of *Cdkl5*$^{-/Y}$ mice revealed locomotor impairments including hindlimb clasping and, in contrast to Wang *et al.* mouse model, hypoactivity [65] together with deficits in hippocampus-dependent learning and memory [73] [70]. Moreover, selective *Cdkl5* knockout in different forebrain population has allowed to correlate the diverse motor behavioural phenotypes with specific neuronal subpopulations: deficits in limb clasping and head tracking was associated with glutamatergic neurons while hypolocomotion with GABAergic neurons.

The localisation of Cdkl5 at synapses and the reported synaptic alteration after *Cdkl5* knock-down pushed up several synaptic studies in *Cdkl5* knockout mice.

Synaptic analyses of knockout mice have been performed in several brain regions including hippocampus [73] [70], somatosensory cortex [74], primary visual cortex (V1) [75] and cerebellum [76] and evidenced region-specific phenotypes.

Hippocampal *Cdkl5*$^{-/Y}$ neurons showed reduced dendritic arborisation with immature dendritic spines and, in CA1 pyramidal neurons, reduced spine density [73] [70] confirming previous evidence obtained *in vitro* and highlighting the role of CDKL5 during neuronal development [51] [58]. Moreover, a reduction in synaptophysin and VGLUT1 presynaptic markers in hippocampal dentate gyrus neurons suggested an impairment in synaptic contact maintenance [73].

Indeed, using two photon imaging, Della Sala *et al.* identified an impairment in dendritic spine maintenance as the cause of reduced spine number in *Cdkl5*$^{-/Y}$ somatosensory cortex [74]. While, in fact, new spines were normally generated, they were more effectively eliminated in the absence of Cdkl5. This resulted in a strong decrease in pyramidal spine density associated with a reduction of PSD95 expression. Morphological defects reflected impaired synaptic transmission and plasticity in terms of miniature EPSCs and LTP (Long-Term Potentiation).

Synaptic connectivity impairments in V1 of *Cdkl5*$^{-/Y}$ mice were described in a recent study [75]. The author evidenced a profound cellular and synaptic disorganisation in V1

characterised by a higher density of parvalbumin positive interneurons which are hyperconnected with pyramidal neurons together with a severe reduction of postsynaptic PSD95 and Homer and an upregulation of VGLUT1. Such alterations may cause a shift in the excitation/inhibition balance and were, indeed, associated with a severe downregulation of c-Fos expression indicating a general circuit hypoactivity in V1 [75].
A recent study evidenced *Cdkl5*-dependent deficits also in the cerebellum [76]. The cerebellum analysis has shown a high reduction of GABA-efflux and, in molecular layer, a selective defect of glutamic acid decarboxylase 67 (GAD67), a specific marker of GABAergic interneurons, suggesting inhibitory deficits. Moreover, Rotarod and Catwalk behavioural tests evidenced impaired motor functions in *Cdkl5* knockout mice [76].

The third mouse model was recently described by Okuda *et al.* deleting *Cdkl5* exon 2 in C57BL/6 genetic background mice [66]. In accordance with previously described *Cdkl5* mice, Okuda *Cdkl5*$^{-/Y}$ mice did not show spontaneous seizures. However, NMDA administration induced severe generalised tonic-clonic seizures in *Cdkl5*$^{-/Y}$ mice, indicating an abnormal NMDAR-mediated response. Electrophysiological analyses in hippocampal CA1 region revealed enhanced synaptic plasticity mediated by GluN2B-containig NMDARs. Indeed, hippocampal subcellular fractionation revealed an accumulation of GluN2B-containig NMDARs and SAP102 at the postsynaptic site of *Cdkl5*$^{-/Y}$ excitatory synapses. This accumulation seems to account for the enhanced seizure susceptibility in knockout mice. Interestingly, the administration of ifenprodil, a GluN2B selective antagonist, abrogated the NMDA-induced hyperexcitability [66].

2.2.4.4 Molecular alterations associated to CDKL5 depletion

Considering the serine/threonine kinase activity of CDKL5, the identification of its substrates is crucial for understanding the consequences of CDKL5 loss.
For these reasons, Wang *et al.* performed a Serine/Threonine (S/T) kinome profiling of different brain areas: striatum, cortex, hippocampus and brainstem. From such analysis emerged alterations in many signal transduction pathways in *Cdkl5* knockout mice and, in particular, in AKT/mTOR signaling cascade, an important pathway regulating protein synthesis. In accordance, a reduction of rpS6 phosphorylation, a ribosomal protein important for protein translation and whose activation depends on AKT, was detected [64]. The downregulation of AKT and rpS6 phosphorylation was confirmed in successive

studies [65] [74] and, interestingly, the administration of Insuline-like Growth Factor 1 (IGF-1), an activator of AKT/mTOR/rpS6 pathway already tested in RTT mice, was able to rescue altered rpS6 phosphorylation, spine deficits and PSD95 expression level [74].

In recent studies, Fuchs *et al.* identified a deregulation of the AKT/GSK-3β signalling pathway in the absence of Cdkl5 [77] [73]. In particular, *Cdkl5*$^{-/Y}$ showed hyperactivation of Glycogen Synthase kinase 3 beta (GSK-3β), a crucial regulator of many neurodevelopmental processes, and generated new-born granule cells with reduced length and number of branches [77]. Considering the elevated activity of GSK-3β, the use of a GSK-3β inhibitor (SB216763) was sufficient to restore both defective dendritic and spine morphology in *Cdkl5*$^{-/Y}$ granule cells and hippocampal pyramidal neurons and to improve impaired learning capabilities of *Cdkl5*$^{-/Y}$ mice [73].

A novel direct phosphorylation target of CDKL5 was recently identified by Trazzi *et al.* [70]. This study reports a downregulation of Histone Deacetylase 4 (HDAC4) phosphorylation in *Cdkl5*-null cells therefore leading to its accumulation into the nucleus and, consequently, to the reduction of H3 acetylation. This hypophosphorylation state makes the protein more active in the nucleus; interestingly, a specific inhibitor for HDAC4/HDAC5 (LMK235) was able to normalise survival and maturation of neuronal precursor cells, dendritic morphology and hippocampus-dependent memory that were impaired in *Cdkl5*$^{-/Y}$ mice [70].

2.2.4.5 CDKL5 roles in proliferating cells

Given the ubiquitous expression of CDKL5 and its belonging to the same family of MAP and cyclin-dependent kinases, its possible roles in proliferating cells have also been investigated.

A study in SH-SY5Y neuroblastoma cell line indicated that CDKL5 can inhibit cell proliferation causing an arrest in G0/G1 phases [78].

Furthermore, we have demonstrated that CDKL5 is important for faithful cell division [79]. Indeed, in proliferating cells, endogenous CDKL5 shows a dynamic localisation during cell cycle: in prophase and in metaphase it is detectable at mitotic spindle poles, while it localises at the midbody during cytokinesis. Importantly, the localisation at the centrosome was also detected in cultured neural progenitors and in post-mitotic primary hippocampal neurons [79].

The role of CDKL5 during cell cycle was more deeply dissected. In particular, *CDKL5* knockdown determines a significant increase in the number of cells with multipolar spindles together with several defects in chromosomal segregation including anaphase/telophase chromosome bridges, micronucleation and binucleated cells. Moreover, the high number of cells positive for phosphorylated histone H3-S10, a mitotic marker, indicates that these cells accumulate in mitosis [79]. Rescue experiments expressing a siRNA resistant *CDKL5* confirmed that these alterations depend on CDKL5. In addition, microscope analyses of si*CDKL5* HeLa cells have evidenced that spindle multipolarity is due to supernumerary centrosomes arising from centrosome accumulation as a consequence of cytokinesis failure [79].

At the molecular level, interfered midbodies have shown decreased levels of HIPK2 (Homeodomain-Interacting Protein Kinase 2) and its cytokinesis target H2B (extrachromosomal histone H2B) phosphorylated at S14 [79]. Importantly, spindle multipolarity of *CDKL5* knocked down cells was overcome using a phosphomimetic H2B-S14D derivative capable of rescuing cytokinesis failure in HIPK2-defective cells [80]. In this work, we have thus demonstrated a novel role of CDKL5 in the regulation of cell division through HIPK2-mediated H2B phosphorylation [79]. Since this topic has been one of the two main focuses of the first year of my PhD studies I have included the paper at the end of this dissertation.

Of interest and as already mentioned, Bergo *et al.* have recently identified an interaction of MeCP2 with centrosome; however, the two proteins seem to have different functions in this organelle [16].

Additional evidence of CDKL5 involvement in cell proliferation was provided by Fuchs *et al.* in the context of adult neurogenesis [77]. In this study, a quantitative analysis of BrdU (Bromodeoxyuridine)-positive or Ki67-positive progenitor cells in P45 hippocampal dentate gyrus (DG) led the authors to suggest an increase of proliferation in both *Cdkl5*$^{-/-}$ and *Cdkl5*$^{Y/-}$ mice compared to wild-type. However, in possible good accordance with our results, the count of BrdU-positive cells in P75 DG showed no difference between *Cdkl5*$^{-/-}$, *Cdkl5*$^{Y/-}$ and wild-type mice indicating that the higher proliferation degree at P45 is associated with a reduction of the survival rate. Accordingly, the expression of cleaved caspase-3 highlighted an increase of apoptotic cell death in newborn postmitotic neurons. Interestingly, the number of astrocytes is not altered suggesting that loss of Cdkl5 does not affect astrogliogenesis [77].

2.3 Therapeutic approaches for *CDKL5*-related pathologies

The identification of logically designed therapeutic approaches requires a profound comprehension of disease pathophysiology.

To date CDKL5 functions and the consequences of its loss are poorly understood therefore postponing the development of logically designed therapies.

Promising alternatives to drug-based therapies are gene- and protein-augmentative therapies. However, in both cases, the subtle regulation of *Cdkl5* mRNA and protein (including subcellular localisation and local translation), the high turnover of the kinase and the dosage issues together with the capability to target in females only cells expressing the mutant X-linked allele, make these approaches unfeasible to date.

However molecular genetics suggests the possibility to test different strategies depending on the specific mutation, therefore, functioning as "personalised medicine". Among these we found worth for testing the therapeutic potentiality of PTC (Premature Stop Codon) suppression.

2.3.1 Read-through approach

Translation termination occurs when a stop codon (UAA, UAG or UGA) enters into the ribosomal A site inducing the release of the polypeptide chain from the peptidyl-tRNA [81].

In the presence of a PTC originating from a nonsense mutation, different mechanisms can be activated including translation termination releasing truncated polypeptides, Nonsense Mediated Decay (NMD) and PTC suppression. NMD is a quality control pathway determining the degradation of PTC-containing mRNA and then avoiding the generation of potentially dominant negative truncated proteins [81]. PTC suppression requires a near-cognate aminoacyl-tRNA that by binding two of the three bases of a PTC bypasses the premature stop codon [82] [81]. This process, also known as read-through, allows protein elongation until the natural stop codon, therefore generating a full-length polypeptide (Fig. 5).

The suppression of an in-frame PTC determines the incorporation of one of several possible amino acids: seven different amino acids could be incorporated at UAG site, while six at UGA or UAA codons (Table 3) [82]. In each case, if PTC arose from a single nucleotide change, one of these amino acids leads to the synthesis of a WT protein.

Different studies have demonstrated that the residue inserted after read-through depends on the PTC. *In vitro* data have identified tryptophan, cysteine and arginine as the preferred inserted amino acids in case of an UGA stop codon, while glutamine is more likely to be found in presence of UAA and UAG stop sites [83] [84] [85] [86]. By establishing a reporter system in yeast, Blanchet *et al.* have recently defined the incorporation rate at different PTCs: 54% for tyrosine, 44% for glutamine, and 2% for lysine at UAA stop codon; 92% tyrosine, 5% glutamine, and 3% lysine at UAG stop codon; 82% tryptophan, 14-17% cysteine, 1-4% arginine at UGA stop codon [87].

As mentioned, the read-through is just one of the possible outcomes in the presence of a PTC; its frequency is affected by several factors, including tRNA abundance, release factors levels, PTC type and the surrounding mRNA sequence. In particular, the highest read-through efficiency was found at UGA stop codon, while UAA appeared as the least efficient [88] [89] [90] [91].

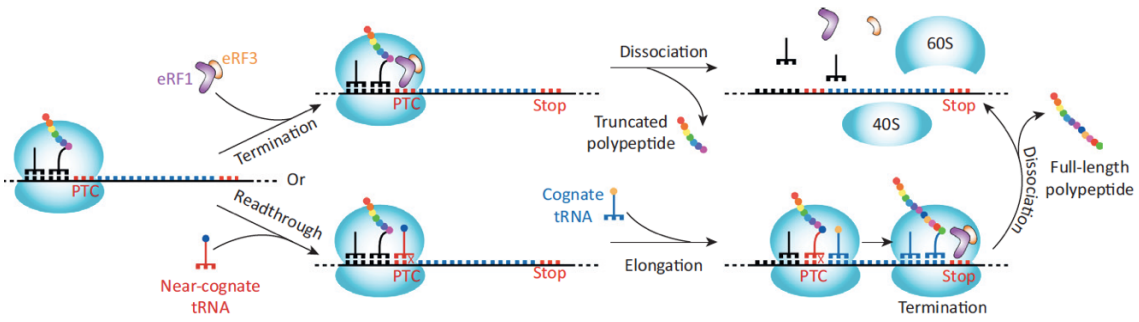

Figure 5. Schematic representation of the main mechanisms occurring when a ribosome encounters a PTC.
The presence of a PTC at the ribosomal A-site can determine translation termination or read-through. In the first case, the binding of eRF1 and eRF3 release factors determines the release of the truncated polypeptide followed by disassociation of ribosomal subunits. Rarely the production of a full-length polypeptide can occur thanks to the association of a near-cognate tRNA [81].

PTC nucleotide context is one of the main factors influencing read-through efficiency. In particular, the CUAG sequence immediately downstream the stop codon or more generally the sequence CARYYA (R for purine and Y for pyrimidine) appeared to facilitate read-through [88]. Moreover, the highest rate of gentamicin-induced read-through was found in the presence of a uridine at -1 and a cytosine at +4 positions respect to PTC [92]. However, the influence of nucleotide context may differ according to the PTC identity. Indeed, Manuvakhova *et al.* have demonstrated that in most cases the best

read-through rate occurs when the position +4 is occupied by a cytosine for UGA and UAA stop codons or by an uracil for UAG [91].

Data from diverse studies have evidenced that basal PTC suppression occurs with a rate between 0.001 to 0.1% at natural stop codons [93] that increases up to 1% at PTCs [94] [91]. However, different types of molecules can be used to induce PTC suppression including suppressor tRNAs or chemical compounds. The former have been generated by modifying the anticodon sequence of an exogenously expressed tRNA in order to allow the recognition of the premature stop codon [95]; however, since the recognition of natural stop codon cannot be excluded, to date their use appears not feasible for PTC suppression therapy [96].

UAA		UAG		UGA	
Near-cognate codon	**Encoded amino acid**	**Near-cognate codon**	**Encoded amino acid**	**Near-cognate codon**	**Encoded amino acid**
AAA	Lys	AAG	Lys	AGA	Arg
CAA	Gln	CAG	Gln	CGA	Arg
GAA	Glu	GAG	Glu	GGA	Gly
UCA	Ser	UCG	Ser	UAA	None
UGA	None	UGG	Trp	UCA	Ser
UUA	Leu	UUG	Leu	UUA	Leu
UAC	Tyr	UAA	None	UGC	Cys
UAG	None	UAC	Tyr	UGG	Tip
UAU	Tyr	UAU	Tyr	UGU	Cys

Table 3. Possible amino acid substitutions during read-through at different PTC sites.
Representation of amino acids deriving from the mispairing between a near-cognate aminoacyl tRNA and a stop codon. For simplicity, this table shows all possible codons deriving from a single mismatch at the three different positions rather than the corresponding tRNA anticodons [82].

On the other hand, the pharmaceutical approach exploits molecules that by binding to ribosomal subunits foster the association of a near-cognate tRNA with the PTC [82].

Considering that about 11% of human genetic diseases can be caused by in-frame nonsense mutations, several studies have tested read-through drugs in different pathological contexts including Duchenne muscular dystrophy (DMD) [97], cystic fibrosis (CF) [98] [99], ataxia-telangiectasia (ATM) [100], Usher syndrome [101], factor VII deficiency [102], retinitis pigmentosa [103] and Rett syndrome [89].

Read-through drugs comprise a wide range of molecules including aminoglycosides, designer aminoglycosides and non-aminoglycosides.

The first one comprises several compounds; among these, drugs carrying a hydroxyl at C6' in the ring I (e.g. G418 or paromomycin) seem to more be more efficient in PTC suppression [104]. Studies in prokaryotic ribosomes have indicated that aminoglycosides

bind the helix 44 of 16S rRNA which is located at the base of ribosomal A site [82]. The binding of paromomycin in the decoding region has been found to induce a conformational rearrangement of the universally conserved nucleotides A1492 and A1493 in the ribosomal A site devoid of a tRNA [105]. The induced conformational change seems to alter the discrimination of near-cognate tRNA and to hinder the entry of release factors, thus stimulating read-though. Although rRNA structure is evolutionary well conserved, the modification of two bases changes in the 18S rRNA with respect to 16S rRNA seems to reduce aminoglycoside binding to eukaryotic decoding site [82].

Aminoglycoside-derived read-through has been extensively tested in different pathological contexts including cell lines and mouse models harboring premature nonsense site in genes such as *CFTR* (Cystic fibrosis transmembrane conductance regulator) and *DMD* (Duchenne muscular dystrophy) [98] [99] [97]. Promising results have led to diverse clinical trials using gentamicin for the treatment of Cystic Fibrosis (CF) and Duchenne Muscular Dystrophy (DMD) patients. While initial clinical trials in DMD patients did not report clinical benefits [106], a subsequent study with an extended time of treatment has shown the expression of dystrophin in DMD patients together with a decrease in serum creatine kinase levels [107]. The clinical trial in CF patients has led to controversial data: two studies reported clinical benefits and enhanced CFTR-mediated chloride transport after gentamicin treatment [108] [109], while Clancy *et al.* did not reported any improvement in sweat chloride measurements [110].

Although different aminoglycosides have shown good capability to induce read-through, their toxicity at therapeutic doses has limited their use in clinical practice. Long-term treatment leads to irreversible ototoxicity and reversible nephrotoxicity that are unrelated to read-through activity [111] [112] [113] [81]. Indeed, the intracellular uptake of aminoglycosides in renal proximal tubules and in hair cells of inner ear is associated with their binding to lysosomal acidic phospholipid and with the inhibition of mitochondrial protein synthesis determining the alteration of different enzyme functions and the generation of reactive oxygen species (ROS).

Different strategies have been explored to decrease the toxicity of this therapeutic approach.

In particular, the advantages of co-administrating together with gentamicin antioxidants [114] or poly-anions, such as poly-L-aspartate and daptomycin have been evaluated. Poly-anions were reported to alleviate nephrotoxicity and ototoxicity by binding aminoglycosides and preventing the association of the antibiotic with lysosomal

phospholipids [115] [116] [117] [82]. Interestingly, poly-L-aspartate administration leads to an increase of aminoglycoside cytoplasmic concentration and improved the read-through efficiency in a CF mouse model [116].
By high-throughput screening in yeast, a new molecule, CDX5-1, was identified [118]. This compound was found to strongly increase the G418-induced read-through *in vitro*. Indeed, while CDX5-1 alone was not able to facilitate the read-through, in co-administration with G418 it enhanced up to 180-fold the PTC suppression efficacy of *TP53* R213X. Moreover, the combination of the two molecules improved also the read-through in patients-derived cells carrying nonsense mutations in *CLN2*, *SMARCAL1* and *DMD* genes [118].

A second approach involves the development of designer derivatives of existing aminoglycosides. Such drugs maintain the natural aminoglycoside backbone but present additional chemical groups that should decrease toxicity and/or enhance bioactivity [119]. Designer aminoglycoside compounds include different groups of molecules: "TC" compounds derived by modification of neomycin, "JL" compounds by kanamycin B, "NB" compounds by paromomycin and geneticin [120]. Among "NB" compounds, the paromomycin derivative NB30 showed dose-dependent read-through activity but its efficacy was found to be lower than paromomycin or gentamicin. On the contrary, subsequent generations of "NB" compounds such as NB54 and NB84 have been reported to induce read-through more effectively than gentamicin [121]. In particular, NB84 demonstrated a reduced ototoxic potential due by its decreased affinity for mitochondrial rRNA [122] and long-term NB84 treatment did not induced toxicity in an MPS I-H (mucopolysaccharidosis type I-Hurler) mouse model [123].

A third solution consists in identifying molecules that induce read-through but are unrelated to aminoglycosides. A group of non-aminoglycoside compounds was identified by high-throughput protein transcription/translation (PTT) ELISA-based assays. Such molecules, known as SMRT (Small Molecular Read-Through) compounds, include RTC13, RTC14 and GJ071, GJ072 [124] [125]. Read-through activity of RTC13 and RTC14 was reported *in vitro* testing different disease-genes, including *ATM* (ataxia telangiectasia) and *dystrophin* genes [124]. GJ071 and GJ072 compounds, identified in a second screen, have shown similar or even a better capability to induce read-through in *ATM* gene if compared to RTC13. In addition, most of the active analogs of GJ072 were

characterized by low partition coefficient (cLogP) indicating their ability to permeate tissues in case of an *in vivo* administration [125].

High throughput screening performed by PTC Therapeutics has led to the identification of another potentially promoting read-through compound, PTC124 (also known as Ataluren or Translarna™) [126].

PTC124-induced read-through has been demonstrated by different *in vitro* and *in vivo* models of disease [127] [128] [129] [130] [131] [132] [133]. In addition, preclinical positive results together with reported low toxicity [134] have encouraged the initiation of different clinical trials in CF and DMD patient cohorts. PTC124 administration in CF patients has induced a substantial improvement in chloride conductance and a trend of improved pulmonary functions were observed [135] [136] [137] [135]; on the other hand, dystrophin protein production and reduction in serum creatine kinase were found in DMD patients [138] [139].

Nevertheless, the read-through activity of PTC124 is still under discussion. Indeed, several preclinical studies did not confirm the capability of PTC124 to suppress PTCs [140] [141] [142] [143], [144] [145] [146] [147] and their clinical efficacy was found to be weak in CF patients [148] [149]. Although the efficacy data lacked robustness, in 2014 PTC124 received a conditional marketing authorization from the European Medicine Agency for DMD patients resulting from a nonsense mutation in *dystrophin* gene [150].

Finally, beyond the toxicity associated with read-through drugs, the ability to cross the blood brain barrier (BBB) is an important issue for the treatment of CNS disorders.

Aminoglycosides are mainly uptaken in mammalian cells through endocytosis mediated by megalin receptor [151]. Megalin is expressed in epithelial cells including brain ependymal cells which can delivery aminoglycosides in the cerebrospinal fluid [152]. Indeed, aminoglycosides such as gentamicin were reported to be able to cross the blood brain barrier to some extent [153] [154] [155]. Moreover, the administration of NB54 and NB84 has significantly reduced lysosomal glycosaminoglycan storage in the brain of nonsense mutation mouse models for MPS I-H disease [156] [123]. Such amelioration in the brain together with the low toxicity reported indicate the possibility to use these designer aminoglycosides in CNS diseases including *CDKL5*-related pathologies.

3. RESULTS

3.1 Analysing the feasibility of PTC suppression in *CDKL5*-related pathologies

As already mentioned, some *CDKL5* patients carry nonsense mutations and might benefit from a read-through strategy as "personalised medicine" approach.

First screenings of read-through drug efficacy are generally performed transfecting cell lines with PTC-containing constructs and verifying the capability of treated cells to generate full-length products. Considering that *CDKL5* pathogenic missense mutations are mainly localised in the N-terminal catalytic domain while nonsense mutations are uniformly distributed in the coding sequence, we have decided to study the read-through of PTCs localised in different *CDKL5* regions.

We selected mutants by analysing the database collecting human genetic alterations in *CDKL5* patients (http://mecp2.chw.edu.au/cdkl5/index.php) and we chose nonsense mutations located either in the N-terminal catalytic domain (R59X, R134X, Fig. 6A) and in the C-terminal tail (Q347X, E364X, R550X, S855X, Fig. 6A). We hypothesized that C-terminal mutations could be more suitable for these studies because the amino acid substitution possibly introduced by PTC suppression might produce a protein that maintains most of its functions. Moreover, considering the importance of stop codon type in the read-through approach [88] [81], drugs have been tested on the three different stop codons codified by the aforesaid pathogenic nonsense mutations: UGA (R59X, R134X, R550X, S855X), UAG (Q347X) and UAA (E364X).

Using the Q5 Site-Directed Mutagenesis Kit (NEB), nonsense sites were introduced in the pEGFPC1-hCDKL5$_{107}$ construct codifying for the human CDKL5 isoform weighting 107 kDa fused to EGFP at the N-terminus (Fig. 6A) [52]. Moreover, since a different amino acid might be introduced at the PTC site after read-through, we mutagenized the aforementioned cDNAs to obtain the most probable full-length protein that may be produced after drug treatment. We thus generated constructs carrying a tryptophan at the TGA nonsense sites (Fig 6A, R59W, R134W, R550W, S855W) whose non-polar nature dramatically contrasts with the polar nature of original arginine [91]. Concerning the two derivatives containing a TAG (Q347X) and TAA (E364X) PTC, glutamine represents the

most probable residue introduced by read-through [91]. Since for the Q347X mutant, the read-through product will have a high chance to reproduce the WT amino acidic sequence, we did not generate any full-length derivative. On the contrary, the E364 residue will be probably substituted with an amino acid (glutamine) that carries quite different chemical properties; considered that this PTC is predicted to be difficult to rescue we decided to postpone the production of a full-length "suppressed" E364Q derivative after having tested read-through.

All constructs were verified by Sanger sequencing and the correct size of the proteins were verified by Western Blot (WB, Fig. 6B). We could thus confirm that all proteins have the expected molecular weight given by the EGFP portion (~27 kDa) fused to the specific cDNA: WT and R/S-W proteins ~134 kDa, R59X ~34 kDa, R550X ~88 kDa, R134X ~42 kDa, Q347X ~65 kDa, E364X ~67 kDa (Fig. 6B).

At the subcellular level, WT CDKL5 is localised both into the nucleus and cytoplasm; on the contrary, truncating or missense mutations can alter the nucleo-cytoplasmic distribution of the kinase and its capability to give rise to dots [54] [52].

In order to understand whether read-through products might retain WT features although containing a missense mutation, tryptophan-substituted proteins were analysed by immunofluorescence (IF). As shown in Fig. 6C, WT protein is equally distributed between the nucleus and the cytoplasm and has a dotted staining in both compartments (Fig. 6C, panels a and b); the nature of this dots is not defined yet. W-containing proteins exhibit a similar distribution and are capable of forming dots (Fig. 6C, panels c-d-e and f). These preliminary results led us to hypothesize that read-through products could have a proper subcellular localisation and therefore possibly a correct functionality and capability to interact with partners, thus, encouraging further studies.

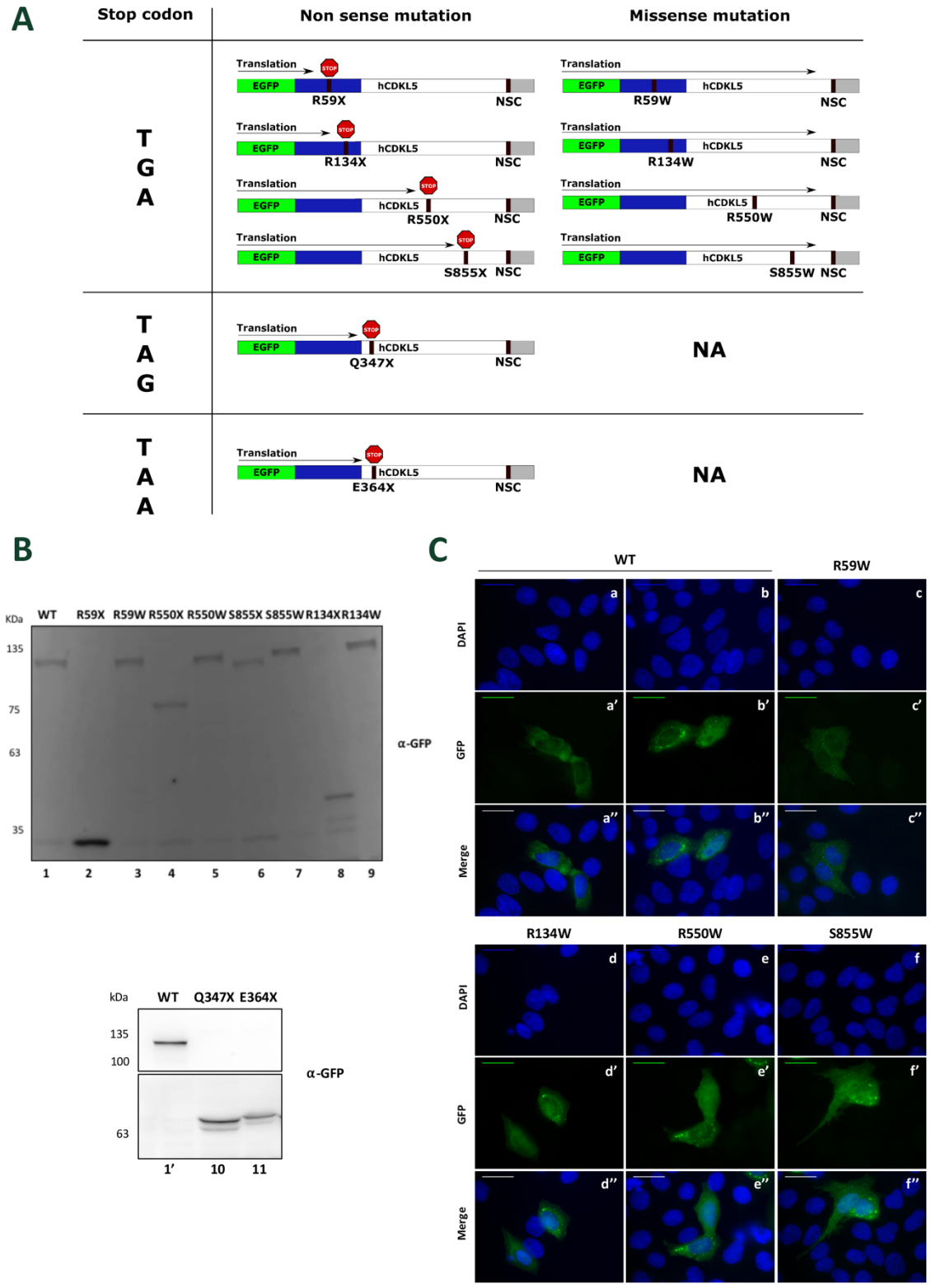

Figure 6. Full-length CDKL5 derivatives containing a missense mutation possibly caused by PTC suppression maintain a proper subcellular distribution.

A) Schematic representation of the GFP-tagged hCDKL5 derivatives generated by site-directed mutagenesis. On the left is highlighted the introduced stop codon. For constructs containing a TGA premature stop codons, full-length derivatives containing a W instead of the PTC were generated. In blue is represented the N-terminal catalytic domain, while in white is shown the C-terminal tail.

NA: Not Available. NSC: Natural Stop Codon.

B) WB (10% SDS-PAGE) analysis assessing the expression and correct size of the generated constructs. Protein lysates were isolated from HeLa cells transfected for 24hrs with WT or mutated constructs. CDKL5 derivatives were revealed using anti-GFP antibody.

C) IF analysis of HeLa cells transfected with WT and mutated CDKL5 cDNAs containing the W-missense mutation. For each CDKL5 derivative, the upper row shows the DAPI stained nuclei (blue), the middle row shows the GFP-expressing cells (green) and the lowest row shows the merge between DAPI and GFP. Images are representative of the subcellular distribution of proteins analysed in at least 60 cells per CDKL5 derivative (n=3). Magnification 100x, scale bar 30 μm.

3.2 Truncated proteins may aberrantly localise in different subcellular compartments

As already mentioned, alterations in CDKL5 have been correlated to its impaired shuttling between nucleus and cytoplasm [52] [54]. For this reason, we have decided to analyse the subcellular distribution of truncated proteins; in fact, the identification of an overt phenotype would facilitate the visualization of an effective read-through process, restoring CDKL5 proper behaviour.

We have thus analysed by IF the localisation of the premature truncated derivatives transfected in HeLa cells (Fig. 7A).

As expected, the analyses revealed a different subcellular distribution of truncated GFP-tagged proteins that seems to depend on the position of the nonsense mutation. Most premature stop codons (R59X, R134X; Fig. 7A, panels d and e) determine the generation of chimeras in which the GFP portion is largely predominant; accordingly, the subcellular distribution of these mutants well overlapped with that one exhibited by GFP (Fig. 7A, panels c). Analogously, mutants carrying nonsense sites in the beginning of the C-terminal tail (Q347X, E364X; Fig. 7A, panels f and g) revealed a similar localisation respect to GFP, suggesting that the presence of NLS1 is not sufficient to determine a nuclear accumulation. On the contrary, R550X protein seems to be enriched into the nucleus (Fig. 7A, panels h). Finally, in cells expressing the S855X mutant (Fig. 7A, panels i) the nuclear DAPI remained quite evident below the green signal of the GFP-tagged protein; this evidence could indicate that NES signal may be sufficient to export the protein in the cytoplasm despite the presence of the two nuclear localisation signals (NLS1 and NLS2).

These results are indicative of a different distribution between the nucleus and the cytoplasm of the diverse derivatives; however, we do realize that in the future we will

have to perform confocal analyses or fractionation experiments (see below) to properly interpret the obtained results.
In addition to altered localisation, truncated proteins seem to have lost the capability to form dots.
Similar results were obtained in HEK293T cells; however, the GFP-CDKL5 R134X mutant manifested the formation of an aggregate close to the nucleus that clearly distinguishes itself from other constructs (Fig. 10A, c).

To better understand the entity of the alterations in the subcellular localisation suggested by IF data, we performed WB analyses using fractionated cell extracts.
As shown in Fig. 7B and C, the analysis of nuclear and cytoplasmic signals seems to confirm that the alteration in the subcellular distribution is dependent on the position of the premature stop codon. Indeed, mutants containing a PTC in the N-terminal domain (R59X, lanes 5-6; R134X, lanes 8-9) and at beginning of the C-terminal tail (Q347X, lanes 11-12) are clearly enriched in the cytoplasmic fraction. Such result is also confirmed by the quantification of the ratio between nuclear and cytoplasmic fraction compared to WT arbitrarily set to 100% (Fig. 7C).
On the contrary, although the WB of the R550X derivative suggested a slight enrichment into the nucleus, this result was not confirmed by quantifying several experiments. Eventually, whereas the S855X protein shows a significant reduction of accumulation in the nuclear compartment with respect to the WT kinase, the presence of the C-terminal E364X and R550X PTCs determines only a tendency in such reduction. It is worthwhile to mention that the observed high variability is probably well justified by the knowledge that CDKL5 subcellular distribution seems to be affected by the cell type, cell cycle and cell physiological conditions.

Altogether, these data confirm that truncating mutations can affect CDKL5 nucleo-cytoplasmic distribution [54] [52] and the identified phenotypes could be used as readout of rescued WT features after read-through.

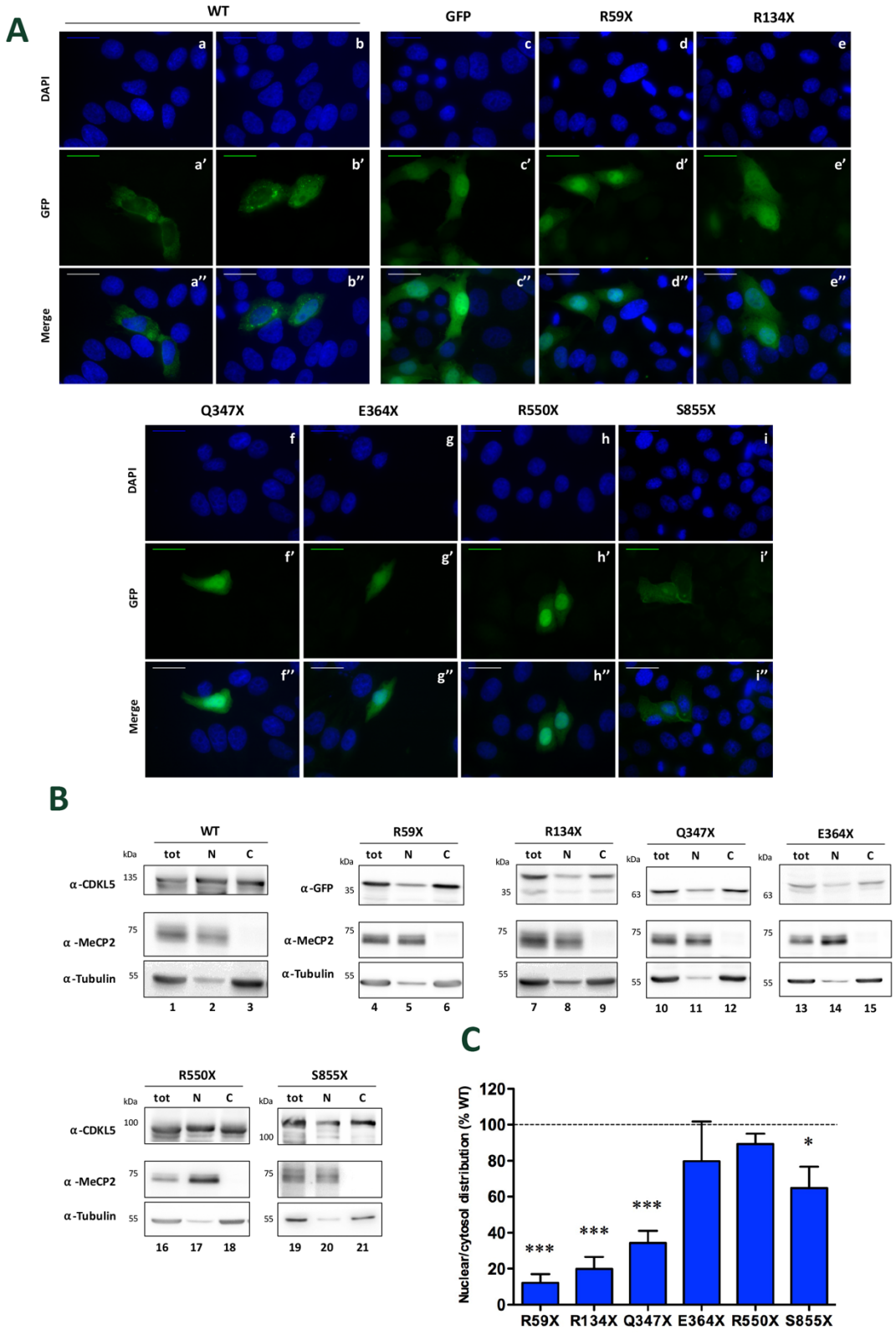

Figure 7. Nucleo-cytoplasmic distribution of almost all truncated GFP-CDKL5 proteins differ from WT GFP-CDKL5.

A) IF assay of HeLa cells transfected with different PTC-containing or WT constructs for 24hrs. Staining was performed using DAPI (blue, upper row) and anti-GFP (green, middle row); the analysis was performed on at least 60 cells per condition (n=3). Magnification 100x, scale bar 30 μm.

B) WB analysis of the subcellular distribution of fractionated HEK293T cells overexpressing GFP-tagged WT or truncated derivatives. The same volume of nuclear and cytoplasmic fraction, corresponding to an identical number of cells, was analysed.
The upper panel shows the CDKL5 specific bands identified by anti-CDKL5 (WT, R550X, S855X) or anti-GFP (R59X, R134X, Q347X, E364X) antibodies; in the middle and lower panels, the quality of fractionation was assessed testing the distribution of MeCP2 and α-tubulin, used as nuclear and cytoplasmic markers, respectively.
Tot: total extract, N: nuclear extract, C: cytoplasmic extract.

C) Graphical representation of the subcellular distribution (nucleus/cytoplasm) of truncated derivatives with respect to WT GFP-CDKL5. Nucleo-cytoplasmic distribution of WT was arbitrarily set to 100% and nucleo-cytoplasmic distribution of truncated derivatives was expressed as values relative to WT. The error was expressed as SEM; the significance was evaluated by one-way ANOVA followed by Bonferroni's post hoc test (* $p < 0.05$, ** $p < 0.01$, *** $p < 0.001$); $n \geq 3$

3.3 Aminoglycoside drugs are able to suppress *CDKL5* UGA stop codons in a dose-dependent manner

The large portion of human genetic diseases that can be caused by nonsense mutations in specific genes have pushed up different studies analysing the possibility to suppress PTCs through chemical compounds. In particular, aminoglycoside read-through activity mediated by gentamicin or G148 has been extensively examined.

We thus started testing whether treatment with different doses of gentamicin or G418 would promote read-through of R59X and R134X mutants causing a UGA premature stop codon.

As shown in Fig. 8, in absence of aminoglycosides no full-length product was generated, while both drugs partially suppressed R59X (Fig. 8A, B) and R134X (Fig. 8A', B') PTCs causing the production of a full-length CDKL5. Read-through efficacy was strictly dependent on the drug dose; in particular, for both mutants an evident signal was detectable when cells were treated with 500-2000 μg/ml of G418 (Fig. 8A, 8A' lanes 7-9) or the same dose of gentamicin (Fig. 8A, 8A' lanes 7-9). However, depending on the specific mutation and the specific experiment, lower drug doses could induce sufficient amounts of full-length CDKL5 to be detected above the background in our experimental conditions (as an example see panel B', lanes 5 and 6). As expected, WT protein size was not affected by treatment with the maximal dose (2000 μg/ml) of G418 (Fig. 8A, lane 2; Fig. 8C, lanes 10-11-12) or gentamicin (Fig. 8B, B', lane 2) confirming that these drugs do not alter the normal arrest of protein synthesis.

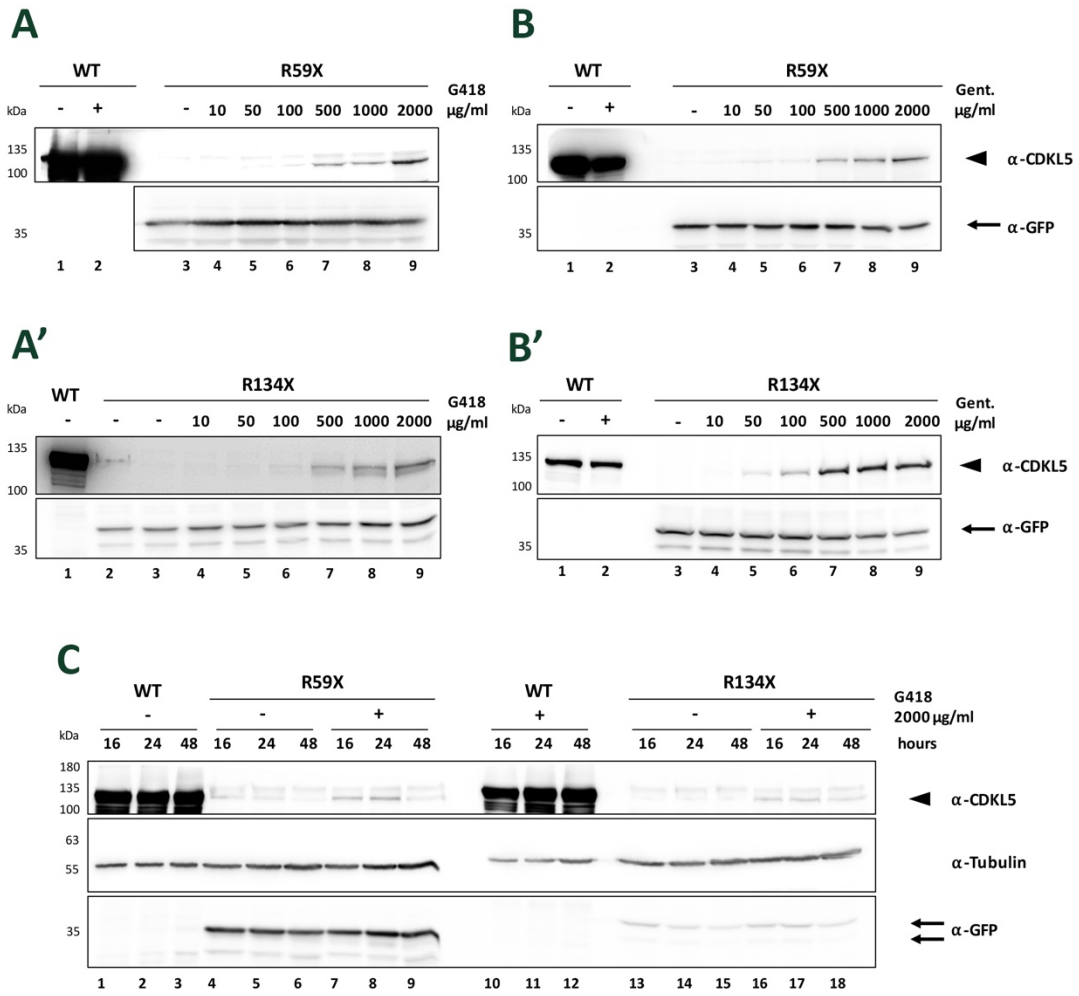

Figure 8. High doses of G418 and gentamicin mediate PTC suppression.
WB (8% SDS-PAGE) analysis of protein lysates from HEK293T cells transfected with R59X (A, B, C) or with R134X (A', B', C) and treated with G418 (A, A') or gentamicin (B, B') at the indicated doses for 24hrs or with G418 (2000µg/ml) for 16, 24 and 48hrs (C). Cells were collected in Sample buffer and the same number of cells transfected with the truncated constructs or half of this number from samples transfected with the WT construct were loaded on the gel. Immunoreactivity was detected using anti-GFP and anti-CDKL5 antibodies. GFP antibody binds to the amino-terminus of the expressed chimera; α–CDKL5 binds a C-terminal epitope (a.a. 636-758). In C, α–tubulin was used as loading control. Arrowheads denote the full-length GFP-CDKL5 protein; arrows highlight each specific mutant form of GFP-CDKL5. n=3
–: untreated cells; +: treated cells with 2000 µg/ml of G418/gentamicin.

These analyses indicate that both drugs are similarly able to induce read-though and that the best efficiency is reached at the higher concentrations. Indeed, although gentamicin has resulted to be more efficient at lower concentration depending on specific mutant (Fig. 8 B', lanes 5 and 6), this trend was not confirmed in all experiments. On the contrary, our experiment shown in Fig. 10 suggests that high doses of G418 have a more robust read-through percentage on all mutants that we identified as read-through sensitive; for such reason, we proceeded performing most analyses with G418.

Then, we assessed the influence of incubation time on read-through. As shown in Fig. 8C, the study of the response to G418 at different time points revealed that most PTC suppression has already occurred in 16 hours of treatment while prolonged exposure did not determine any increase of the full-length signal.

3.4 Read-through occurs at different *CDKL5* PTC types but it is probably dependent on the position of the PTC

In the context of PTC suppression two main factors should be considered: the identity of PTC and its nucleotide context. Different studies have indicated that UGA is the easiest stop codon to be read-through [88] [81], while a cytosine or uridine immediately downstream the stop codon (+4 position) give rise to the highest rate of PTC suppression [91]. In addition, gentamicin read-through was found to be more efficient when a uridine is present at -1 position [92].

Concerning *CDKL5*-related pathologies, only about 30% of nonsense mutations codify for UGA stop codon, while about 40% and 30% give rise to UAG and UAA PTCs, respectively. Understanding whether PTC suppression can occur at different PTC types is thus mandatory for the treatment of *CDKL5* patients carrying nonsense mutations.

The analysis of the nucleotide context of chosen PTCs revealed that none of them has the most favourable surrounding sequence for read-through (Fig. 9A', B', C'). Nevertheless, G418 mediated the read-through of all PTC types: UGA (Fig. 9A, lanes 6-7-8), UAG (Fig. 9B, lane 4) and UAA (Fig. 9B, lane 6). The only PTC studied that was not suppressed neither by gentamicin (Gent.) or G418 causes the generation of a truncated protein containing 855 amino acids (S855X mutant, Fig. 9C). Such result was unexpected since S855X mutant codifies for a UGA stop codon and the surrounding context is similar to the other PTCs analysed. Being so close to the natural stop codon, we hypothesize that the S855 PTC might exploit the close 3'-poly-(A) tail for the recruitment of releasing factors to the poly-(A) binding proteins, thus increasing the efficiency of translation termination and, therefore, significantly limiting the efficacy of read through drugs.

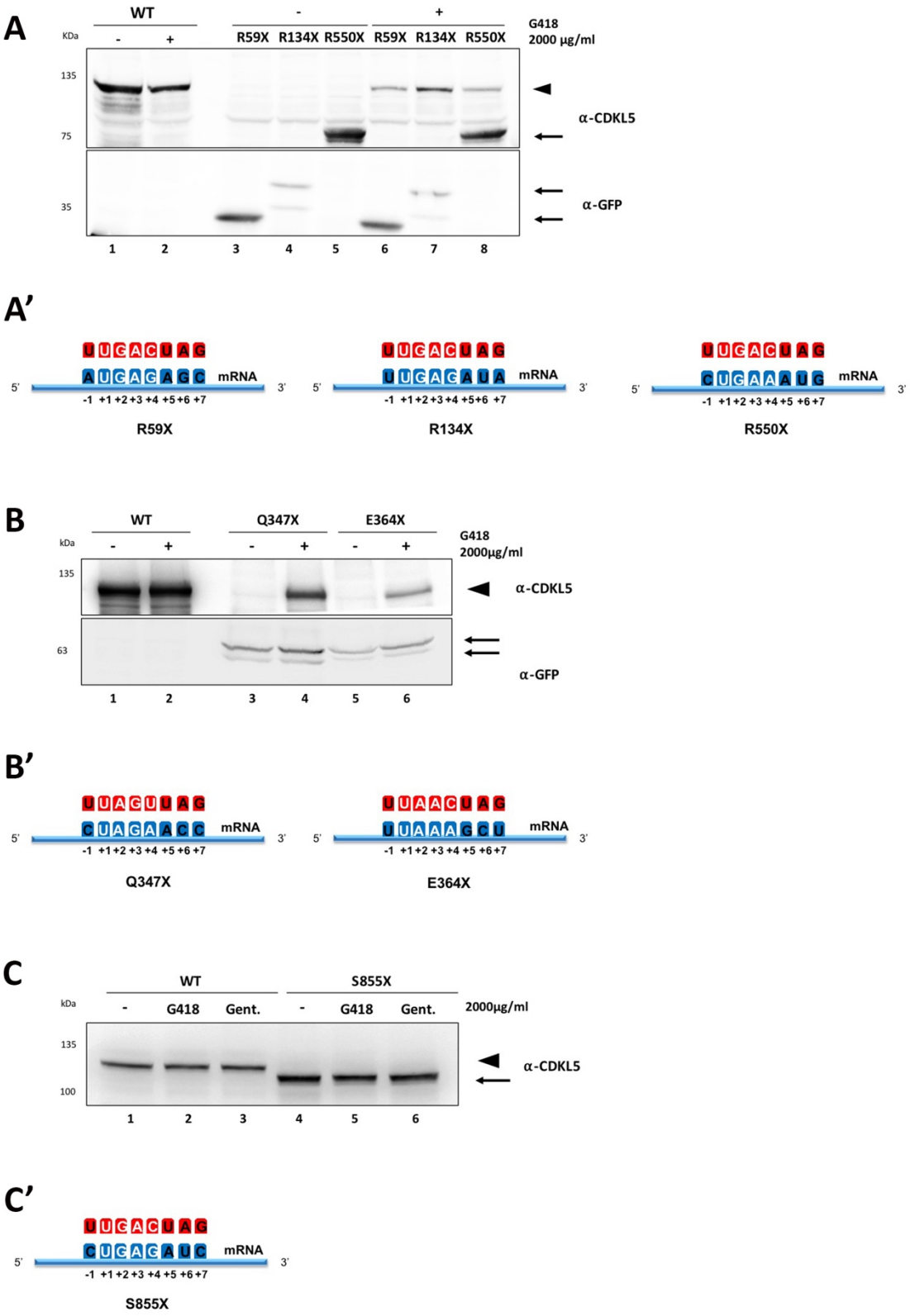

Figure 9. G148 facilitates the suppression of different PTCs.
WB (8% SDS-PAGE) assays of samples extracted from transfected HEK293T cells and treated with G418 (2000 µg/ml, A, B, C) or gentamicin (2000 µg/ml, C) for 24hrs. Cells were transfected with TGA- (R59X, R134X, R550X, S855X; A, C), TAG- (Q347X) or TAA- (E364X) containing constructs (B) and collected in Sample buffer; the same number of cells transfected with the truncated constructs or half of this number

from samples transfected with the WT construct were loaded on the gel. Immunoreactivity was detected using anti-GFP or anti-CDKL5 antibodies. n≥3
Arrowheads identify the full-length GFP-CDKL5 protein; arrows show specific truncated mutant of GFP-CDKL5. A', B', C' show the nucleotide context of the different PTCs (blue) together with the best nucleotide context for read-through (red) [91] [92]
–: untreated cells; +: treated cells with 2000 μg/ml of G418 or gentamicin (Gent.)

3.5 Aminoglycosides differentially suppress *CDKL5* PTCs

It is well known that the efficiency of aminoglycoside-derived read-through is dependent on the stop codon type. We thus proceeded trying to establish the efficiency of gentamicin and G418 to suppress the PTCs of the already described *CDKL5* mutants. In particular, we focused on R59X, R134X and R550X mutants that in previous WBs (Figs. 8 and 9) had demonstrated a good recovery of the full-length protein.

To this purpose, we used IF experiments with the aim of exploiting an anti-CDKL5 antibody that by recognizing a C-terminal epitope permits to detect only full-length CDKL5 derivatives. Indeed, in the absence of aminoglycosides only cells transfected with the WT construct permitted to detect the CDKL5 signal (Fig. 10A, a'; red cells) while, as expected, cells transfected with the truncated derivatives did not show any red signal (Fig. 10A, b', c', d').

Importantly, a (presumably) full-length CDKL5 could be identified after G418 treatment (Fig. 10A, f', g', h'; red cells). By comparing the subcellular distribution of the read-through red products with respect to the WT protein, it appears that rescued molecules well phenocopy CDKL5. On the contrary by comparing red and green signals, we found that the two signals do not coincide, possibly because most of GFP signal is given by truncated derivatives. Furthermore, the strong variability in subcellular distribution of WT CDKL5 transfected in HEK293T cells together with the intrinsic features of such cells (i.e. huge nucleus and little cytoplasm) did not allow us to well compare by IF the subcellular distribution of the diverse mutants with respect to WT CDKL5.

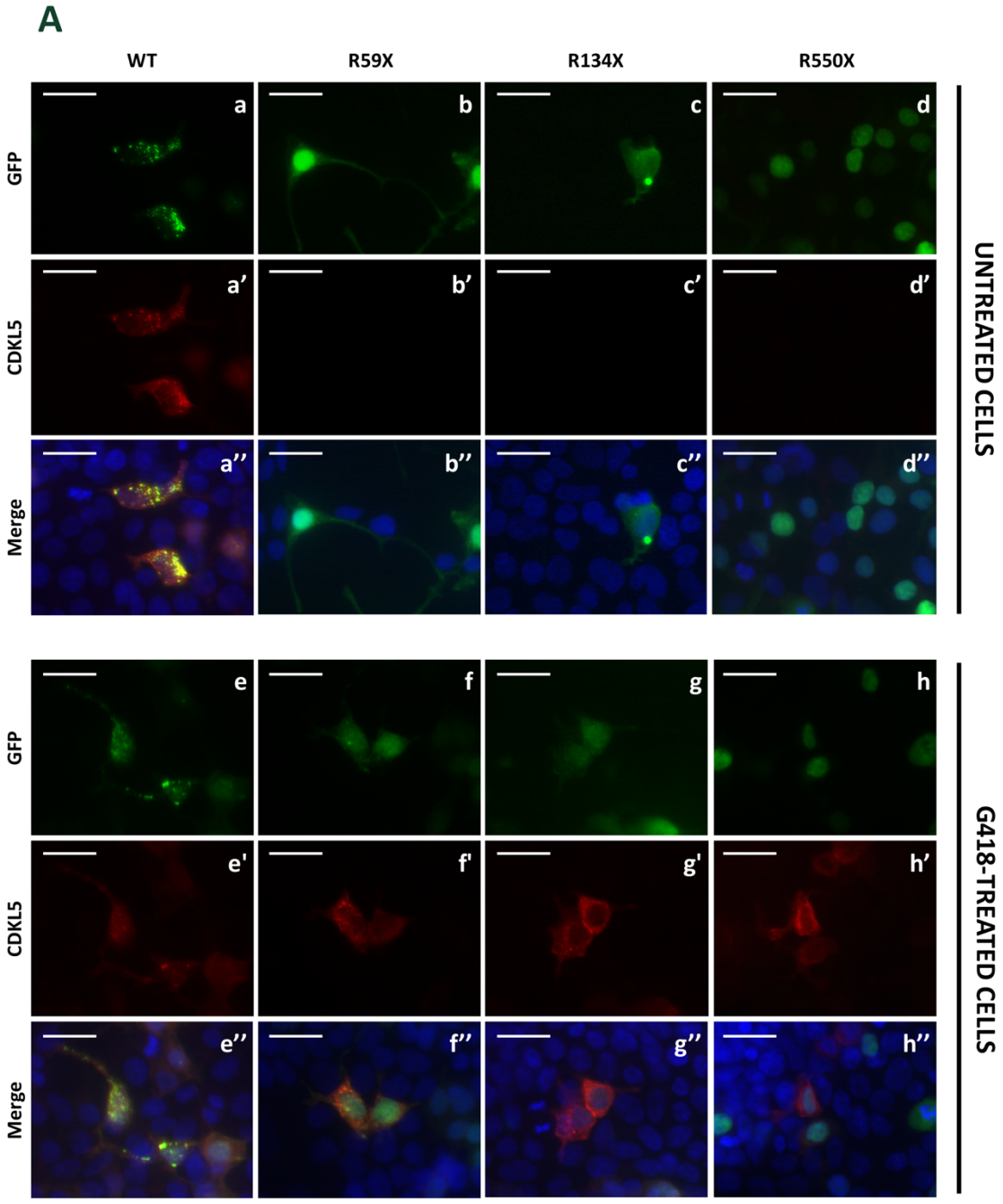
A
WT
R59X
R134X
R550X
GFP
CDKL5
Merge
a
b
c
d
a'
b'
c'
d'
a''
b''
c''
d''
UNTREATED CELLS
e
f
g
h
e'
f'
g'
h'
e''
f''
g''
h''
G418-TREATED CELLS

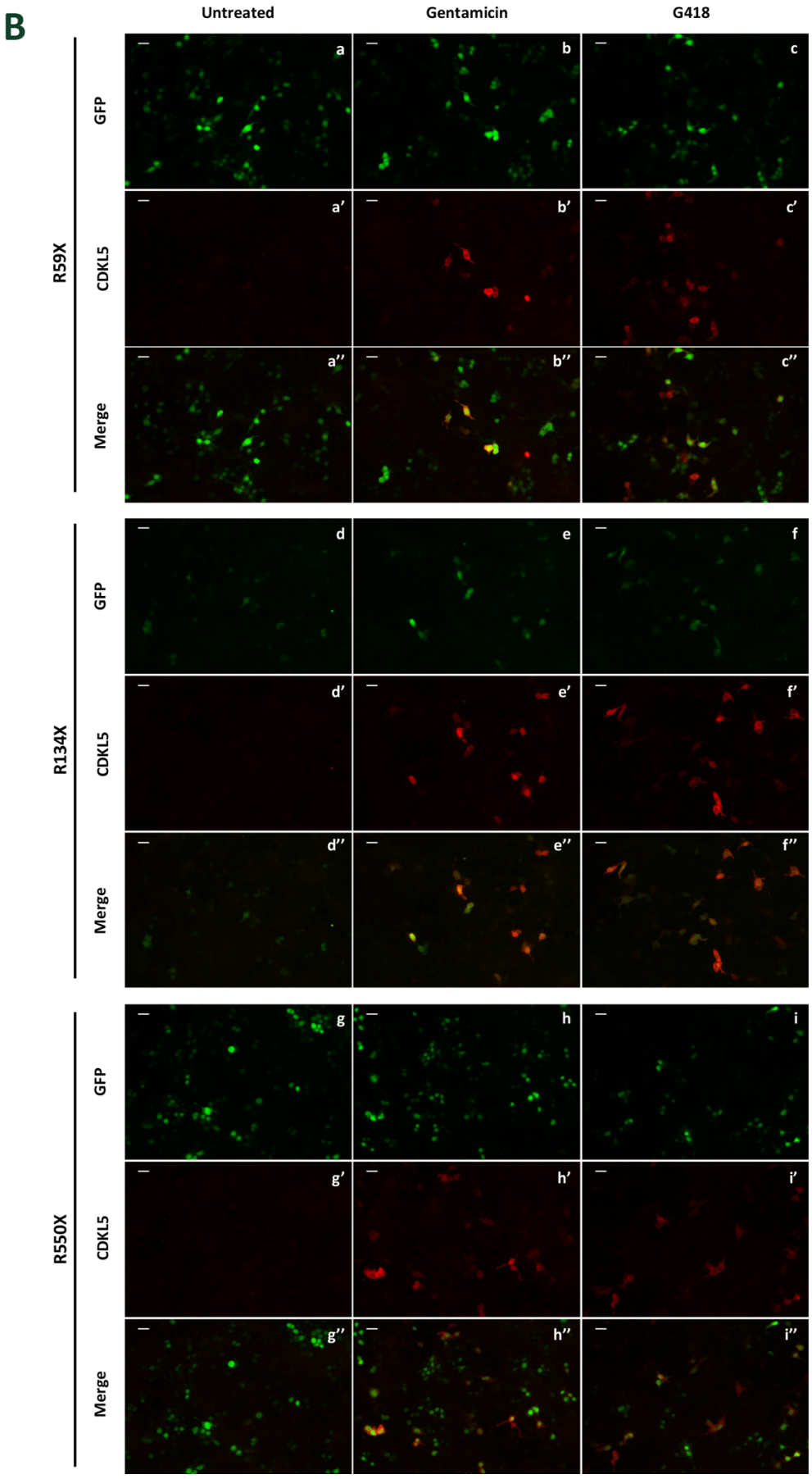
B
Untreated
Gentamicin
G418
R59X
R134X
R550X
GFP
CDKL5
Merge
a
b
c
a'
b'
c'
a''
b''
c''
d
e
f
d'
e'
f'
d''
e''
f''
g
h
i
g'
h'
i'
g''
h''
i''

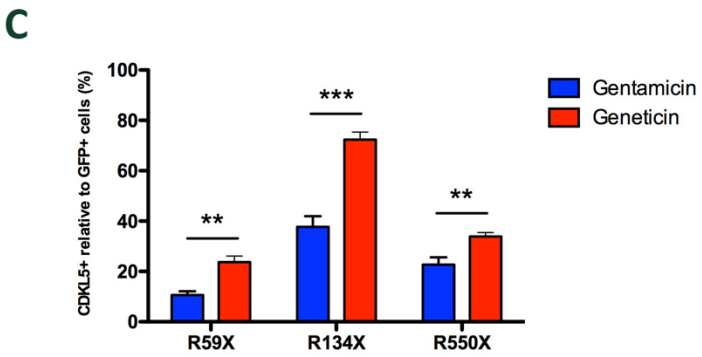

Figure 10. Aminoglycoside read-through efficiency varies according to the specific R-X mutant.

A, B) IF analyses of HEK293T cells transfected with WT, R59X, R134X or R550X mutants and treated with 2000 µg/ml of G418 (A, B) or gentamicin (B) for 24hrs. In untreated cells, GFP signal allows to identify only WT or truncated proteins. To evaluate GFP-R134X signal the brightness was strongly increased. CDKL5 signal is specific for full-length proteins (WT or read-through products; antibody epitope: a.a. 636-758). In A, merge panels result from overlapping of GFP (green), CDKL5 (red) and DAPI (blue); in B from GFP (green), CDKL5 (red). Magnification 40x (A) or 20x (B), scale bar 30 µm. n=3

C) Graphical representation of gentamicin (blue) and G418 (red) read-though efficiency. The percentage of read-through was determined by counting full-length CDKL5 positive cells over GFP positive cells. The error was expressed as SEM; the significance was evaluated by Student's t test (* $p < 0.05$, ** $p < 0.01$, *** $p < 0.001$); n=3

However, by overlapping GFP-R-X (green) and full-length CDKL5 signals after treatments (red; Fig. 10B, b'', c'', e'', f'', h'', i''), it emerged that not all transfected cells generate detectable full-length CDKL5 derivatives and such result depends on the specific mutation and read-through drug. In fact, by quantifying the results, calculating the percentage of read-through CDKL5 positive cells (red) over transfected cells expressing the truncated derivatives (green), we found that G418 more strongly induces read-through of selected PTC sites (Fig. 10C). In particular, the suppression of R134X stop codon appeared particularly efficient (>75%), followed by R550X (>35%) and R59X (>25%).

By observing the IF results of R550X and R59X mutants, we can state that some cells were more susceptible to treatment, while others did not respond at all or produced a too little amount of full-length protein to be detected above background.

Concerning the R134X mutant we have observed that its transfection leads to very few cells weakly expressing it (in Fig.10B compare panel d with panels a and g), its frequent accumulation in perinuclear aggregates (Fig. 10A, c) and a low signal in WB presenting several degradation products (see WB in Figs 6B, 7B, 8A', 8B', 11A', 11B', 13A). Moreover, cells co-transfected with R134X and GFP expressed the truncated construct at

a low level in spite of equal expression of GFP (data not shown) therefore demonstrating that this phenotype is not caused by transfection deficiency and/or cell lethality. We hypothesize that the herein observed highly efficient read-through might simply reflect a stabilization of the full-length CDKL5.

3.6 PTC124 and GJ072 are not able to induce read-through of selected *CDKL5* premature stops

The results described above demonstrate that in our experimental conditions we can observe an effective read-though of *CDKL5* PTCs at high aminoglycoside doses, known to be toxic [81].

This consideration led us to test the efficacy of alternative compounds and, in particular, of non-aminoglycosides. We have verified whether different doses and incubation times of PTC124 or GJ072 may promote the read-through of *CDKL5* R59X or R134X mutants.

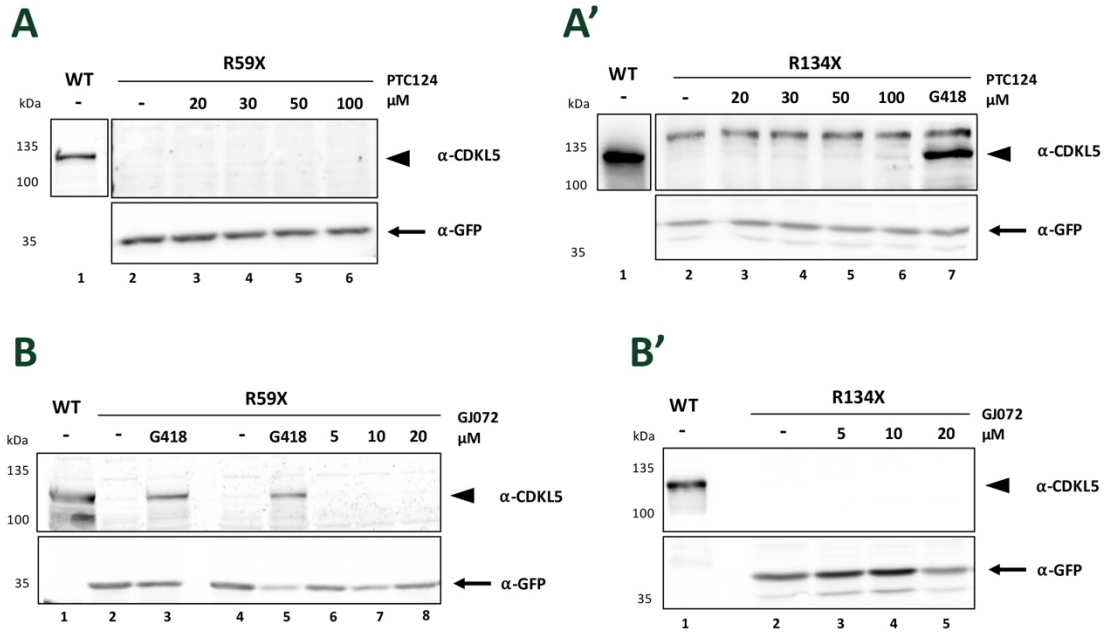

Figure 11. PTC124 and Gj072 do not induce read-through.
WB (8% SDS-PAGE) analyses of protein lysates from HEK293T cells transfected with R59X (A, B) and R134X (A', B') truncated derivatives and treated with PTC124 (A, A') or GJ072 (B, B') for 24hrs; increasing drug doses were used as indicated in the figure. Cells were collected in Sample buffer and the same number of cells transfected with the truncated constructs or half of this number from cells transfected

with the WT construct were analysed. Immunoreactivity was detected using anti-GFP for R59X and R134X truncated proteins or anti-CDKL5 for WT and full-length read-through derivatives. n=3
Arrowheads indicate the full-length GFP-CDKL5 protein; arrows identify each specific mutant form of CDKL5.
–: untreated cells (DMSO at the maximal dose used with the highest drug concentration); G418: treatment with 2000 μg/ml of G418.

As shown in Fig. 11A, A', PTC124 at any dose (lanes 3 to 6) was not able to give rise to full-length GFP-CDKL5, while a full-length product was detectable after G418 treatment (Fig. 11A', lane 7); the same result was obtained administering GJ072 (Fig. 11B, lanes 6 to 8; Fig. 11B' lanes 3 to 5). These results were obtained either after 24 hours (Fig. 11) or 48 hours (not shown) of treatment. Moreover, in GJ072 experiments a higher dose of 30 μM was used, but cell toxicity became evident after 24 hours (data not shown).
These experiments demonstrate that, at least in our experimental conditions, PTC124 and GJ072 show no efficacy for *CDKL5* PTC suppression, therefore supporting previous published data questioning PTC124 capability to facilitate read-through [141] [140, 157] [146]. In future studies, we will certainly test whether cell lines can affect the sensitivity to specific read-through drugs.

3.7 CDKL5 subcellular localisation can be rescued after read-through

As already stated, the generation of a full-length product after read-through does not guarantee a proper functionality of rescued proteins. Thus, to investigate whether read-through GFP-CDKL5 proteins well mimic the WT protein, we started analysing the subcellular distribution of read-through products.
Nucleo-cytoplasmic localisation was analysed by WB of fractionated extracts derived from transfected and G418-treated HEK293T cells.
As shown in Fig. 12, the read-through products can rescue an appropriate subcellular distribution but this capability seems to depend on the specific nonsense mutation. Indeed, the ratio between nuclear and cytoplasmic fraction relative to WT CDKL5 (arbitrarily set to 100%) revealed that full-length proteins derived from the suppression of R59X and R134X PTCs showed a recover of the phenotype. Importantly, R59X and R134X truncated proteins display an altered subcellular distribution both in the absence (truncated -) or in the presence (truncated +) of G418 confirming, as expected, an

enrichment in the cytoplasmic fraction. On the contrary, the read-through of C-terminal PTCs did not restore a correct nuclear-cytoplasmic distribution. Indeed, Q347X full-length derivative maintained a significantly different sub-cellular distribution compared to the WT although the cytoplasmic enrichment is reduced respect to the truncated Q347X protein. Vice versa, the subcellular distribution of the R550X truncated protein was comparable to WT, while the product of its read-through got significantly different.

All in all, these results indicate that after read-through a rescue of a proper subcellular distribution is possible but, as expected, the position of PTC could be critical. In particular, the introduction of a missense mutation in the C-terminal tail of CDKL5 may hinder a proper localisation of CDKL5.

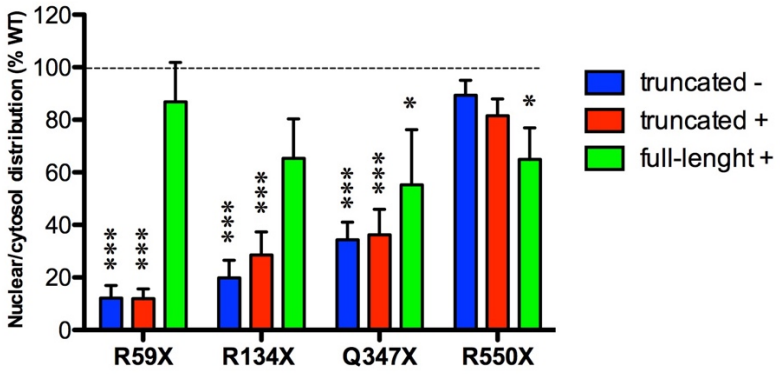

Figure 12. Read-through derivatives can have a proper nucleo-cytoplasmic distribution.
Graphical representation of the subcellular distribution (nucleus/cytoplasm) of truncated and read-through derivatives compared to WT. Nucleo-cytoplasmic distribution of WT was arbitrarily set to 100% (dotted line) and nucleo-cytoplasmic distribution of truncated derivatives was expressed as values relative to WT. The error was expressed as SEM; the significance was evaluated by one-way ANOVA followed by Bonferroni's post hoc test (* $p < 0.05$, ** $p < 0.01$, *** $p < 0.001$); $n \geq 3$

3.8 Read-through derivatives are impaired in their catalytic activity

We proceeded by testing to what extent read-through full-length CDKL5 proteins have rescued their proper catalytic activity.

As already mentioned the catalytic domain of CDKL5 resides in the protein N-terminus, while C-terminal tail has been reported to negatively regulate the kinase activity [55]. Indeed, C-terminal truncated proteins display a higher catalytic activity than full-length CDKL5 [55] [54], possibly suggesting that kinase activity of CDKL5 should be finely regulated.

For these reasons, we have considered necessary to establish whether full-length CDKL5 derivatives may recover an appropriate kinase activity by evaluating the TEY motif auto-phosphorylation. As other members of the CMGC family, the dual TEY motif phosphorylation at threonine and tyrosine residues is necessary for maximal activation [158] [55] [54]. Accordingly, no TEY auto-phosphorylation can be observed in the "kinase-dead" CDKL5 K42R mutant, a construct carrying a missense mutation in the ATP binding site that impairs the capability to bind ATP and transfer the phosphoryl group to the substrate [55] [54].

TEY phosphorylation level of each read-through mutant was thus assessed by dividing the signal obtained using an anti-phospho-ERK1/2 (Thr 202/Tyr 204) to total CDKL5 and comparing such ratio to the one of WT samples arbitrarily set to 100.

As shown in Fig. 13 A, A', a discrete auto-phosphorylation signal can be detected, suggesting that full-length derivatives derived from the read-through process own some catalytic activity (upper panel, lanes 4-6-8); however, they are clearly hypomorphic (Fig. 13A'). It is worth noting that the evaluation of TEY phosphorylation in R59X and R134X truncated protein cannot be possible since such motif is located downstream the PTCs (a.a. 169-171); further, for these mutants we could not exploit the CDKL5 antibody (recognising a.a. ~370-520) for normalization. On the contrary, preliminary experiments indicated that R550X kinase activity seems to be similar to WT (data not shown).

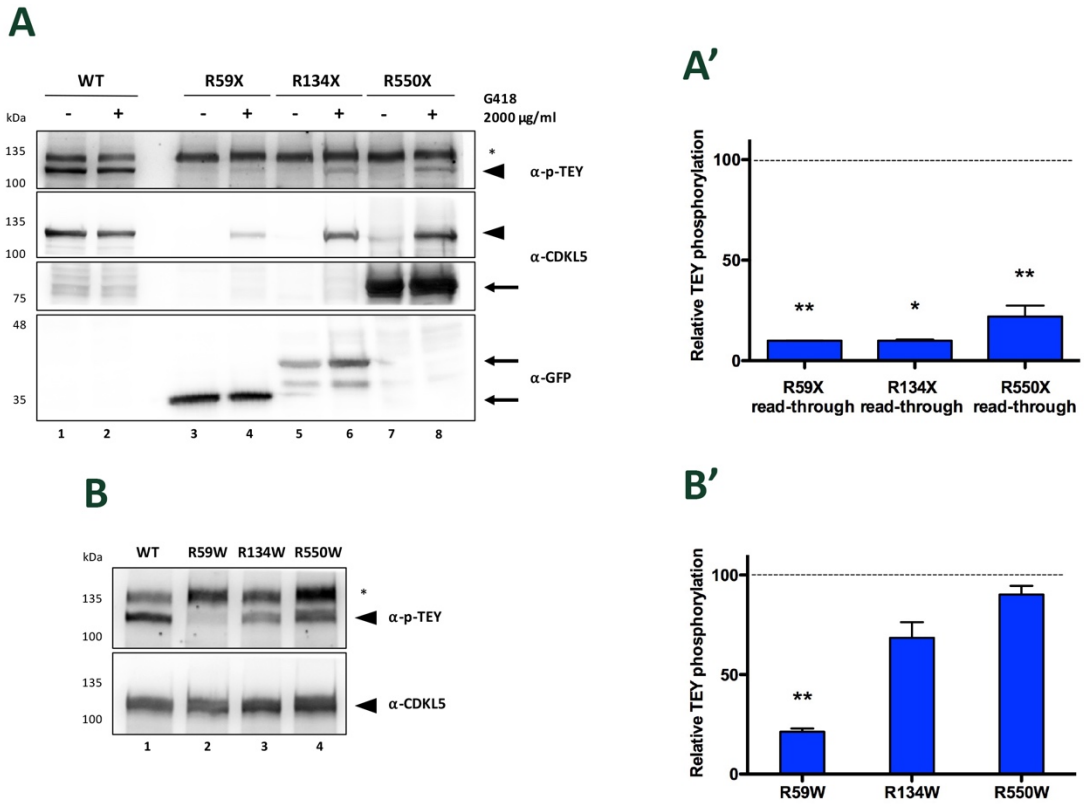

Figure 13. Read-through proteins appear to have an hypomorphic catalytic activity.

A, B) WB (8% SDS-PAGE) assays evaluating the auto-phosphorylation of the TEY motif through an anti-phospho-ERK antibody (upper panel, arrowhead; * indicates an aspecific product). HEK293T cells were transfected with WT, R59X, R134X or R550X constructs and treated with G418 (2000 µg/ml) for 24hrs (A) or WT, R59W, R134W or R550W constructs (B). Full-length CDKL5 and R550X truncated proteins were detected using an anti-CDKL5 antibody, the remaining truncated proteins with anti-GFP antibody.
Arrowheads identify the full-length GFP-CDKL5 protein; arrows show specific truncated mutant of GFP-CDKL5.
–: untreated cells; +: treated cells with 2000 µg/ml of G418

A', B') Graphic representation of the mean relative phosphorylation normalised to CDKL5 signal of different experiments. TEY phosphorylation of WT was arbitrarily set to 100 (dotted line) and TEY auto-phosphorylation of read-through products was expressed as values relative to WT. The error was expressed as SEM; the significance was evaluated by Student's t test (* $p < 0.05$, ** $p < 0.01$, *** $p < 0.001$); n=3

To understand whether the possible amino acid substitution at PTC sites can be responsible for the observed reduced catalytic activity, we analysed the auto-phosphorylation signal of W-containing mutants. As shown in Fig. 13B, B', only R59W protein has revealed a significant lower auto-phosphorylation activity, while R134W and R550W derivatives were comparable to WT.

These results suggested that read-through products can be catalytically active and that, in accordance with our hypothesis, the position of PTCs and the type of amino acid inserted

can influence the extent of their activity. Accordingly, analysing dbSNP database no missense variant can be found at 59, 134 positions, possibly suggesting that the complete recovery of kinase activity may be obtained only if arginine will be introduced at analysed PTC sites. On the other hand, a possibly non-pathogenic missense variant introducing a glutamine at 550 position can be found (rs745508309) indicating that amino acid substitutions are probably tolerated at this site.

3.9 Read-through full-length derivatives can rescue the impaired neuronal branching in transfected *Cdkl5*-null neurons

To understand whether the generated read-through protein may be sufficient to rescue the pathological phenotype associated with CDKL5 deficiency, we tested G418 in transfected *Cdkl5*-null neurons.

We started evaluating cell viability of cortical neurons after G418 treatment through MTT assay. As shown in Fig.14A, the MTT reduction normalised to controls has revealed that about 90% of neurons are viable after G418 treatment at different doses. Considering that in HEK cells a good level of full-length CDKL5 was detected at 500 μg/ml dose (Fig. 8), we started these preliminary studies by testing such concentration in transfected *Cdkl5*-null neurons.

Cdkl5 depletion is associated with reduced dendritic arborisation [58] [73] [70]; we thus decided to analyse whether read-through of a PTC mutant could rescue a proper neuronal branching in *Cdkl5*-null neurons.

To this purpose, cortical neurons from E15 *Cdkl5*$^{Y/-}$ mouse embryos were prepared and transfected at DIV12 with WT GFP-CDKL5 or GFP-CDKL5 R134X. The mutant was chosen for its strong susceptibility to read-through. 24 hours later, neurons were treated with G418 and fixed at DIV14, when functional synapses can be found [50]. Using anti-CDKL5 antibodies recognising C-terminal regions of the kinase (Sigma: a.a. 636-758 or Santa Cruz: a.a. ~370-520), no specific CDKL5 signal could be detected above the background by IF. However, such observation does not exclude the generation of small amounts of the full-length kinase; in fact, exploiting *Cdkl5*-null brains, we have already demonstrated that by IF no CDKL5 antibody is able to distinguish the protein above the

background when the kinase is present (as testified by western blot) but very low in abundance.

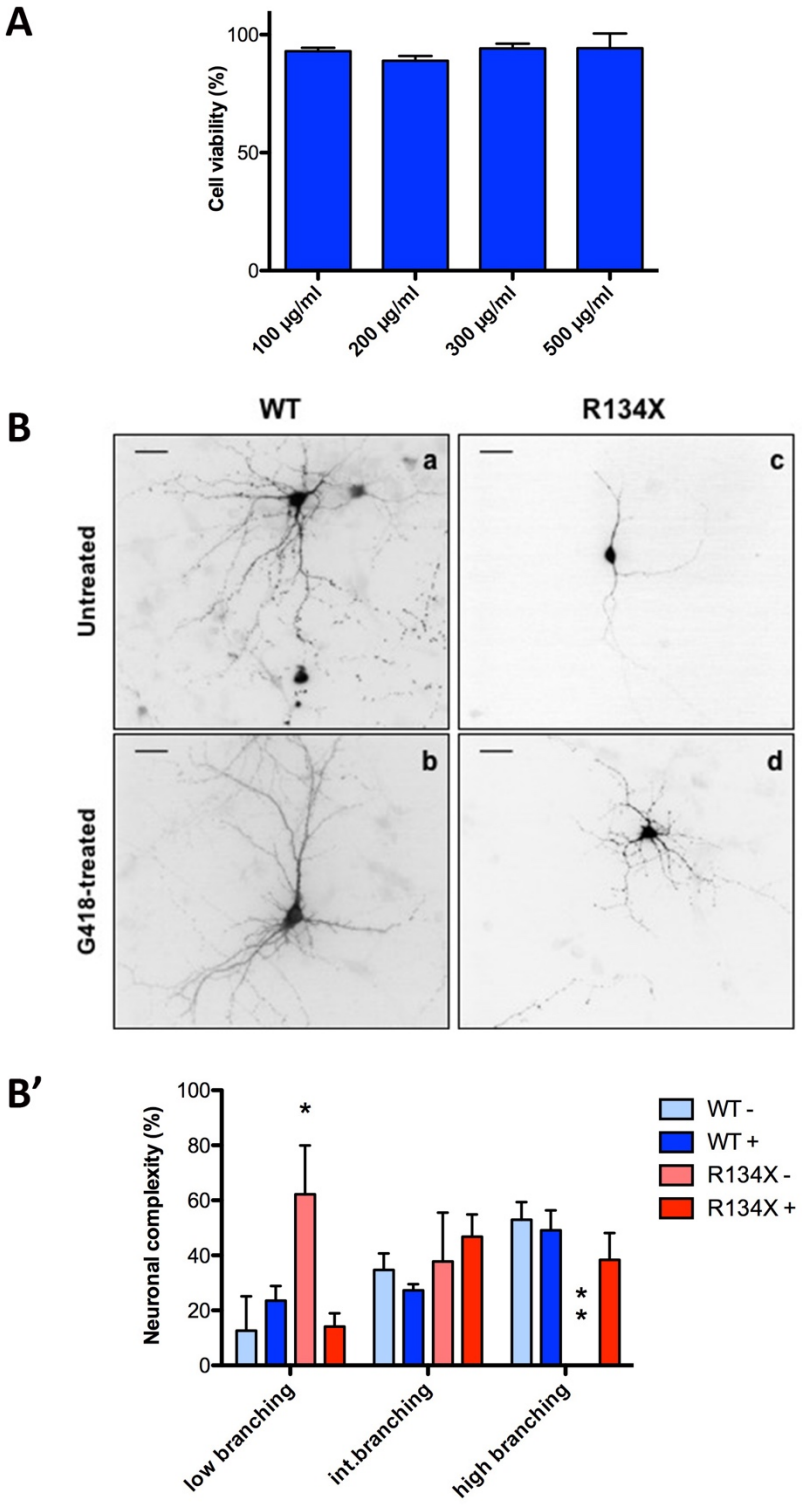

Figure 14. Neuronal defects can be rescued after G418 treatment.

A) MTT assay assessing viability of neurons treated with indicated doses of G418 for 24hrs. Absorbance of treated samples was normalized dividing by values obtained from control neurons. n=2

B) Representative images from DIV14 cortical neurons transfected with WT GFP-CDKL5 (a, b) or GFP-CDKL5 R134X (c, d) constructs and treated with 500 μg/ml G418 for 24hrs. Magnification 40x, scale bar 30 μm. n=2

B') Graphical representation of neuronal branching evaluation in transfected and treated neurons (B). The error was expressed as SEM; the significance was evaluated by two-way ANOVA followed by Bonferroni's post hoc test (* $p < 0.05$, ** $p < 0.01$, *** $p < 0.001$); n=2

The possibility that some read-through CDKL5 is present appears to be supported by a phenotype amelioration in neurons transfected with R134X construct and treated with G418 (Fig. 14B). Indeed, by counting neurons with low, intermediate or high number of branches, we can observe that the expression of WT GFP-CDKL5 seems to promote neuronal branching of otherwise null neurons (Fig. 14B, a-b, and B'). On the contrary, neurons expressing the R134X derivative reveal the presence of a reduced and shorter number of neurites (Fig. 14B, c, and B'). On the other hand, treatment with G418 clearly ameliorated the branching defects determining an increase of neurons with more and longer neurites (Fig. 14B, d, and B').

These results suggest that few amounts of full-length, possibly hypomorphic, CDKL5 could ameliorate neuronal impairment given by the absence of the kinase.

Nevertheless, we are aware that to confirm our results we have to test aminoglycosides on different PTC-containing constructs and to more deeply analyse their impact on neuronal morphology. Moreover, to better evaluate the read-through efficiency in neurons we will generate constructs codifying for a C-terminal RFP.

4. DISCUSSION

Mutations in *CDKL5*, a complex gene located on Xp22, have been associated with different neurological disorders including the *early seizure variant* of RTT syndrome [32], also known as the Hanefeld variant [29].

CDKL5 is an ubiquitously expressed serine/threonine kinase localised both in the nucleus and cytoplasm of neurons and proliferating cells [54] [52] [57]. Different functions have been associated with the kinase according to its subcellular compartment. In the nucleus, CDKL5 seems to regulate gene expression through the interaction with DNMT1 [61] and MeCP2 [60]. In the cytoplasm, CDKL5 has a role in neural polarisation via the interaction with shootin1 [63], in the regulation of cytoskeleton dynamics by association with Rac1 [51] and IQGAP1 [67], in spine development and synaptic stability by NGL1 phosphorylation and association with PSD95 [58]. Moreover, we have recently demonstrated that in proliferating cells CDKL5 affects cell division via the phosphorylation of H2B mediated by HIPK2 [79].

The generation of different *Cdkl5*-null mouse models has permitted to better understand CDKL5 functions [64] [65] [66]. However, although epileptic encephalopathy is considered the prominent clinical feature of *CDKL5*-related pathologies, none of these models has shown spontaneous seizures and all are characterized by moderate phenotypes.

Although different studies have been published in recent years, CDKL5 roles have not been completely elucidated yet. For this reason, no cure exists for *CDKL5* patients and current treatments are only intended to ameliorate secondary symptoms, in particular epilepsy.

In the brain, CDKL5 expression is finely regulated during development, getting strongly induced in early postnatal day (P14) while low levels can be found during embryogenesis [52]. Moreover, the kinase expression is modulated in response to stimuli. In fact, sustained glutamate stimulation of mature neurons determines a massive proteasome-dependent degradation of CDKL5 that occurs through extrasynaptic NMDA receptors [57]. In addition, neuronal activation quickly induces CDKL5 expression; the increased levels are obtained through two main molecular mechanisms: an increase in gene transcription and the activation of localised protein synthesis in dendritic fractions. Importantly, neuronal maturation influences the extent of this activation. Indeed, while in

immature neurons CDKL5 levels remain up-regulated for about 1 hour after KCl stimulation, neuronal maturation determines a proteasomal-dependent demolition of the kinase and, consequently, the decline to basal levels within few minutes [50]. These observations indicate that CDKL5 levels have to be strictly modulated and that both gain or loss of functions may alter brain development. Accordingly, patients carrying *CDKL5* duplications have been reported [38]. This evidence leads some concern about the possibility to use gene- and protein-augmentative therapies for the treatment of *CDKL5* patients; in fact, both these approaches will not reproduce the subtle regulation of the kinase expression. In addition, the large dimension of *CDKL5* gene, the absence of information about regions involved in mRNA localisation in dendrites and spines and the activation of protein synthesis by neuronal depolarization limit the design of the best vector.

We thus reasoned that some *CDKL5* patients might benefit from therapeutic approaches, tailored in function of the specific genetic lesion.

In particular, PTC suppression might be a valid therapeutic approach for *CDKL5* patients carrying a nonsense mutation, accounting for about 15% of all cases described so far. Several chemical compounds have been discovered or specifically designed to induce read-through and some of them (i.e. aminoglycosides and PTC124) revealed a sufficient efficacy to be used in clinical trials; this seems to be particularly promising for nonsense *CDKL5* patients although the capability of these drugs to cross the BBB is still under discussion. BBB permeation is favoured by different factors including lipophilicity and reduced molecular dimension of compounds. On the contrary, aminoglycosides are hydrophilic molecules with a molecular mass of about 400 Da whose penetration in cerebrospinal fluid is low in the absence of meningeal inflammation [159]. However, the ability to improve neurological defects by administering two designer aminoglycosides promoting read-through, NB54 and NB84, in a nonsense MPS I-H mouse model suggests that these drugs could be able to reach brain tissues [156] [123]. Of note, aminoglycosides are principally endocytosed in cells via the megalin receptor whose expression has been found in different neural cells including astrocytes, oligodendrocytes and neurons [160] indicating that such drugs can be uptaken by different cell types in CNS.

In this study, we tried to understand whether nonsense mutations causing the onset of *CDKL5*-related encephalopathy can be suppressed using read-through compounds and whether the obtained full-length derivatives exhibit molecular and cellular features

largely overlapping with the WT protein. In particular, with these analyses we wanted to comprehend i) the efficacy of read-through on different *CDKL5* nonsense mutations; ii) whether read-through products have the capability to rescue some features of the kinase and iii) whether the possible rescue of the phenotype may depend on PTC localisation. Considering the distribution of pathogenic missense mutations, we hypothesized that the suppression of PTCs located in the catalytic domain would have lower capability to recover the kinase properties (catalytic activity and possibly subcellular distribution), while the read-through of C-terminal PTCs could generate full-length proteins maintaining most of the biochemical and cellular properties of the WT protein. Indeed, while several missense mutations within the catalytic domain determine a clinical condition, very few if any missense pathogenic mutations have been identified in the C-terminal region of CDKL5.

Finally, we wanted to identify the most effective drug, verify the possibility of enhancing read-through using non-toxic molecules, and, eventually, evaluate whether the read-through of nonsense derivatives of CDKL5 exogenously expressed in mouse *Cdkl5*-null neurons would allow the rescue of some typical phenotypes [73] [70].

To verify our hypothesises and obtain a first indication of the feasibility of our studies, we have compared the subcellular distribution of WT protein with truncated and full-length derivatives characterized by a tryptophan residue at the PTC site; such amino acid was chosen because it was found to be frequently inserted at UGA non-sense sites after read-through [87].

As already mentioned, in proliferating cells WT CDKL5 can be found both in the nucleus and the cytoplasm, while different types of mutations can alter its shuttling capability between the two compartments [54] [52]. Our analyses indicate that some truncated proteins have an altered subcellular distribution (Fig. 7). Conversely, the nucleo-cytoplasmic distribution of W-containing proteins was comparable to the WT, suggesting that the recovery of WT protein features is possible after read-though (Fig. 6). These preliminary results have encouraged us to test read-through drugs and to understand whether the generated full-length proteins can be functional.

Transient transfection experiments have permitted to ascertain that aminoglycoside drugs can induce full-length protein generation in a dose-dependent manner (Fig. 8), as previously observed in several studies [89] [161] [90] [162]. Read-through was evident only at high doses of aminoglycosides (Fig. 8) and obtained results suggest that PTC

position can be critical for read-through. In particular, we speculate that the proximity of a PTC to the poly-(A) tail might facilitate the association between eRF3 and the poly-(A) binding proteins, thus reinforcing translation termination and hindering the read-through process (Fig. 9) [82].

Several studies have indicated that the type of stop codon can be critical for read-through and UGA stop site was identified as the most responsive to PTC suppression [88] [89] [90] [91]. Our results have shown that G418 is able to facilitate the read-through of different PTC types at high doses (Fig. 9) and a higher efficiency at UGA stop codon has been confirmed. In fact, although WB analyses allowed us to identify the suppression of different types of PTCs (Fig. 9), the signal of full-length CDKL5 can be detectable by IF only in cells transfected with UGA constructs (Fig. 10). On the contrary, the aminoglycoside treatment of cells expressing Q347X (UAG) or E364X (UAA) constructs did not permit the evaluation of full-length derivatives in IF assays. These observations may suggest that cells transfected with Q347X or E364X constructs produced such a little amount of full-length CDKL5 that could not be detected above the background.

In addition, the percentage of cells generating full-length CDKL5 over transfected cells indicates that G418 is more effective than gentamicin [163] [89] [90] [91] and it determines a particularly efficient PTC suppression in our conditions that could vary from almost 25% to 75% of transfected cells. The higher percentage of read-through (~75%) was found in cells transfected with the R134X derivative and treated with G418. However, our transfection experiments performed both in cell lines and in neurons demonstrate a lower expression of this mutant with respect to the WT or other PTC-containing constructs. Currently, we are investigating whether this phenotype might be caused by an instable mRNA and/or the activation of NMD. If this would be the case, we hypothesize that translation might stabilize the transcript therefore leading to a more robust read-through. Interestingly, the description of the clinical features of an R134X patient evidences a phenotype similar to other *CDKL5* patients, although very severe. In fact, seizures started already in the second month of life and are refractory to any medication [164].

IF analyses permitted to deduce that cells do not uniformly respond to aminoglycoside treatment; indeed, some cells seem to not be able to respond or to very less extent than others (Fig. 10). To the best of our knowledge, no one has ever addressed whether the cell cycle may influence the read-through efficiency. Considering that cells were not synchronised, we speculate that cells visibly responding to aminoglycoside treatment

might be in a phase immediately before the cell division, when protein synthesis is particularly increased. In the future, it would be interesting to understand whether the different phases of cell cycle may influence the read-through efficiency by starving cells transfected with a destabilised GFP. Considering that neurons have a high rate of protein synthesis, it might be relevant to discover that read-through efficacy depends on the rate of protein translation.

In addition, by measuring the fluorescence of the full-length CDKL5 signal from each cell, we identified a trend where fluorescence intensity is higher in cells treated with gentamicin with respect to G418 (data not shown). This observation may suggest that G418 is able to induce read-through in a larger number of cells, while gentamicin determines the generation of higher amount of full-length protein but in few cells.

Despite the significant efficiency in read-through facilitation, several studies have evidenced a high toxicity associated with the administration of aminoglycoside drugs [111] [112] [113]. We have thus tried to understand whether the read-though could be induced by alternative compounds, in particular by two non-aminoglycoside drugs, GJ072 and PTC124. WB analyses of lysates from transfected and treated cells have shown that these drugs are not able to facilitate read-through in our experimental conditions (Fig. 11).

Nevertheless, the inefficacy of PTC124 treatment was not entirely unexpected. Indeed, although different reports have indicated its capability to induce PTC suppression [127] [128] [129] [130] [131] [132] [133], several preclinical studies have not been able to detect read-through products after PTC124 administration [140] [141] [142] [143], [144] [145] [146] [147]. However, considering that GJ072 read-through activity was found in an *in vitro* assay and in A-T lymphoblastoid cell-lines from patients carrying *ATM* nonsense mutations, we are going to use different cell types and experimental settings to evaluate whether drug inefficacy might be due to our experimental setup.

Given the negative results obtained with non-aminoglycoside drugs treatments, we tried to comprehend whether it was possible to reduce the minimum effective dose of G418 using the CDX5-1 molecule, a powerful read-through enhancer [118]. Our results indicated a slight increase of full-length protein only with high doses of G418 in transfected HEK293T cells. HEK293T is an excellent cell line to be used for transfection experiments but we are aware that the drug efficiency might be influenced by the cell type. We will thus test CDX5-1 in different cell lines; furthermore, considering that

CDKL5 alterations are primarily causative of neurological disorders, in the future we want to thoroughly investigate read-through, including CDX5-1 sensitivity, in neurons.

To understand whether CDKL5 read-through products are functional we compared some of their molecular and cellular features to those of the WT protein. From IF analyses (Fig. 10) and fractionation experiments (Fig. 12), it appeared that read-through induced the production of full-length proteins whose subcellular localisation well overlapped with the WT. On the contrary, truncated proteins displayed an altered subcellular localisation even in presence of the read-through drug. Nevertheless, the R550X and Q347X full-length derivatives were unable to reach a proper nucleo-cytoplasmic distribution. These results suggest that the PTC position can be relevant for the correct localisation of the full-length protein and, in contrast with our initial hypothesis, they indicate that read-through of PTCs contained in the catalytic domain might be feasible.
However, the dbSNP database analysis allowed us to identify a non-conservative (R/Q) missense mutation at 550 position which is not associated with a clinical condition; we cannot thus exclude that variations may be tolerated. On the contrary, no polymorphisms or missense mutations can be found at 59, 134 or 347 positions in the dbSNP database.
By deleting the C-terminal of CDKL5, Mari *et al.* [60] have identified that the region containing amino acids 450-550 is necessary for the association with MeCP2, while amino acids 551-650 reinforce such interaction. It would be thus interesting to understand whether the suppression of truncated mutants will generate full-length proteins with a restored full capability to interact with the methyl-binding protein.

Verifying whether read-through products are catalytically active is also crucial for understanding their functionality.
In the activation loop of CDKL5 is located a TEY motif whose intermolecular auto-phosphorylation is suggested to be indicative of the enzymatic activity of CDKL5 [54] [55]. By analysing the TEY motif auto-phosphorylation emerged that full-length read-through derivatives only partially recovered the catalytic activity and might, therefore, be hypomorphic (Fig. 13); a hypothesis that however remains to be demonstrated. Nevertheless, the results from the W-containing full-length CDKL5 derivatives revealed that only the amino acid substitution at 59 position is particularly critical for the TEY phosphorylation, while R134W and R550W mutants showed a phosphorylation level similar to the WT (Fig. 13). These results, as hypothesized, indicate that an amino acid

substitution can interfere with the catalytic activity and the type of amino acid and the position of PTC can be crucial. Since at premature UGA stop codons, tryptophan, cysteine or arginine are preferably inserted [83] [84] [85] [86] [87], in the future it would be interesting to test the consequences on the catalytic activity of having a cysteine as missense mutation.

On the other hand, considering that ribosomal toeprinting studies have proposed a protracted ribosomal pausing at PTCs [165] and that the co-translational folding depends on the timing of protein synthesis [166], we can speculate that during read-through the prolonged ribosomal pausing may alter the folding of the nascent polypeptide possibly impairing its catalytic activity and, therefore, justifying the apparently contrasting results obtained comparing the catalytic activity of read-through products and W-substituted CDKL5 derivatives.

CDKL5 depletion causes a decrease of axon and dendrites length [51], defects in dendritic arborisation [73] [70] and neuronal polarisation [63] [67]. Concordantly, by transfecting R134X mutant in cortical *Cdkl5*-null neurons we identified clear neuronal branching defects that were ameliorated by G418 administration (Fig. 14).

Although further studies are necessary to fully understand the PTC suppression efficiency in neurons and which morphological and molecular *CDKL5*-associated alterations can be restored by treatment with read-through drugs, our preliminary data suggest that small amounts of possibly hypomorphic CDKL5 can greatly improve the phenotypes associated with the absence of the kinase. To better understand the read-through efficiency in neurons we are planning to generate PTC containing constructs carrying an in-frame C-terminal RFP and thus to verify whether low doses of read-through drugs are sufficient to obtain full-length CDKL5 proteins and, possibly, rescue typical *Cdkl5*-null neurons. Considering the low efficiency of neuronal transfection, lentiviral particles will be exploited.

In the future, it will be also important to study read-through in a more physiological system. For this reason, we will test aminoglycoside drugs on knock-in neurons obtained from the mouse *Cdkl5*^{R59X} carrying UGA nonsense mutation at arginine 59 (Jackson Laboratory). Complementary, CRISPR/Cas9 directed genome editing will be used to generate knock-in neural stem cells carrying different nonsense sites, including those studied in this dissertation.

Eventually, to verify whether aminoglycoside drugs are able to induce read-through of endogenous *CDKL5* PTCs, we started performing analyses on heterozygous female patients-derived fibroblasts carrying Q347X, E364X and R550X nonsense premature codons. WB analyses revealed that the expression of full-length CDKL5 is similar to healthy control fibroblasts, therefore suggesting the presence of very few cells expressing the mutated allele, rendering thus quite difficult the study of read-through drugs in such fibroblasts.

For future experiments, we believe that male neurons derived from differentiated iPS could be more suitable for testing read-through.

Eventually, the possibility to test read-through on endogenous premature stop codons will allow us to identify whether PTCs stimulate the NMD mechanism. The effectiveness of read-through can, in fact, be strongly affected by the activation of NMD, a surveillance pathway leading to degradation of mRNAs containing PTCs [81]; accordingly, in a previous study *CDKL5* L42X mRNA was reported to be unstable because of NMD activation [37]. Importantly, amlexanox, a drug able to both inhibit NMD and promote read-through, has been identified [167].

In conclusion, the above data suggest that the read-though strategy may be a promising therapeutic approach for *CDKL5* patients carrying nonsense mutations. However, preclinical studies in mouse models are necessary to establish the extent of phenotypic amelioration due to the administration of read-through drugs. Moreover, considering that our results indicate that aminoglycoside might be used at high doses, the identification of molecules capable to enhance their activity will be fundamental.

Finally, as for other neurological diseases, the design of drugs capable to efficiently cross the BBB or effective strategies for drug delivery will be mandatory for the treatment of *CDKL5* patients harbouring a premature stop codon.

5. MATERIAL AND METHODS

5.1 Plasmids and site-directed mutagenesis

pEGFPC1-hCDKL5$_{107}$ plasmid codifies for human CDKL5 weighting 107kDa, fused to EGFP at N-terminal [52]; it is defined as WT in this dissertation. Such plasmid was mutagenised to insert the selected human nonsense sites (175 C>T for R59X, 400 C>T for R134X, 1648 C>T R550X, 2564 C>G for S855X, 1039 C>T for Q347X and 1090 G>T for E364X) or to generate constructs codifying the W-containing proteins at PTCs (175 to 177 CGA>TGG for R59W, 400 to 402 CGA>TGG for R134W, 1648 to 1640 CGA>TGG for R550W, 2564 to 2565 CA>GG). Site-directed mutagenesis was performed through Q5 Site-Directed Mutagenesis Kit (New England Biolabs) following the manufacturer's protocol and using specific primers (Table 4). All PCR-generated constructs were verified by sequencing.

	Forward primers	**Reverse primers**
R59X	AACGACTTTATGAGAGCTTAAAATG	TCTTTGACTTCTTCATTTTCTTC
R134X	TATTGTCCATTGAGATATAAAACCAG	TCATTCTTATGGCACCAG
R550X	AAGAAATAACTGAAATGAGGGAACG	CCAGAAGGGCTGAGCAAAG
S855X	CCGGCTTCCTGAGATCCCCGC	GTGATTTGAGGCCGAAGAGAGATG
Q347X	CAAGGACATCTAGAACCTGAG	CTGTTAGATCTGTGGTGAG
E364X	CCCTGCCAATTAAAGCTTCCTAAATGG	AGACCTTCGTCAGCCCGG
R59W	AACGACTTTATGGGAGCTTAAAATG	TCTTTGACTTCTTCATTTTCTTC
R134W	TATTGTCCATTGGGATATAAAACCAG	TCATTCTTATGGCACCAG
R550W	AAGAAATAACTGGAATGAGGGAACGC	CCAGAAGGGCTGAGCAAAG
S855W	CCGGCTTCCTGGGATCCCCGCT	GTGATTTGAGGCCGAAGAG

Table 4. Primers used in site-directed mutagenesis.
Specific primers have been drawn using NEBaseChanger following the manufacturer's protocol.

5.2 Antibodies

Antibodies used are the following: mouse monoclonal anti-α-tubulin (Sigma-Aldrich, T6074), mouse monoclonal anti-GFP (Roche, 1814460), chicken polyclonal anti-GFP (Invitrogen, A10262), rabbit polyclonal anti-phospho-ERK1/2 (Thr 202/Tyr 204, Santa Cruz, sc-16982), rabbit polyclonal anti-CDKL5 1 isolated from our lab ([54]; a.a. 301-751), rabbit polyclonal anti-CDKL5 2 (Sigma-Aldrich, HPA002847, a.a. 636-758), mouse monoclonal anti-CDKL5 3 (Santa Cruz, sc-376314, a.a. 222-520). Binding sites of GFP, CDKL5 1, 2 and 3 antibodies are shown in Fig. 15.
HRP-conjugated anti-mouse and anti-rabbit secondary antibodies were purchased from Thermo Scientific. DAPI and secondary Alexa anti-mouse 488, anti-chicken 488, and anti-rabbit 568 antibodies were purchased from Life Technologies Corporation.

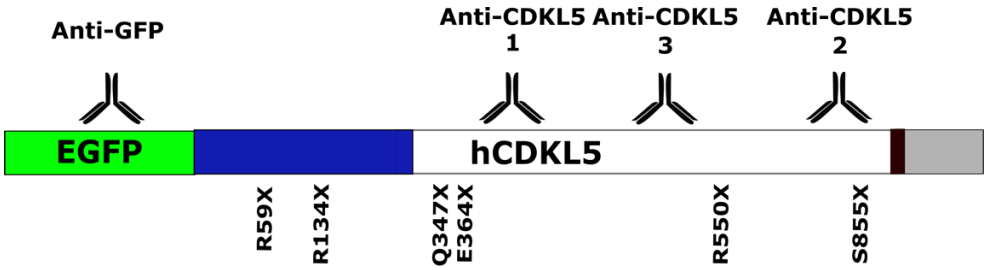

Figure 15. Antibodies binding sites on GFP-CDKL5.
GFP antibody binds the amino-terminus of the expressed hCDKL5 protein; anti-CDKL5 1 recognizes a C-terminal region of the full-length protein (a.a. 301-751); anti-CDKL5 2 binds a more C-terminal epitope (a.a. 636-758); monoclonal anti-CDKL5 3 was raised against a.a. 222-520 and recognises a region between ~ a.a. 370 and a.a. 550. In blue is represented the N-terminal catalytic domain, while in white is shown the C-terminal tail.

5.3 Cell cultures and transfection

HEK293T and HeLa cells were maintained in DMEM (Dulbecco's modified Eagle's medium, Sigma Aldrich) supplemented with 10% FBS (Gibco), 1% L-glutamine (Sigma Aldrich), 1% penicillin/streptomycin (Sigma Aldrich) at 37°C with 5% CO_2 in T75 flasks.

Cells were seeded in 6-, 12- or 24-well dishes and transfected when they have reached the opportune confluence (approximately 70-80%). Both cell lines, were transiently transfected with the constructs using Lipofectamine 2000 (Life Technologies Incorporated, following manufacturer's protocol) or calcium phosphate method. The amount of DNA used for transfection varies according to number of cell seeded and dishes utilised. Cells seeded in 12-well plates were transfected with a total amount of 1.6 μg DNA/well and 4μl Lipofectamine/well or 2 μg DNA/well when calcium phosphate method was used.

5.4 Drug treatments

Eight hrs after transfection, read-through drugs were added in fresh medium without penicillin and streptomycin:

Drug	**Stock solution**	**Working concentrations**
Geneticin (Gibco)	50mg/ml in H_2O	10, 50, 100, 500, 1000, 2000 μg/ml
Gentamicin (Sigma Aldrich)	50mg/ml in H_2O	10, 50, 100, 500, 1000, 2000 μg/ml
PTC124 (Selleckem)	200mM in DMSO	20, 30, 50, 100 μM
GJ072 (Ambinter)	10mM in DMSO	10, 20 μM

Table 5. Drug tested in the different experiments.
The powders were dissolved using the shown vehicles (H_2O or DMSO) and stored at -20°C or -80°C. Drugs were diluted at the indicated working concentrations in DMEM supplemented with 10% FBS and 1% L-glutamine.

Cells were treated for 16, 24 or 48 hrs with the drug or vehicle. At selected time point, cells were collected in 1X PBS (Phosphate Buffered Saline) for fractionation experiment, in Sample buffer or lysis buffer for Western blot analysis or fixed in 4% PFA (Paraformaldehyde in 1X PBS) for immunofluorescence.

5.5 Western Blot

Cells were lysed using Sample or lysis buffer (50mM Tris HCl pH8, 150mM NaCl, 2mM EDTA, 1% Triton X-100, 1mM DTT) supplemented with protease inhibitor cocktail

(PIC, Sigma Aldrich) and sonicated for 10 s at 30% amplitude. Lysates were maintained on ice for 30 min and then clarified by centrifugation at 14000 rpm for 15 min. Total protein content was measured by colorimetric Bradford assay. Samples were heated at 95°C for 5 min or, to preserve phosphorylations, at 70°C for 10 min. Proteins were separated on a 10% or 8% SDS-PAGE under reducing conditions and then electrophoretically transferred to a nitrocellulose membrane (Biorad). Blotting was verified through ponceau staining and membranes were saturated for 1 h at room temperature using 5% non-fat dry milk in TBS-T (20mM TrisHCl pH 7.5, 150mM NaCl, 0.2% Tween). Blots were incubated with primary antibodies overnight at 4°C or 1h at room temperature in mild shaking (Table 6), washed in TBS-T and incubated with appropriate secondary HRP-conjugated antibody (1:10000 in 5% non-fat dry milk in TBS-T) for 1 h at room temperature. After incubation with secondary antibody, membranes were extensively washed with TBS-T and finally immunocomplexes were visualized by chemiluminescence using the ECL kit (Genespin) by the Uvitec instrument (Cleaver Scientific).

Densitometric analysis of the immunoblot was performed using Uvitec software. The mean value of the control group was set to 1.0 and the data of treated and/or mutated samples were expressed as percentage of controls.

Antibody	**Dilution**	**Incubation time**
anti-α-tubulin	1:10000 in 5% non-fat dry milk TBS-T	1 h at room temperature
anti-GFP	1:1000 in 5% non-fat dry milk TBS-T	overnight at 4°C
anti-CDKL5 1	1:1000 in 5% non-fat dry milk TBS-T	overnight at 4°C
anti-CDKL5 2	1:1000 in 5% non-fat dry milk TBS-T	overnight at 4°C
anti-CDKL5 3	1:1000 in 5% non-fat dry milk TBS-T	overnight at 4°C
anti-phospho-ERK1/2	1:300 in 5% BSA TBS-T	overnight at 4°C

Table 6. Antibodies used in WB experiments.
Nitrocellulose membranes were incubated with the opportune antibodies as indicated in the table.

5.6 Immunofluorescence

For immunofluorescence (IF) assay, cells were seeded on slides coated with 1 mg/ml poly-L-lysine hydrobromide (Sigma Aldrich) to allow the cell adhesion of neurons and

HEK293T cells. HeLa cells did not require coating. At selected time point (24 hrs or 32 hrs after transfection), cells were washed with 1X PBS and fixed in 4% PFA for 20 min at room temperature. For CDKL5 staining, cells were permeabilised overday using blocking solution (5% horse serum, 0.2% Triton X-100 in 1X PBS) and thus incubated with primary antibody (anti-CDKL5 2, 1:500 in blocking solution) overnight at 4°C. Slides were washed for several times with 1X PBS and incubated with Alexa anti-rabbit 568 secondary antibody for 1 h at room temperature. After washes, DAPI (1:1000 for 10 min; Life Technologies Incorporated) staining was performed and slides were mounted using Fluoromount-G (eBioscience). Analyses and acquisition were performed using a NikonEclipse Ni upright microscope, while cell counting was done using ImageJ (http://rsbweb.nih.gov/ij/). When required, images were adjusted in brightness and contrast using Adobe Photoshop.

5.7 Subcellular fractionation

For fractionation experiments, HEK293T cells were seeded in 6-well plates 40 hrs before transfection that was performed at 70-80% of confluence. 24 hrs after G418 administration, cells were collected in 1X PBS and pelleted at 1000g for 5 min at 4°C. Cells were lysed in hypotonic buffer (10mM Tris HCl pH 7.5, 1,5 mM $MgCl_2$, 10 mM KCl, 0,1 mM EDTA, 1X PIC) and incubated on ice for 8 min. ¼ of lysate was conserved as total extract and cytoplasmic fraction was separated from nuclei by centrifugation at 1000g for 5 min at 4°C. The resulting pellet, enriched in nuclei, was washed in hypotonic buffer, kept on ice for 5 min to better purify the nuclear fraction. Nuclei were pelleted at 1000g for 5 min at 4°C, resuspendend in nuclear lysis buffer (50mM Tris HCl pH8, 150 mM NaCl, 2mM EDTA, 1% Triton X-100, 1mM DTT, 1X PIC) and incubated on ice for 30 min. Subsequently, genomic DNA was destroyed by sonication and cellular debris removed by centrifugation at 14000 rpm for 15 min. The same volume of total extracts, cytoplasmic and nuclear fractions (correspondent to the same number of cells) was separated by SDS-PAGE. Subcellular distribution was calculated dividing the signal revealed in the nuclear fraction by the one of the cytoplasmic fraction and normalized to control samples arbitrarily set to 1.0.

5.8 Primary neuronal cell cultures

Primary cortical cultures were obtained from WT and *CDKL5* knockout (*Cdkl5*$^{Y/-}$) [65] brains of mouse embryos at 15 days (E15) obtained by crossing heterozygous females (*Cdkl5*$^{+/-}$) [65] with WT males (Charles River Laboratories). Mice were sacrificed by cervical decapitation and embryo brains were removed under a microscope. Embryos were genotyped by PCR on genomic DNA as described by Fuchs *et al.* [77]. Cerebral cortex was rapidly dissected and maintained in cold 1X HBSS. After washes with 1X HBSS, cortices were digested with 0.25% Trypsin/EDTA (Life Technologies) by 7 min of incubation at 37°C. Trypsin was eliminated and inactivated by washing with 1X HBSS and then with a Neurobasal medium containing 10% FBS (Gibco), 2% B27 (Gibco), 1% L-glutamine (Sigma Aldrich), 0.5% penicillin/streptomycin (Sigma Aldrich). By gentle pipetting, cells were dissociated and counted in a Bürker chamber after dilution in 0.4% Trypan Blue. Dissociated neurons were diluted in Neurobasal medium supplemented with 10% FBS, 2% B27, 1% L-glutamine and 0.5% penicillin/streptomycin, plated on coated slides (1 mg/ml poly-L-lysine hydrobromide) in 24-well dishes (70000 cells/well) and maintained at 37°C with 5% CO_2. Two hrs later, medium was removed and replaced with the definitive medium composed by Neurobasal supplemented with 2% B27, 1% L-glutamine. At DIV12 cortical neurons were transfected using calcium phosphate method (2μg DNA/well) and 500 μg/ml G418 was administered 24 hrs later. At DIV14 neurons were fixed for 15 min in 4% PFA at room temperature and analysed by IF.

5.8.1 Morphological analysis.

Morphological analyses were performed on cortical *CDKL5*-null neurons at DIV14.
IF was performed as described using a chicken anti-GFP (1:500) and DAPI (1:1000 in 1X PBS). GFP positive neurons were acquired using a NikonEclipse Ni upright microscope at 40X magnification; neuronal branching was evaluated defining the following parameters: ≤ 5 branches: low branching; 6-11 branches: intermediate branching; >11 branches: high branching.

5.8.2 3-(4,5-dimethylthiazol-2-yl)2-5-diphenyltetrazolium bromide (MTT) assay

WT cortical neurons were plated in 96 well dishes (10000 cells/well) and cultured in Neurobasal supplemented with 2% B27, 1% L-glutamine without penicillin and streptomycin. At DIV12 cortical neurons were treated with different doses of G418 (100, 200, 300, 500 μg/ml) or vehicle (1X PBS, untreated); G418 was dissolved in Neurobasal supplemented with 2% B27, 1% L-glutamine. 24 hrs later, neurons were incubated with 0.4 mg/ml of MTT (Sigma, 5655) at 37°C with 5% CO_2 for 4 hrs. Thereafter the medium was aspirated, wells were allowed to dry and 100 μl of a solution containing HCl 1:25 in isopropanol was added to each well. After formazan had dissolved, the absorbance was determined at 540 nm using a spectrophotometer (Wallac 1420 VICTOR2™; Perkin Elmer). Cell viability was evaluated dividing the mean of absorbance values of treated sample by the one of untreated neurons.

5.9 Statistical analysis

All values are expressed as means ± standard error (SEM). The significance of results was evaluated by Student's t test, one way or two-way ANOVA followed by Bonferroni's post hoc test using Prism software (GraphPad Software, Inc. La Jolla CA, USA). Statistical significance was established as $p < 0.05$.

6. BIBLIOGRAPHY

1. Chahrour, M. and H.Y. Zoghbi, *The story of Rett syndrome: from clinic to neurobiology.* Neuron, 2007. **56**(3): p. 422-37.
2. Rett, A., *U ber ein eigenartiges hirnatrophisches Syndrome bei Hyperammona ¨mie im Kindesalter.* Wien Med Wochenschr, 1966. **116**: p. 723-726.
3. Hagberg B, A.J., Dias K, Ramos O., *A progressive syndrome of autism, dementia, ataxia, and loss of purposeful hand use in girls: Rett's syndrome: report of 35 cases.* Ann Neurol, 1983. **14**: p. 471-479.
4. Amir, R.E., et al., *Rett syndrome is caused by mutations in X-linked MECP2, encoding methyl-CpG-binding protein 2.* Nat Genet, 1999. **23**(2): p. 185-8.
5. Hagberg, B., et al., *Rett syndrome: criteria for inclusion and exclusion.* Brain Dev, 1985. **7**(3): p. 372-3.
6. Hagberg, B., et al., *An update on clinically applicable diagnostic criteria in Rett syndrome. Comments to Rett Syndrome Clinical Criteria Consensus Panel Satellite to European Paediatric Neurology Society Meeting, Baden Baden, Germany, 11 September 2001.* Eur J Paediatr Neurol, 2002. **6**(5): p. 293-7.
7. Neul, J.L., et al., *Rett syndrome: revised diagnostic criteria and nomenclature.* Ann Neurol, 2010. **68**(6): p. 944-50.
8. Bellini, E., et al., *MeCP2 post-translational modifications: a mechanism to control its involvement in synaptic plasticity and homeostasis?* Front Cell Neurosci, 2014. **8**: p. 236.
9. Lewis, J.D., et al., *Purification, sequence, and cellular localization of a novel chromosomal protein that binds to methylated DNA.* Cell, 1992. **69**(6): p. 905-14.
10. Skene, P.J., et al., *Neuronal MeCP2 is expressed at near histone-octamer levels and globally alters the chromatin state.* Mol Cell, 2010. **37**(4): p. 457-68.
11. Shahbazian, M., et al., *Mice with truncated MeCP2 recapitulate many Rett syndrome features and display hyperacetylation of histone H3.* Neuron, 2002. **35**(2): p. 243-54.
12. Ricciardi, S., et al., *Reduced AKT/mTOR signaling and protein synthesis dysregulation in a Rett syndrome animal model.* Hum Mol Genet, 2011. **20**(6): p. 1182-96.
13. Li, Y., et al., *Global transcriptional and translational repression in human-embryonic-stem-cell-derived Rett syndrome neurons.* Cell Stem Cell, 2013. **13**(4): p. 446-58.
14. Long, S.W., et al., *A brain-derived MeCP2 complex supports a role for MeCP2 in RNA processing.* Biosci Rep, 2011. **31**(5): p. 333-43.
15. Cheng, T.L., et al., *MeCP2 suppresses nuclear microRNA processing and dendritic growth by regulating the DGCR8/Drosha complex.* Dev Cell, 2014. **28**(5): p. 547-60.
16. Bergo, A., et al., *Methyl-CpG binding protein 2 (MeCP2) localizes at the centrosome and is required for proper mitotic spindle organization.* J Biol Chem, 2015. **290**(6): p. 3223-37.
17. Matijevic, T., et al., *Rett syndrome: from the gene to the disease.* Eur Neurol, 2009. **61**(1): p. 3-10.
18. Van Esch, H., *MECP2 Duplication Syndrome.* Mol Syndromol, 2012. **2**(3-5): p. 128-136.
19. Kishi, N. and J.D. Macklis, *MECP2 is progressively expressed in post-migratory neurons and is involved in neuronal maturation rather than cell fate decisions.* Mol Cell Neurosci, 2004. **27**(3): p. 306-21.
20. Matarazzo, V., et al., *The transcriptional repressor Mecp2 regulates terminal neuronal differentiation.* Mol Cell Neurosci, 2004. **27**(1): p. 44-58.
21. Francke, U., *Mechanisms of disease: neurogenetics of MeCP2 deficiency.* Nat Clin Pract Neurol, 2006. **2**(4): p. 212-21.
22. Belichenko, P.V., et al., *Widespread changes in dendritic and axonal morphology in Mecp2-mutant mouse models of Rett syndrome: evidence for disruption of neuronal networks.* J Comp Neurol, 2009. **514**(3): p. 240-58.
23. Chapleau, C.A., et al., *Dendritic spine pathologies in hippocampal pyramidal neurons from Rett syndrome brain and after expression of Rett-associated MECP2 mutations.* Neurobiol Dis, 2009. **35**(2): p. 219-33.
24. Fukuda, T., et al., *Delayed maturation of neuronal architecture and synaptogenesis in cerebral cortex of Mecp2-deficient mice.* J Neuropathol Exp Neurol, 2005. **64**(6): p. 537-44.
25. Dani , V.S., Chang, Q., Maffei, A., Turrigiano, G.G., Jaenisch, R., Nelson, S.B., *Reduced cortical activity due to a shift in the balance between excitation and inhibition in a mouse model of Rett syndrome.* Proc Natl Acad Sci U S A, 2005. **102**: p. 12560-5.
26. Zhang, L., He, J., Jugloff, D.G., Eubanks, J.H. , *The MeCP2-null mouse hippocampus displays altered basal inhibitory rhythms and is prone to hyperexcitability.* Hippocampus, 2008. **18**: p. 294-309.

27. Asaka, Y., et al., *Hippocampal synaptic plasticity is impaired in the Mecp2-null mouse model of Rett syndrome.* Neurobiol Dis, 2006. **21**(1): p. 217-27.
28. Della Sala, G. and T. Pizzorusso, *Synaptic plasticity and signaling in Rett syndrome.* Dev Neurobiol, 2014. **74**(2): p. 178-96.
29. Hanefeld, F., *The clinical pattern of the Rett syndrome.* Brain Dev, 1985. **7**(3): p. 320-5.
30. Bahi-Buisson, N. and T. Bienvenu, *CDKL5-Related Disorders: From Clinical Description to Molecular Genetics.* Mol Syndromol, 2012. **2**(3-5): p. 137-152.
31. Kalscheuer, V.M., et al., *Disruption of the serine/threonine kinase 9 gene causes severe X-linked infantile spasms and mental retardation.* Am J Hum Genet, 2003. **72**(6): p. 1401-11.
32. Fehr, S., et al., *The CDKL5 disorder is an independent clinical entity associated with early-onset encephalopathy.* Eur J Hum Genet, 2013. **21**(3): p. 266-73.
33. Russo, S., et al., *Novel mutations in the CDKL5 gene, predicted effects and associated phenotypes.* Neurogenetics, 2009. **10**(3): p. 241-50.
34. Bahi-Buisson, N., et al., *The three stages of epilepsy in patients with CDKL5 mutations.* Epilepsia, 2008. **49**(6): p. 1027-37.
35. Liang, J.S., et al., *CDKL5 alterations lead to early epileptic encephalopathy in both genders.* Epilepsia, 2011. **52**(10): p. 1835-42.
36. Saitsu, H., et al., *A girl with early-onset epileptic encephalopathy associated with microdeletion involving CDKL5.* Brain Dev, 2012. **34**(5): p. 364-7.
37. Bahi-Buisson, N., et al., *Key clinical features to identify girls with CDKL5 mutations.* Brain, 2008. **131**(Pt 10): p. 2647-61.
38. Szafranski, P., et al., *Neurodevelopmental and neurobehavioral characteristics in males and females with CDKL5 duplications.* Eur J Hum Genet, 2015. **23**(7): p. 915-21.
39. Saletti, V., et al., *A CDKL5 mutated child with precocious puberty.* Am J Med Genet A, 2009. **149A**(5): p. 1046-51.
40. Bahi-Buisson, N., et al., *Epileptic encephalopathy in a girl with an interstitial deletion of Xp22 comprising promoter and exon 1 of the CDKL5 gene.* Am J Med Genet B Neuropsychiatr Genet, 2010. **153B**(1): p. 202-7.
41. Moseley, B.D., et al., *Historic, clinical, and prognostic features of epileptic encephalopathies caused by CDKL5 mutations.* Pediatr Neurol, 2012. **46**(2): p. 101-5.
42. Kilstrup-Nielsen, C., et al., *What we know and would like to know about CDKL5 and its involvement in epileptic encephalopathy.* Neural Plast, 2012. **2012**: p. 728267.
43. Mei, D., et al., *Xp22.3 genomic deletions involving the CDKL5 gene in girls with early onset epileptic encephalopathy.* Epilepsia, 2010. **51**(4): p. 647-54.
44. Elia, M., et al., *CDKL5 mutations in boys with severe encephalopathy and early-onset intractable epilepsy.* Neurology, 2008. **71**(13): p. 997-9.
45. Sartori, S., et al., *A novel CDKL5 mutation in a 47,XXY boy with the early-onset seizure variant of Rett syndrome.* Am J Med Genet A, 2009. **149A**(2): p. 232-6.
46. Montini, E., et al., *Identification and characterization of a novel serine-threonine kinase gene from the Xp22 region.* Genomics, 1998. **51**(3): p. 427-33.
47. Hector, R.D., et al., *Characterisation of CDKL5 Transcript Isoforms in Human and Mouse.* PLoS One, 2016. **11**(6): p. e0157758.
48. Williamson, S.L., et al., *A novel transcript of cyclin-dependent kinase-like 5 (CDKL5) has an alternative C-terminus and is the predominant transcript in brain.* Hum Genet, 2012. **131**(2): p. 187-200.
49. Hector, R.D., et al., *Characterisation of Cdkl5 transcript isoforms in rat.* Gene, 2017. **603**: p. 21-26.
50. La Montanara, P., et al., *Synaptic synthesis, dephosphorylation, and degradation: a novel paradigm for an activity-dependent neuronal control of CDKL5.* J Biol Chem, 2015. **290**(7): p. 4512-27.
51. Chen, Q., et al., *CDKL5, a protein associated with rett syndrome, regulates neuronal morphogenesis via Rac1 signaling.* J Neurosci, 2010. **30**(38): p. 12777-86.
52. Rusconi, L., et al., *CDKL5 expression is modulated during neuronal development and its subcellular distribution is tightly regulated by the C-terminal tail.* J Biol Chem, 2008. **283**(44): p. 30101-11.
53. Hanks, S.K. and T. Hunter, *Protein kinases 6. The eukaryotic protein kinase superfamily: kinase (catalytic) domain structure and classification.* FASEB J, 1995. **9**(8): p. 576-96.
54. Bertani, I., et al., *Functional consequences of mutations in CDKL5, an X-linked gene involved in infantile spasms and mental retardation.* J Biol Chem, 2006. **281**(42): p. 32048-56.
55. Lin, C., B. Franco, and M.R. Rosner, *CDKL5/Stk9 kinase inactivation is associated with neuronal developmental disorders.* Hum Mol Genet, 2005. **14**(24): p. 3775-86.
56. Krishnaraj, R., G. Ho, and J. Christodoulou, *RettBASE: Rett syndrome database update.* Hum Mutat, 2017. **38**(8): p. 922-931.

57. Rusconi, L., C. Kilstrup-Nielsen, and N. Landsberger, *Extrasynaptic N-methyl-D-aspartate (NMDA) receptor stimulation induces cytoplasmic translocation of the CDKL5 kinase and its proteasomal degradation.* J Biol Chem, 2011. **286**(42): p. 36550-8.
58. Ricciardi, S., et al., *CDKL5 ensures excitatory synapse stability by reinforcing NGL-1-PSD95 interaction in the postsynaptic compartment and is impaired in patient iPSC-derived neurons.* Nat Cell Biol, 2012. **14**(9): p. 911-23.
59. Oi, A., et al., *Subcellular distribution of cyclin-dependent kinase-like 5 (CDKL5) is regulated through phosphorylation by dual specificity tyrosine-phosphorylation-regulated kinase 1A (DYRK1A).* Biochem Biophys Res Commun, 2017. **482**(2): p. 239-245.
60. Mari, F., et al., *CDKL5 belongs to the same molecular pathway of MeCP2 and it is responsible for the early-onset seizure variant of Rett syndrome.* Hum Mol Genet, 2005. **14**(14): p. 1935-46.
61. Kameshita, I., et al., *Cyclin-dependent kinase-like 5 binds and phosphorylates DNA methyltransferase 1.* Biochem Biophys Res Commun, 2008. **377**(4): p. 1162-7.
62. Ricciardi, S., et al., *CDKL5 influences RNA splicing activity by its association to the nuclear speckle molecular machinery.* Hum Mol Genet, 2009. **18**(23): p. 4590-602.
63. Nawaz, M.S., et al., *CDKL5 and Shootin1 Interact and Concur in Regulating Neuronal Polarization.* PLoS One, 2016. **11**(2): p. e0148634.
64. Wang, I.T., et al., *Loss of CDKL5 disrupts kinome profile and event-related potentials leading to autistic-like phenotypes in mice.* Proc Natl Acad Sci U S A, 2012. **109**(52): p. 21516-21.
65. Amendola, E., et al., *Mapping pathological phenotypes in a mouse model of CDKL5 disorder.* PLoS One, 2014. **9**(5): p. e91613.
66. Okuda, K., et al., *CDKL5 controls postsynaptic localization of GluN2B-containing NMDA receptors in the hippocampus and regulates seizure susceptibility.* Neurobiol Dis, 2017. **106**: p. 158-170.
67. Barbiero, I., et al., *The neurosteroid pregnenolone reverts microtubule derangement induced by the loss of a functional CDKL5-IQGAP1 complex.* Hum Mol Genet, 2017.
68. Lin, J.C., et al., *The netrin-G1 ligand NGL-1 promotes the outgrowth of thalamocortical axons.* Nat Neurosci, 2003. **6**(12): p. 1270-6.
69. Sekiguchi, M., et al., *Identification of amphiphysin 1 as an endogenous substrate for CDKL5, a protein kinase associated with X-linked neurodevelopmental disorder.* Arch Biochem Biophys, 2013. **535**(2): p. 257-67.
70. Trazzi, S., et al., *HDAC4: a key factor underlying brain developmental alterations in CDKL5 disorder.* Hum Mol Genet, 2016. **25**(18): p. 3887-3907.
71. Livide, G., et al., *GluD1 is a common altered player in neuronal differentiation from both MECP2-mutated and CDKL5-mutated iPS cells.* Eur J Hum Genet, 2015. **23**(2): p. 195-201.
72. Schmeisser, M.J., et al., *Autistic-like behaviours and hyperactivity in mice lacking ProSAP1/Shank2.* Nature, 2012. **486**(7402): p. 256-60.
73. Fuchs, C., et al., *Inhibition of GSK3beta rescues hippocampal development and learning in a mouse model of CDKL5 disorder.* Neurobiol Dis, 2015. **82**: p. 298-310.
74. Della Sala, G., et al., *Dendritic Spine Instability in a Mouse Model of CDKL5 Disorder Is Rescued by Insulin-like Growth Factor 1.* Biol Psychiatry, 2016. **80**(4): p. 302-11.
75. Pizzo, R., et al., *Lack of Cdkl5 Disrupts the Organization of Excitatory and Inhibitory Synapses and Parvalbumin Interneurons in the Primary Visual Cortex.* Front Cell Neurosci, 2016. **10**: p. 261.
76. Sivilia, S., et al., *CDKL5 knockout leads to altered inhibitory transmission in the cerebellum of adult mice.* Genes Brain Behav, 2016. **15**(5): p. 491-502.
77. Fuchs, C., et al., *Loss of CDKL5 impairs survival and dendritic growth of newborn neurons by altering AKT/GSK-3beta signaling.* Neurobiol Dis, 2014. **70**: p. 53-68.
78. Valli, E., et al., *CDKL5, a novel MYCN-repressed gene, blocks cell cycle and promotes differentiation of neuronal cells.* Biochim Biophys Acta, 2012. **1819**(11-12): p. 1173-85.
79. Barbiero, I., et al., *CDKL5 localizes at the centrosome and midbody and is required for faithful cell division.* Sci Rep, 2017. **7**(1): p. 6228.
80. Rinaldo, C., et al., *HIPK2 controls cytokinesis and prevents tetraploidization by phosphorylating histone H2B at the midbody.* Mol Cell, 2012. **47**(1): p. 87-98.
81. Bidou, L., et al., *Sense from nonsense: therapies for premature stop codon diseases.* Trends Mol Med, 2012. **18**(11): p. 679-88.
82. Keeling, K.M., et al., *Suppression of premature termination codons as a therapeutic approach.* Crit Rev Biochem Mol Biol, 2012. **47**(5): p. 444-63.
83. Hirsh, D., *Tryptophan transfer RNA as the UGA suppressor.* J Mol Biol, 1971. **58**(2): p. 439-58.
84. Feng, Y.X., et al., *Identification of amino acids inserted during suppression of UAA and UGA termination codons at the gag-pol junction of Moloney murine leukemia virus.* Proc Natl Acad Sci U S A, 1990. **87**(22): p. 8860-3.

85. Urban, C. and H. Beier, *Cysteine tRNAs of plant origin as novel UGA suppressors.* Nucleic Acids Res, 1995. **23**(22): p. 4591-7.
86. Zerfass, K. and H. Beier, *The leaky UGA termination codon of tobacco rattle virus RNA is suppressed by tobacco chloroplast and cytoplasmic tRNAs(Trp) with CmCA anticodon.* EMBO J, 1992. **11**(11): p. 4167-73.
87. Blanchet, S., et al., *New insights into the incorporation of natural suppressor tRNAs at stop codons in Saccharomyces cerevisiae.* Nucleic Acids Res, 2014. **42**(15): p. 10061-72.
88. Loughran, G., et al., *Evidence of efficient stop codon readthrough in four mammalian genes.* Nucleic Acids Res, 2014. **42**(14): p. 8928-38.
89. Popescu, A.C., et al., *Aminoglycoside-mediated partial suppression of MECP2 nonsense mutations responsible for Rett syndrome in vitro.* J Neurosci Res, 2010. **88**(11): p. 2316-24.
90. Bukowy-Bieryllo, Z., et al., *Aminoglycoside-stimulated readthrough of premature termination codons in selected genes involved in primary ciliary dyskinesia.* RNA Biol, 2016. **13**(10): p. 1041-1050.
91. Manuvakhova, M., K. Keeling, and D.M. Bedwell, *Aminoglycoside antibiotics mediate context-dependent suppression of termination codons in a mammalian translation system.* RNA, 2000. **6**(7): p. 1044-55.
92. Floquet, C., et al., *Statistical analysis of readthrough levels for nonsense mutations in mammalian cells reveals a major determinant of response to gentamicin.* PLoS Genet, 2012. **8**(3): p. e1002608.
93. Parker, J., *Errors and alternatives in reading the universal genetic code.* Microbiol Rev, 1989. **53**(3): p. 273-98.
94. Cassan, M. and J.P. Rousset, *UAG readthrough in mammalian cells: effect of upstream and downstream stop codon contexts reveal different signals.* BMC Mol Biol, 2001. **2**: p. 3.
95. Kuchino, Y. and T. Muramatsu, *Nonsense suppression in mammalian cells.* Biochimie, 1996. **78**(11-12): p. 1007-15.
96. Turner, K.A., Choy F. Y. M., *Treatment of Nonsense Mutations Using Stop Codon Read-through Therapeutics and Creation of Animal Models Using CRISPR-Cas9.* J Mol Genet Med, 2015. **9**(3).
97. Barton-Davis, E.R., et al., *Aminoglycoside antibiotics restore dystrophin function to skeletal muscles of mdx mice.* J Clin Invest, 1999. **104**(4): p. 375-81.
98. Bedwell, D.M., et al., *Suppression of a CFTR premature stop mutation in a bronchial epithelial cell line.* Nat Med, 1997. **3**(11): p. 1280-4.
99. Du, M., et al., *Aminoglycoside suppression of a premature stop mutation in a Cftr-/- mouse carrying a human CFTR-G542X transgene.* J Mol Med (Berl), 2002. **80**(9): p. 595-604.
100. Lai, C.H., et al., *Correction of ATM gene function by aminoglycoside-induced read-through of premature termination codons.* Proc Natl Acad Sci U S A, 2004. **101**(44): p. 15676-81.
101. Rebibo-Sabbah, A., et al., *In vitro and ex vivo suppression by aminoglycosides of PCDH15 nonsense mutations underlying type 1 Usher syndrome.* Hum Genet, 2007. **122**(3-4): p. 373-81.
102. Pinotti, M., et al., *Intracellular readthrough of nonsense mutations by aminoglycosides in coagulation factor VII.* J Thromb Haemost, 2006. **4**(6): p. 1308-14.
103. Guerin, K., et al., *Systemic aminoglycoside treatment in rodent models of retinitis pigmentosa.* Exp Eye Res, 2008. **87**(3): p. 197-207.
104. Pfister, P., et al., *The molecular basis for A-site mutations conferring aminoglycoside resistance: relationship between ribosomal susceptibility and X-ray crystal structures.* Chembiochem, 2003. **4**(10): p. 1078-88.
105. Fourmy, D., et al., *Structure of the A site of Escherichia coli 16S ribosomal RNA complexed with an aminoglycoside antibiotic.* Science, 1996. **274**(5291): p. 1367-71.
106. Wagner, K.R., et al., *Gentamicin treatment of Duchenne and Becker muscular dystrophy due to nonsense mutations.* Ann Neurol, 2001. **49**(6): p. 706-11.
107. Malik, V., et al., *Gentamicin-induced readthrough of stop codons in Duchenne muscular dystrophy.* Ann Neurol, 2010. **67**(6): p. 771-80.
108. Wilschanski, M., et al., *Gentamicin-induced correction of CFTR function in patients with cystic fibrosis and CFTR stop mutations.* N Engl J Med, 2003. **349**(15): p. 1433-41.
109. Sermet-Gaudelus, I., et al., *In vitro prediction of stop-codon suppression by intravenous gentamicin in patients with cystic fibrosis: a pilot study.* BMC Med, 2007. **5**: p. 5.
110. Clancy, J.P., et al., *Evidence that systemic gentamicin suppresses premature stop mutations in patients with cystic fibrosis.* Am J Respir Crit Care Med, 2001. **163**(7): p. 1683-92.
111. Swan, S.K., *Aminoglycoside nephrotoxicity.* Semin Nephrol, 1997. **17**(1): p. 27-33.
112. Forge, A. and J. Schacht, *Aminoglycoside antibiotics.* Audiol Neurootol, 2000. **5**(1): p. 3-22.
113. Priuska, E.M. and J. Schacht, *Formation of free radicals by gentamicin and iron and evidence for an iron/gentamicin complex.* Biochem Pharmacol, 1995. **50**(11): p. 1749-52.

114. Kawamoto, K., et al., *Antioxidant gene therapy can protect hearing and hair cells from ototoxicity.* Mol Ther, 2004. **9**(2): p. 173-81.
115. Thibault, N., et al., *Protection against gentamicin nephrotoxicity by daptomycin in nephrectomized rats.* Life Sci, 1995. **56**(22): p. 1877-87.
116. Du, M., et al., *Poly-L-aspartic acid enhances and prolongs gentamicin-mediated suppression of the CFTR-G542X mutation in a cystic fibrosis mouse model.* J Biol Chem, 2009. **284**(11): p. 6885-92.
117. Beauchamp, D., et al., *Protection against gentamicin-induced early renal alterations (phospholipidosis and increased DNA synthesis) by coadministration of poly-L-aspartic acid.* J Pharmacol Exp Ther, 1990. **255**(2): p. 858-66.
118. Baradaran-Heravi, A., et al., *Novel small molecules potentiate premature termination codon readthrough by aminoglycosides.* Nucleic Acids Res, 2016. **44**(14): p. 6583-98.
119. Richardson, R., et al., *Mechanism and evidence of nonsense suppression therapy for genetic eye disorders.* Exp Eye Res, 2017. **155**: p. 24-37.
120. Nagel-Wolfrum, K., et al., *Targeting Nonsense Mutations in Diseases with Translational Read-Through-Inducing Drugs (TRIDs).* BioDrugs, 2016. **30**(2): p. 49-74.
121. Brendel, C., et al., *Readthrough of nonsense mutations in Rett syndrome: evaluation of novel aminoglycosides and generation of a new mouse model.* J Mol Med (Berl), 2011. **89**(4): p. 389-98.
122. Shulman, E., et al., *Designer aminoglycosides that selectively inhibit cytoplasmic rather than mitochondrial ribosomes show decreased ototoxicity: a strategy for the treatment of genetic diseases.* J Biol Chem, 2014. **289**(4): p. 2318-30.
123. Gunn, G., et al., *Long-term nonsense suppression therapy moderates MPS I-H disease progression.* Mol Genet Metab, 2014. **111**(3): p. 374-381.
124. Du, L., et al., *Nonaminoglycoside compounds induce readthrough of nonsense mutations.* J Exp Med, 2009. **206**(10): p. 2285-97.
125. Du, L., et al., *A new series of small molecular weight compounds induce read through of all three types of nonsense mutations in the ATM gene.* Mol Ther, 2013. **21**(9): p. 1653-60.
126. Welch, E.M., et al., *PTC124 targets genetic disorders caused by nonsense mutations.* Nature, 2007. **447**(7140): p. 87-91.
127. Du, M., et al., *PTC124 is an orally bioavailable compound that promotes suppression of the human CFTR-G542X nonsense allele in a CF mouse model.* Proc Natl Acad Sci U S A, 2008. **105**(6): p. 2064-9.
128. Schwarz, N., et al., *Translational read-through of the RP2 Arg120stop mutation in patient iPSC-derived retinal pigment epithelium cells.* Hum Mol Genet, 2015. **24**(4): p. 972-86.
129. Pibiri, I., et al., *Enhancement of premature stop codon readthrough in the CFTR gene by Ataluren (PTC124) derivatives.* Eur J Med Chem, 2015. **101**: p. 236-44.
130. Goldmann, T., et al., *PTC124-mediated translational readthrough of a nonsense mutation causing Usher syndrome type 1C.* Hum Gene Ther, 2011. **22**(5): p. 537-47.
131. Wang, B., et al., *Membrane blebbing as an assessment of functional rescue of dysferlin-deficient human myotubes via nonsense suppression.* J Appl Physiol (1985), 2010. **109**(3): p. 901-5.
132. Yu, H., et al., *Comparison of read-through effects of aminoglycosides and PTC124 on rescuing nonsense mutations of HERG gene associated with long QT syndrome.* Int J Mol Med, 2014. **33**(3): p. 729-35.
133. Goldmann, T., et al., *A comparative evaluation of NB30, NB54 and PTC124 in translational read-through efficacy for treatment of an USH1C nonsense mutation.* EMBO Mol Med, 2012. **4**(11): p. 1186-99.
134. Hirawat, S., et al., *Safety, tolerability, and pharmacokinetics of PTC124, a nonaminoglycoside nonsense mutation suppressor, following single- and multiple-dose administration to healthy male and female adult volunteers.* J Clin Pharmacol, 2007. **47**(4): p. 430-44.
135. Kerem, E., et al., *Effectiveness of PTC124 treatment of cystic fibrosis caused by nonsense mutations: a prospective phase II trial.* Lancet, 2008. **372**(9640): p. 719-27.
136. Sermet-Gaudelus, I., et al., *Ataluren (PTC124) induces cystic fibrosis transmembrane conductance regulator protein expression and activity in children with nonsense mutation cystic fibrosis.* Am J Respir Crit Care Med, 2010. **182**(10): p. 1262-72.
137. Wilschanski, M., et al., *Chronic ataluren (PTC124) treatment of nonsense mutation cystic fibrosis.* Eur Respir J, 2011. **38**(1): p. 59-69.
138. Finkel, R.S., et al., *Phase 2a study of ataluren-mediated dystrophin production in patients with nonsense mutation Duchenne muscular dystrophy.* PLoS One, 2013. **8**(12): p. e81302.
139. Bushby, K., et al., *Ataluren treatment of patients with nonsense mutation dystrophinopathy.* Muscle Nerve, 2014. **50**(4): p. 477-87.

140. Auld, D.S., et al., *Mechanism of PTC124 activity in cell-based luciferase assays of nonsense codon suppression.* Proc Natl Acad Sci U S A, 2009. **106**(9): p. 3585-90.
141. Auld, D.S., et al., *Molecular basis for the high-affinity binding and stabilization of firefly luciferase by PTC124.* Proc Natl Acad Sci U S A, 2010. **107**(11): p. 4878-83.
142. Dranchak, P.K., et al., *Nonsense suppressor therapies rescue peroxisome lipid metabolism and assembly in cells from patients with specific PEX gene mutations.* J Cell Biochem, 2011. **112**(5): p. 1250-8.
143. Brumm, H., et al., *Rescue of melanocortin 4 receptor (MC4R) nonsense mutations by aminoglycoside-mediated read-through.* Obesity (Silver Spring), 2012. **20**(5): p. 1074-81.
144. Koopmann, T.T., et al., *The chemical compound PTC124 does not affect cellular electrophysiology of cardiac ventricular myocytes.* Cardiovasc Drugs Ther, 2012. **26**(1): p. 41-5.
145. Harmer, S.C., et al., *Readthrough of long-QT syndrome type 1 nonsense mutations rescues function but alters the biophysical properties of the channel.* Biochem J, 2012. **443**(3): p. 635-42.
146. McElroy, S.P., et al., *A lack of premature termination codon read-through efficacy of PTC124 (Ataluren) in a diverse array of reporter assays.* PLoS Biol, 2013. **11**(6): p. e1001593.
147. Bolze, F., et al., *Aminoglycosides, but not PTC124 (Ataluren), rescue nonsense mutations in the leptin receptor and in luciferase reporter genes.* Sci Rep, 2017. **7**(1): p. 1020.
148. Kerem, E., et al., *Ataluren for the treatment of nonsense-mutation cystic fibrosis: a randomised, double-blind, placebo-controlled phase 3 trial.* Lancet Respir Med, 2014. **2**(7): p. 539-47.
149. O'Sullivan, B.P., *Targeting nonsense-mediated cystic fibrosis: is it premature to stop now?* Lancet Respir Med, 2014. **2**(7): p. 509-11.
150. Haas, M., et al., *European Medicines Agency review of ataluren for the treatment of ambulant patients aged 5 years and older with Duchenne muscular dystrophy resulting from a nonsense mutation in the dystrophin gene.* Neuromuscul Disord, 2015. **25**(1): p. 5-13.
151. Moestrup, S.K., et al., *Evidence that epithelial glycoprotein 330/megalin mediates uptake of polybasic drugs.* J Clin Invest, 1995. **96**(3): p. 1404-13.
152. Christensen, E.I. and H. Birn, *Megalin and cubilin: multifunctional endocytic receptors.* Nat Rev Mol Cell Biol, 2002. **3**(4): p. 256-66.
153. McCracken, G.H., Jr., D.F. Chrane, and M.L. Thomas, *Pharmacologic evaluation of gentamicin in newborn infants.* J Infect Dis, 1971. **124 Suppl**: p. S214- 23.
154. Newman, R.L. and R.J. Holt, *Intrathecal gentamicin in treatment of ventriculitis in children.* Br Med J, 1967. **2**(5551): p. 539-42.
155. Strausbaugh, L.J. and G.S. Brinker, *Effect of osmotic blood-brain barrier disruption on gentamicin penetration into the cerebrospinal fluid and brains of normal rabbits.* Antimicrob Agents Chemother, 1983. **24**(2): p. 147-50.
156. Wang, D., et al., *The designer aminoglycoside NB84 significantly reduces glycosaminoglycan accumulation associated with MPS I-H in the Idua-W392X mouse.* Mol Genet Metab, 2012. **105**(1): p. 116-25.
157. Peltz, S.W., et al., *Nonsense suppression activity of PTC124 (ataluren).* Proc Natl Acad Sci U S A, 2009. **106**(25): p. E64; author reply E65.
158. Pearson, G., et al., *Mitogen-activated protein (MAP) kinase pathways: regulation and physiological functions.* Endocr Rev, 2001. **22**(2): p. 153-83.
159. Nau, R., F. Sorgel, and H. Eiffert, *Penetration of drugs through the blood-cerebrospinal fluid/blood-brain barrier for treatment of central nervous system infections.* Clin Microbiol Rev, 2010. **23**(4): p. 858-83.
160. Alvira-Botero, X., et al., *Megalin interacts with APP and the intracellular adapter protein FE65 in neurons.* Mol Cell Neurosci, 2010. **45**(3): p. 306-15.
161. Cogan, J., et al., *Aminoglycosides restore full-length type VII collagen by overcoming premature termination codons: therapeutic implications for dystrophic epidermolysis bullosa.* Mol Ther, 2014. **22**(10): p. 1741-52.
162. Gomez-Grau, M., et al., *Evaluation of Aminoglycoside and Non-Aminoglycoside Compounds for Stop-Codon Readthrough Therapy in Four Lysosomal Storage Diseases.* PLoS One, 2015. **10**(8): p. e0135873.
163. Goldmann, T., et al., *Beneficial read-through of a USH1C nonsense mutation by designed aminoglycoside NB30 in the retina.* Invest Ophthalmol Vis Sci, 2010. **51**(12): p. 6671-80.
164. Rademacher, N., et al., *Identification of a novel CDKL5 exon and pathogenic mutations in patients with severe mental retardation, early-onset seizures and Rett-like features.* Neurogenetics, 2011. **12**(2): p. 165-7.
165. Amrani, N., et al., *A faux 3'-UTR promotes aberrant termination and triggers nonsense-mediated mRNA decay.* Nature, 2004. **432**(7013): p. 112-8.

166. Buchan, J.R. and I. Stansfield, *Halting a cellular production line: responses to ribosomal pausing during translation.* Biol Cell, 2007. **99**(9): p. 475-87.
167. Gonzalez-Hilarion, S., et al., *Rescue of nonsense mutations by amlexanox in human cells.* Orphanet J Rare Dis, 2012. **7**: p. 58.

SCIENTIFIC REPORTS

OPEN

CDKL5 localizes at the centrosome and midbody and is required for faithful cell division

Received: 25 January 2017
Accepted: 5 June 2017
Published online: 24 July 2017

Isabella Barbiero[1], Davide Valente[2], Chetan Chandola[1,5], Fiorenza Magi[3,6], Anna Bergo[1], Laura Monteonofrio[2], Marco Tramarin[1], Maria Fazzari[4], Silvia Soddu[2], Nicoletta Landsberger[4], Cinzia Rinaldo[2,3] & Charlotte Kilstrup-Nielsen[1]

The cyclin-dependent kinase-like 5 (*CDKL5*) gene has been associated with rare neurodevelopmental disorders characterized by the early onset of seizures and intellectual disability. The CDKL5 protein is widely expressed in most tissues and cells with both nuclear and cytoplasmic localization. In post-mitotic neurons CDKL5 is mainly involved in dendritic arborization, axon outgrowth, and spine formation while in proliferating cells its function is still largely unknown. Here, we report that CDKL5 localizes at the centrosome and at the midbody in proliferating cells. Acute inactivation of CDKL5 by RNA interference (RNAi) leads to multipolar spindle formation, cytokinesis failure and centrosome accumulation. At the molecular level, we observed that, among the several midbody components we analyzed, midbodies of CDKL5-depleted cells were devoid of HIPK2 and its cytokinesis target, the extrachromosomal histone H2B phosphorylated at S14. Of relevance, expression of the phosphomimetic mutant H2B-S14D, which is capable of overcoming cytokinesis failure in HIPK2-defective cells, was sufficient to rescue spindle multipolarity in CDKL5-depleted cells. Taken together, these results highlight a hitherto unknown role of CDKL5 in regulating faithful cell division by guaranteeing proper HIPK2/H2B functions at the midbody.

CDKL5 is a serine-threonine kinase that was identified through a transcriptional mapping study aimed at identifying disease causing genes in the Xp22 region[1]. The subsequent identification of mutations in the *CDKL5* gene in patients with the Hanefeld variant of Rett syndrome or early infantile epileptic encephalopathy (OMIM #300672) suggested the involvement of this gene in human brain functions[2]. In agreement, the two existing *Cdkl5* knock-out mouse models are characterized by impaired learning and memory, autistic-like features, and motor deficits reconciling several aspects of the clinical spectrum present in patients with mutations in *CDKL5*[3,4].

The *CDKL5/Cdkl5* gene is widely transcribed and the protein can be detected in most tissues and cells, both in the nucleus and in the cytoplasm[5,6]. However, CDKL5 expression reaches highest levels in the brain[6] and because of the evident brain-associated functions, most studies have focused on the neuronal roles of CDKL5. In the brain CDKL5 expression is low at embryonic stages but a significant induction can be observed in the neuronal compartment in the first post-natal days supporting a role during neuronal maturation[5]. In post-mitotic neurons the levels and distribution of CDKL5 are regulated by neuronal activity indicating that the protein responds promptly to external stimuli[7,8]. Of relevance, neurons devoid of the kinase are characterized by defects in axon formation and outgrowth, dendritic arborization, spine morphology, and synaptic transmission, underscoring the importance of CDKL5 for brain development and functioning[4,6,9,10].

[1]Department of Biotechnology and Life Sciences, University of Insubria, 21052, Busto Arsizio, Italy. [2]Unit of Cellular Networks and Molecular Therapeutic Targets, Department of Research, Advanced Diagnostic, and Technological Innovation, Regina Elena National Cancer Institute – IRCCS, 00144, Rome, Italy. [3]Institute of Molecular Biology and Pathology (IBPM), National Research Council (CNR), c/o Sapienza University, 00185, Rome, Italy. [4]Department of Medical Biotechnology and Translational Medicine, University of Milan, 20090, Segrate, Italy. [5]Present address: Centre for Drug Research, Division of Pharmaceutical Biosciences, University of Helsinki, Helsinki, Finland. [6]Present address: Laboratory of Biomedical Research "Fondazione Niccolò Cusano per la Ricerca Medico-Scientifica", Niccolò Cusano University, Rome, Italy. Isabella Barbiero, Davide Valente, Chetan Chandola and Fiorenza Magi contributed equally to this work.Cinzia Rinaldo and Charlotte Kilstrup-Nielsen jointly supervised this work. Correspondence and requests for materials should be addressed to C.R. (email: cinzia.rinaldo@uniroma1.it) or C.K.-N. (email: c.kilstrup-nielsen@uninsubria.it)

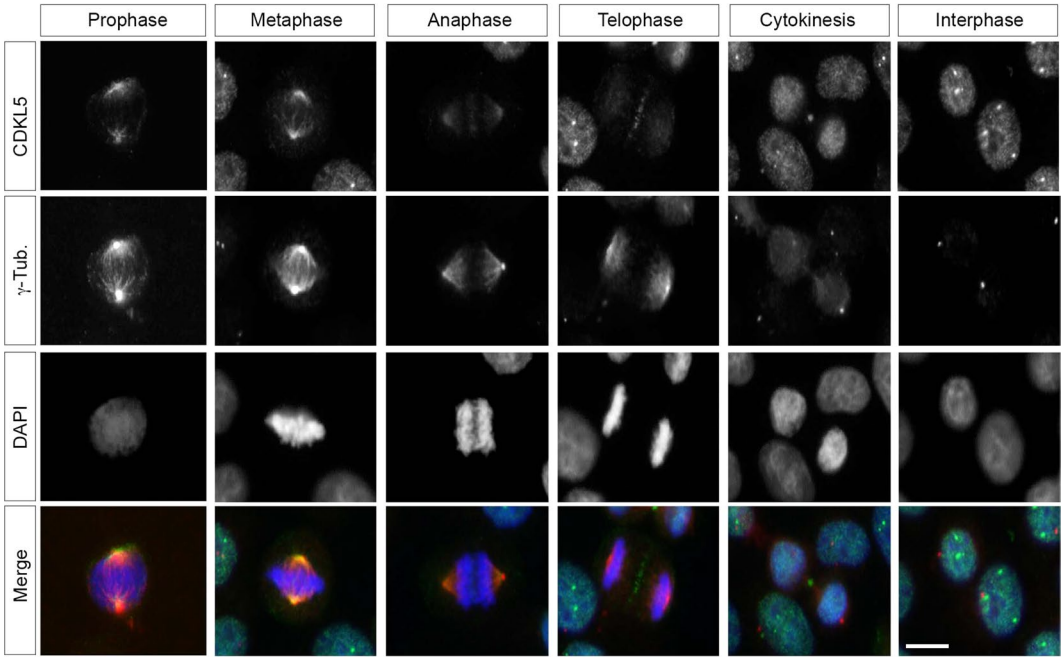

Figure 1. CDKL5 localizes at the centrosome and at the midbody in proliferating cells. HeLa cells were stained with Abs against CDKL5 (polyclonal, green) and γ-tubulin (red) and, to visualize DNA, with DAPI (blue). Scale bar, 10 μm.

While the functions of CDKL5 in post-mitotic neurons are under continuous investigation, its role in proliferating cells is still largely unknown. CDKL5 overexpression induces cell cycle arrest in neuroblastoma cells[11] whereas CDKL5 inhibition, by RNAi or targeted gene disruption, was shown to increase bromodexoyuridine incorporation[11,12]. Although these data suggest the involvement of CDKL5 in cell proliferation, no information is available regarding the functions and the subcellular localization of the kinase during the cell cycle. In the current study we examined the localization of CDKL5 in interphase, mitosis, and cytokinesis of proliferating cells. Besides the typical nuclear punctuate staining of CDKL5 in interphase cells[13], we also found CDKL5 to be localized at the centrosomes and at the midbody.

In animal cells, centrosomes form when a pair of orthogonally positioned centrioles assemble and organize a matrix of proteinaceous pericentriolar material around themselves. Centrioles act as the centrosome organizer and their duplication controls centrosome number. Like DNA, centrioles duplicate semi-conservatively exactly once per cell cycle[14]. The centrosome serves as the main microtubule-organizing center that contributes to cell adhesion, motility, and polarity in interphase and to bipolar spindle formation and timely mitotic progression in mitosis[15,16]. During mitosis, the presence of two centrosomes per cell ensures the bipolar nature of the spindle and the equal segregation of chromosomes to two daughter cells. Quantitative or qualitative centrosome defects may lead to multipolar spindle formation and, eventually, loss of mitotic fidelity and acquisition of chromosome instability[17,18].

The midbody is the narrow intercellular bridge containing bundles of microtubules derived from the mitotic spindle that connects the two daughter cells in cytokinesis. A complex network of components impacting on vesicle and membrane trafficking, cytoskeleton, chromosomes, cell cycle and lipid rafts affects midbody formation and cleavage[19]. Among the numerous midbody components, we have shown that HIPK2, an evolutionary conserved kinase whose large number of substrates includes the Rett syndrome associated factor MeCP2[20], localizes at the midbody and is required for faithful cytokinesis[21]. HIPK2 contributes to abscission, the last step of cell division, by phosphorylating extrachromosomal histone H2B at serine 14 (S14) at the midbody. In HIPK2-defective cells, expression of a phosphomimetic H2B-S14D mutant overcomes the cytokinesis failure[21].

By biochemical and functional assays, we confirmed the presence of CDKL5 both at centrosomes and at the midbody and highlighted the involvement of CDKL5 in cell division through the regulation of HIPK2/H2B functions.

Results

CDKL5 localizes at the centrosome and midbody. To investigate the function(s) of the ubiquitously expressed CDKL5 in proliferating cells we started evaluating the subcellular localization of the kinase during the cell cycle. The distribution of endogenous CDKL5 was analyzed in HeLa cells by immunofluorescence (IF) during interphase, mitosis, and cytokinesis (Fig. 1). We observed a quite dynamic localization of CDKL5 at different mitotic and cytokinetic subcompartments. In prophase and metaphase, CDKL5 is detectable at the mitotic spindle poles where it colocalizes with the centrosomal marker γ-tubulin. As cells progress in telophase, CDKL5 is no longer detectable at the centrosome but localizes at the midzone. In the subsequent steps of cytokinesis

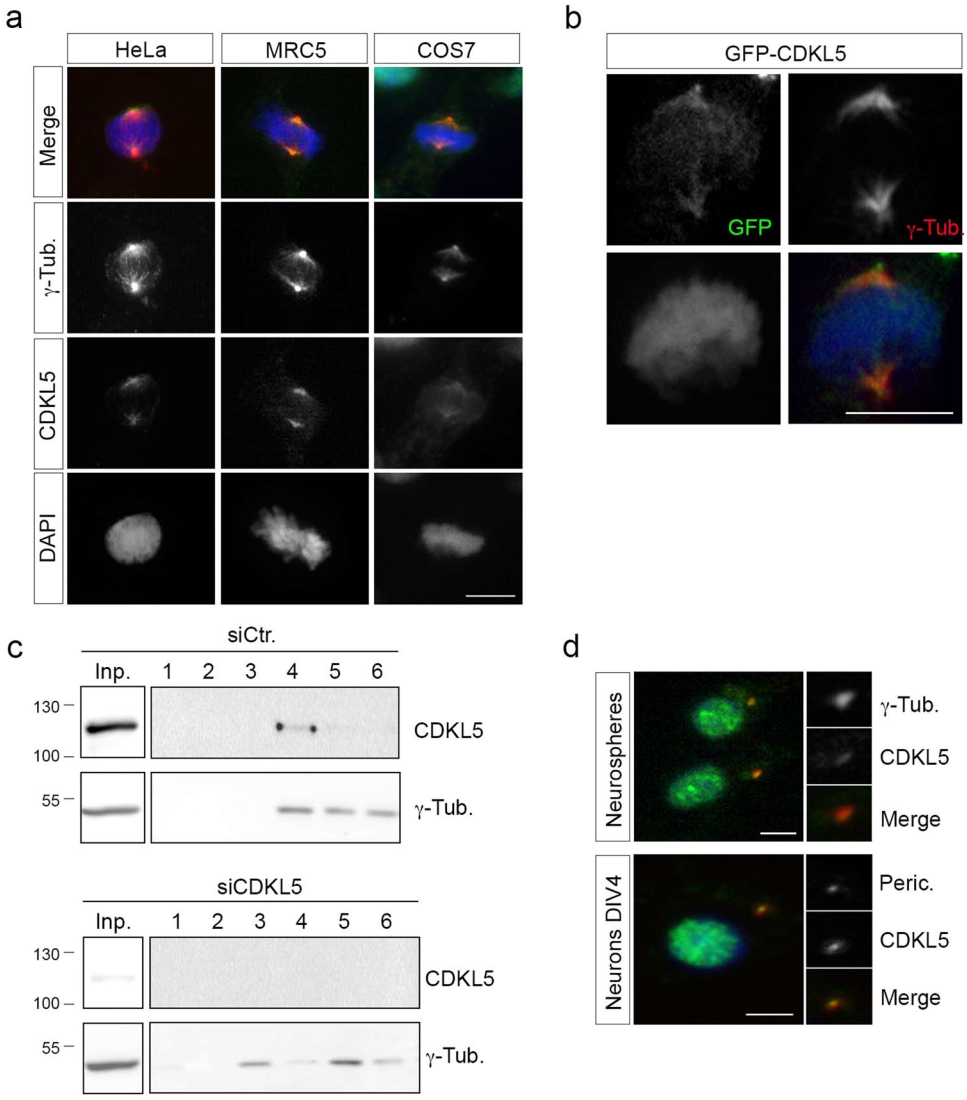

Figure 2. CDKL5 is localized at the centrosome. (**a**) The indicated cells were stained as in Fig. 1. (**b**) Exogenously expressed GFP-CDKL5 (green) localizes at the γ-tubulin positive (red) centrosome in HeLa cells. DAPI staining (blue) was used to visualize DNA. (**c**) HeLa cells were transfected with siCDKL5#1 or a control siRNA (siCtr.); centrosomes were purified 60 h post-transfection and the obtained fractions analyzed by WB with Abs against CDKL5 and γ-tubulin. Input corresponds to approximately 0.6% of the whole cell extract before fractionation. Fractions 1 and 6 are the bottom and top ones, respectively (n = 3 independent experiments). Input and fractions 1–6 are shown as different exposures of the same membrane; full-length blots are presented in Supplementary Figure S7a. (**d**) Neurospheres (upper) and primary hippocampal neurons (DIV4; lower) were stained with Abs against CDKL5 (polyclonal, green) and either γ-tubulin or pericentrin (both red) and DAPI (blue). The panels to the right show the magnified centrosome. Scale bar, 10 μm.

CDKL5 is clearly detectable at the midbody, where it remains during abscission. As expected, in interphase we observed the typical punctuate nuclear staining of CDKL5, which corresponds to nuclear speckles enriched in mRNA splicing factors[13].

Next, through additional studies we validated the centrosomal and midbody localization of CDKL5 suggested by the above IF results.

Regarding the centrosomal localization, we confirmed the overlapping staining of CDKL5 and γ-tubulin in different cells, such as SV40-transformed COS7 cells and human fibroblasts, MRC-5 (Fig. 2a). In the latter cells, the centrosomal localization of CDKL5 could be detected also in interphase by using two different antibodies (Abs) (Supplementary Fig. S1a,b). The specificity of the result was further confirmed through siRNA mediated silencing of CDKL5, which led to a significant reduction of the centrosomal CDKL5 staining (Supplementary Fig. S1b,c). Similar to endogenous CDKL5, exogenous green fluorescent protein (GFP)-tagged CDKL5 can be detected at the centrosome in metaphase cells (Fig. 2b). Finally, the presence of CDKL5 at the centrosome was verified by biochemical fractionation of centrosomal proteins obtained from nocodazole/cytochalasin B-treated HeLa cells transfected with a CDKL5 specific siRNA (siCDKL5) or the relative control (siCtr). Western blot (WB)

analyses show the presence of endogenous CDKL5 in the γ-tubulin positive centrosomal fractions from siCtr cells but not from siCDKL5 cells (Fig. 2c). Considering the importance of the centrosome for neuronal functions, we also analyzed whether CDKL5 is present at the centrosome in cultured neuronal progenitors and post-mitotic primary hippocampal neurons. Interestingly, CDKL5 is detectable at the centrosome in both cell types (Fig. 2d).

To validate the midbody localization, we first performed IF to confirm the co-staining of CDKL5 with two midbody markers, α-tubulin and PLK-1[22] in different cell types using two different anti-CDKL5 Abs (Fig. 3a and Supplementary Figure S2). As above, the specificity of the Ab was tested by silencing CDKL5 expression in HeLa cells (Fig. 3b). As biochemical approach, we isolated and purified midbodies from proliferating HeLa cells enriched in telophase by nocodazole treatment, mitotic shake off, and release after nocodazole washout[21]. Successful midbody isolation was assessed by IF (Fig. 3c, lower panel). Midbody extracts (MID) were analyzed by WB and compared with total cell extracts (TCE) from the same number of cells in interphase (TCE-I) and telophase (TCE-T). WB for the mitotic kinases Aurora A and cytoplasmic AKT was used to validate the fractionation protocol. In line with the results obtained by IF, endogenous CDKL5 can be detected in the midbody extracts both by WB (Fig. 3c) and by immunoprecipitation (Fig. 3d). Finally, similar to endogenous CDKL5, exogenous GFP-CDKL5 is detectable at the midbody by IF (Fig. 3e) and in midbody extracts by WB (Fig. 3f).

Altogether, these results show that, beside its well-defined nuclear and cytoplasmic localization, CDKL5 also localizes at the centrosome and midbody in different cell types.

CDKL5 depletion triggers mitotic spindle multipolarity by centrosome accumulation. We then evaluated the phenotype of CDKL5-depleted cells during cell division. IF analyses were performed with HeLa cells 60 h after siRNA transfection when CDKL5 expression is strongly reduced (Fig. 4a). Compared with siCtr, siCDKL5 HeLa cells showed a significant increase in the number of cells with multipolar spindles (Fig. 4b) associated with different chromosome segregation defects including anaphase/telophase chromosome bridges, micronucleation, and binucleated cells (Fig. 4c). In addition, a significant increase in the number of cells positive for the mitotic marker phosphorylated histone H3-S10 (Fig. 4d) supported that an increased number of cells accumulate in mitosis. Similar defects were observed also in siCDKL5 MRC-5 cells (Supplementary Figure S3). To exclude that the observed phenotypes were due to off-target effects, we performed rescue experiments in which siRNA-resistant CDKL5 was co-expressed with GFP from a bicistronic cassette in silenced HeLa cells. As shown in Fig. 4e–g, cells re-expressing CDKL5 have a percentage of multipolar spindles similar to siCtr cells expressing only GFP.

Spindle multipolarity can be due to defects in microtubule (MT) dynamics or to numeral and structural centrosome alterations[23]. To assess the underlying cause of multipolarity in CDKL5 depleted cells, we first evaluated whether silencing of CDKL5 impairs MT dynamics in COS7 and MRC-5 cells by analyzing the regrowth of MTs after their nocodazole mediated disruption. No significant difference was observed in the aster size of newly formed MTs between siCtr and siCDKL5 cells, suggesting that CDKL5 depletion does not alter the microtubule nucleation activity of these cells (Supplementary Figure S4).

We proceeded evaluating whether CDKL5 depletion might lead to loss of centrosome integrity. Microscopy analyses of siCDKL5 HeLa cells revealed a large number of mitotic spindles with more than two centrosomes, that appear grossly normal, as shown by the staining with the centriolar marker centrin-2 (*i.e.*, each centrosome presents two spots of centrin-2; Fig. 5a and Supplementary Figure S5). Notably, we never observed either one centrin-2 dot per spindle pole or a centrin-2 negative spindle pole (*i.e.*, zero out of 140 spindles); we thus excluded loss of centriole cohesion or centrosome fragmentation as causative of the multipolar spindles. Furthermore, a significant increase of interphase cells with supernumerary centrioles (more than four per cell) was detected in siCDKL5 compared to siCtr cells (Fig. 5b). Altogether, these data support the hypothesis that spindle multipolarity might be due to supernumerary centrosomes rather than to the loss of structural centrosome integrity.

Supernumerary centrosomes can arise through centriole overduplication or accumulation[24]. To distinguish between these two events, double IF analysis for centrin-2 and Cep170 was performed[25,26]. Cep170, a marker for mature, maternal centrioles, can be used to assess the ratio of mature, maternal centrioles and immature, daughter centrioles. This ratio is balanced during centrosome accumulation whilst centrosome duplication causes an excessive number of daughter centrioles compared to maternal ones. Quantification of the Cep170 and centrin-2 staining revealed that CDKL5-deficient cells show a significant increase in centriole accumulation compared to siCtr cells whereas no significant difference was observed in centriole overduplication (Fig. 5c).

Taken together, these results indicate that CDKL5 depletion triggers mitotic spindle multipolarity through centrosome accumulation.

CDKL5 depleted cells show polyploidization and cytokinesis failure. Centrosome accumulation can originate via different pathways, including endoreduplication, mitotic slippage (mitosis without chromosome segregation), cytokinesis failure, and cell fusion[24]. We thus analyzed siCDKL5 cells by *in vivo* time-lapse imaging. Compared to controls, siCDKL5 cells show a significantly longer prometaphase time [from the round-up to chromosome segregation; $t = 148.3 \pm 91.34$ min in siCDKL5 ($n = 74$) *versus* 59.07 ± 33.64 min in siCtr ($n = 73$); $p < 0.001$]. In these cells, we also observed a significantly longer cytokinesis time [from the cleavage furrow ingression to cell daughter separation; t = mean ± Standard deviation = 186.38 ± 78.39 min in siCDKL5 ($n = 66$) *versus* 139.81 ± 62.81 min in siCtr ($n = 62$); $p < 0.001$] and cytokinesis failure resulting in the formation of binucleated cells (Fig. 6a,b and Supplementary Movies S1, S2 and S3). We did not observe any sign of cell death or mitotic slippage (*i.e.* no cells that, after round-up, re-adhere without chromosome segregation) in either siCtr or siCDKL5 cells during the imaging session (Fig. 6a,b, Supplementary Movies S1 and S2 data not shown).

Altogether, these findings show that CDKL5 depletion leads to polyploidization and cytokinesis failure.

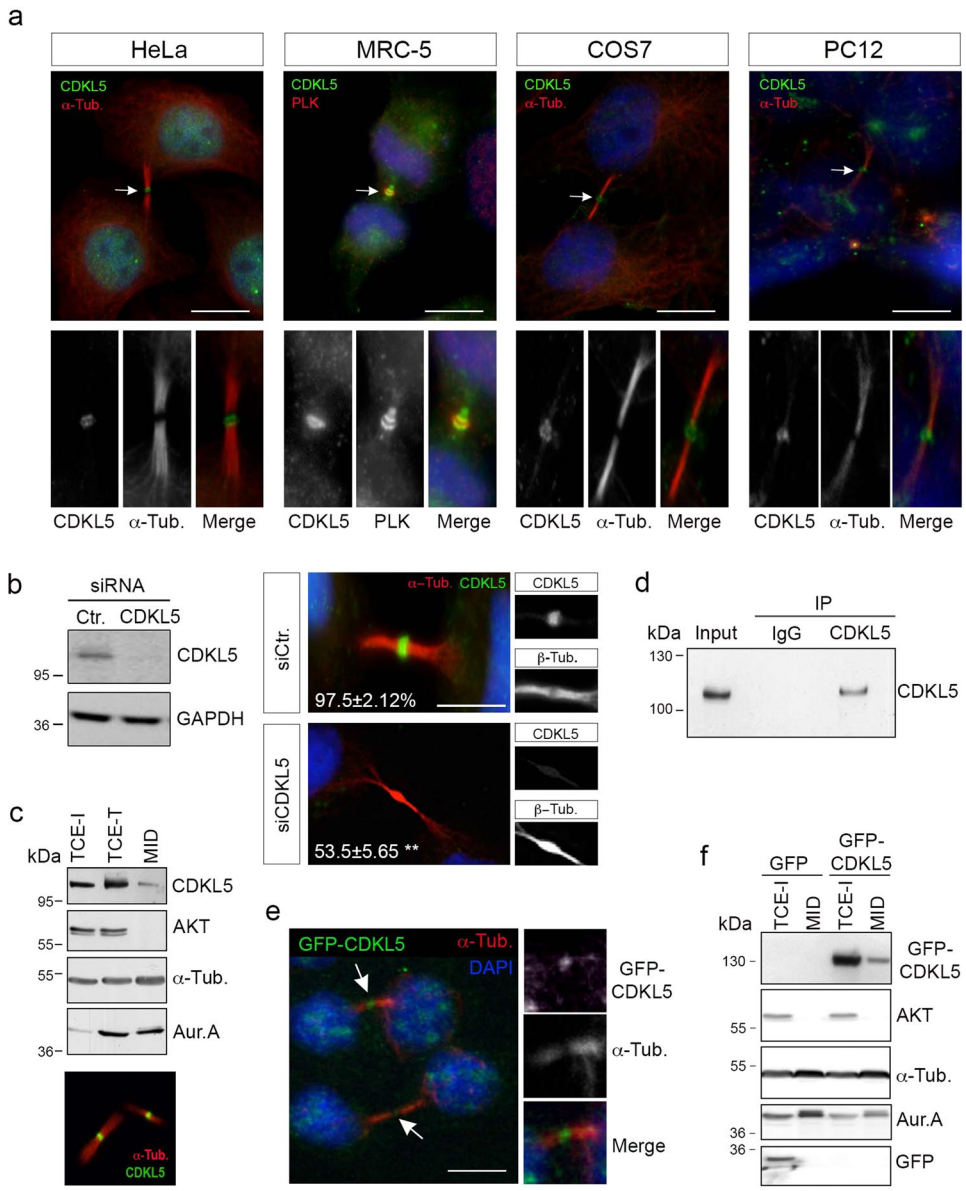

Figure 3. CDKL5 localizes at the midbody. (**a**) The indicated cells were immunostained with Abs against CDKL5 (polyclonal, green) and α-tubulin or PLK-1 (red) to mark the midbody. DAPI staining (blue) was used to visualize DNA. Arrows indicate the CDKL5 positive midbodies, shown enlarged in the lower panels. (**b**) HeLa cells were treated as in Fig. 2c and silencing of CDKL5 expression was verified by western blotting 60 h post siRNA transfection (left). Immunofluorescence analysis (right) showed that only 53.5% ± 5.65 of siCDKL5-treated cells were positive for staining with CDKL5 Ab (polyclonal) at the midbody as opposed to 97.5% ± 2.12 of siCtr cells (n = 2; **p < 0.01; unpaired t-test; 160 midbodies analyzed per condition). Scale bar, 5 µm. (**c**) Total cell extracts of interphase (TCE-I) and telophase (TCE-T) cells were analyzed by WB together with extracts of purified midbodies (MID) with the indicated Abs. Midbody isolation was confirmed by immunofluorescence with Abs against CDKL5 and α-tubulin before extraction (lower panel), (n = 3). (**d**) WB showing immunoprecipitation of a midbody protein extract with polyclonal anti-CDKL5 or anti-IgG. Input corresponds to 10% of the midbody extract before the immunoprecipitation. (n = 2). (**e**) Exogenously expressed GFP-CDKL5 (green) could be detected at the midbody in transfected Hela cells. Arrows indicate GFP-CDKL5 at the midbody. Right panels show the magnified midbody. (**f**) Midbodies (MID) were purified from HeLa cells expressing GFP or GFP-CDKL5 and the extracted proteins were analyzed by WB with the indicated Abs together with an interphase total cell extract (TCE-I) (n = 2). Scale bars in **a** and **e**, 10 µm.

CDKL5 depletion impairs HIPK2/H2B midbody activity. The midbody localization of CDKL5, the longer cytokinesis time, and the increment of binucleated cells upon silencing of CDKL5 (Figs 4c and 6a,b and Supplementary Figure S3c) support the hypothesis that depletion of the kinase might affect cytokinesis. Thus, to get insight into the molecular mechanism involved in the observed cytokinesis failure, we evaluated whether

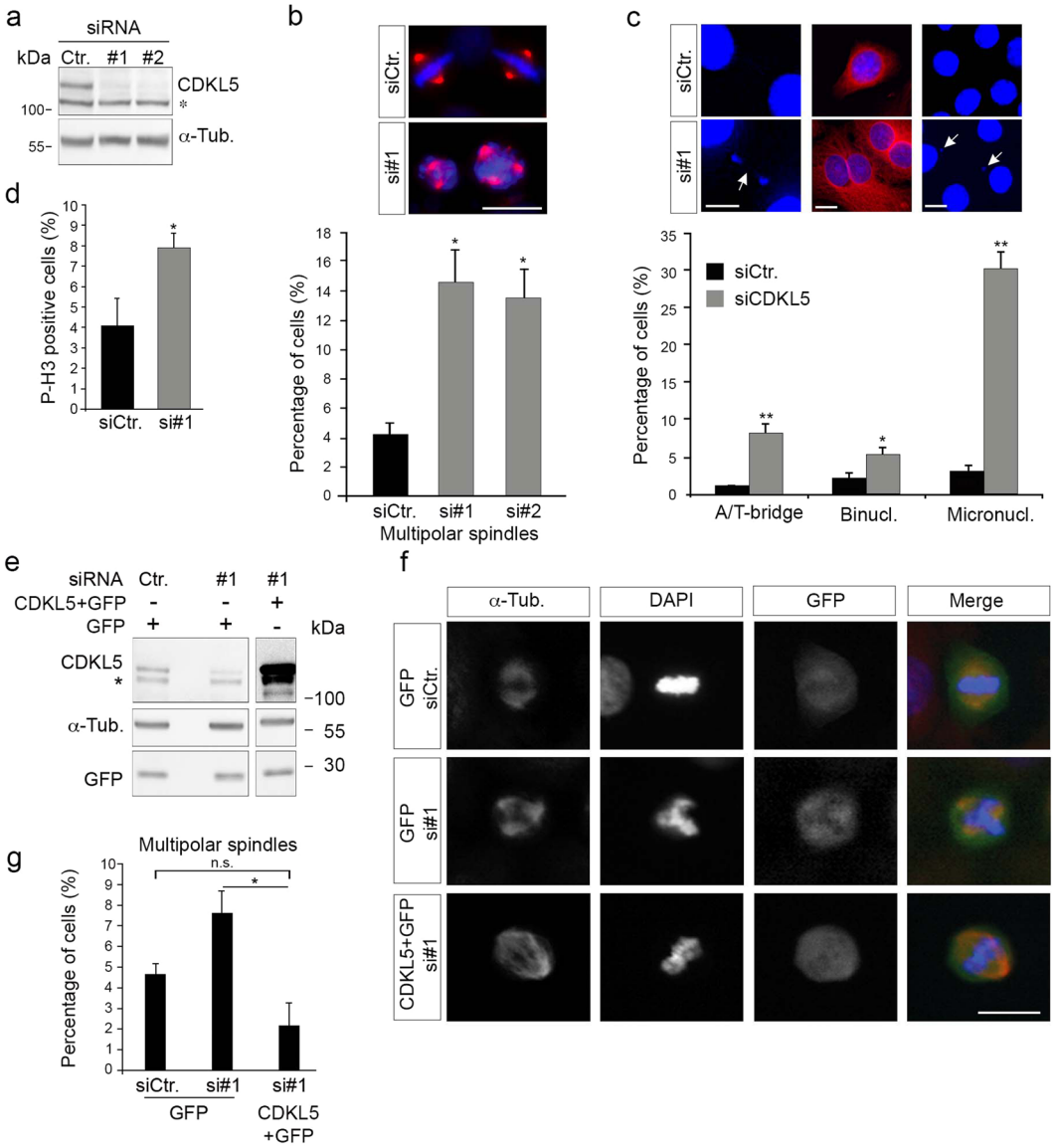

Figure 4. Silencing of CDKL5 is associated with multipolar spindle formation and chromosome segregation defects. (**a**) CDKL5 expression in HeLa cells 60 h after transfection with two different siRNAs targeting CDKL5 or a control siRNA. α-tubulin was used as loading control. The asterisk indicates an unspecific band (**b**,**c**) HeLa cells treated as in **a** were stained against α-tubulin and DAPI 60 h post-transfection. In **b**, the percentage of mitotic multipolar spindles is reported as mean ± S.E.M. (n = 3; *$p < 0.05$, ANOVA followed by Dunnet's *post hoc* analysis). In **c**, the frequency of the indicated phenotypes is shown as mean ± S.E.M. (n = 2; *$p < 0.05$; **$p < 0.01$; unpaired t-test; approximately 1000 counted cells per condition). In **b** and **c**, representative images of the indicated cells are shown above the graphs with DAPI in blue and α-tubulin in red; scale bar, 10 µm. In **c**, arrows indicate a chromosome bridge and micronuclei. A/T = ana-/telo-phase. (**d**) HeLa cells were treated as in **a** and analyzed for phosphorylated histone H3 (P-H3) 60 h after silencing. The percentage of P-H3 positive cells was calculated in three independent experiments counting approximately 2000 cells (mean ± S.E.M., unpaired t-test). (**e**) CDKL5 was expressed in HeLa cells 60 h post-silencing by transfection of a bicistronic vector expressing also GFP. Vertical cropping was performed to show different exposures of the same membrane; full-length blots are shown in Supplementary Figure S7b. (**f**) Representative images of spindles in GFP-positive cells (green) treated as in **e** by staining against α-tubulin (red) and with DAPI (blue). Scale bar, 10 µm. (**g**) Graph showing number of cells with multipolar spindles upon CDKL5 re-expression in silenced cells. ≥ 60 counted cells per condition (n = 3; mean ± S.E.M, *$p < 0.05$; ANOVA followed by Dunnet's *post hoc* analysis). n.s. = not statistically significant.

CDKL5-depleted cells show any midbody defects. The localization of different structural and functional mid-body factors including kinases (*i.e.*, Aurora B, PLK1, HIPK2) and microtubule-associated proteins (*i.e.*, MKLP1, MgcRacGap1, PRC1, and Spastin)[21,22,27,28] were assessed by IF in siCtr and siCDKL5 HeLa cells. Among the

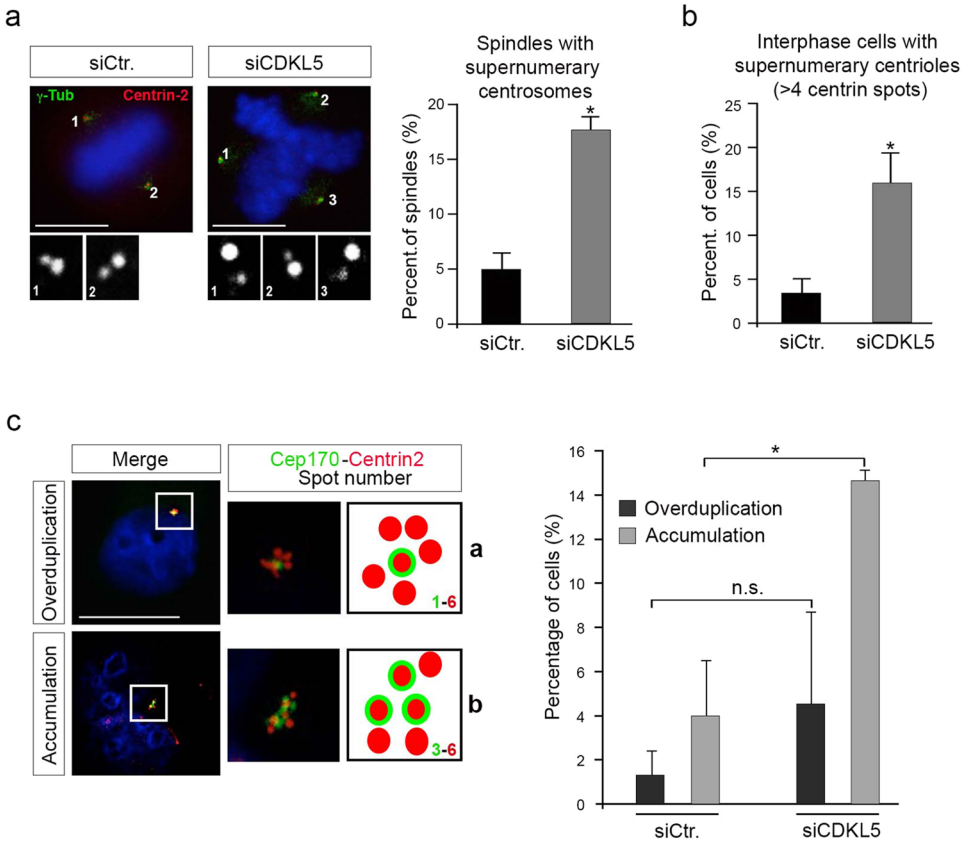

Figure 5. Spindle multipolarity in CDKL5 depleted cells is due to centrosome accumulation. (**a**–**c**) HeLa cells were silenced as in Fig. 4a and analyzed by IF 60 h after transfection. In (**a**) cells were stained with Abs anti-γ-tubulin and anti-centrin-2 to mark the spindle poles and the centrioles, respectively. DAPI staining (blue) was used to visualize DNA. The insets below show the magnified centrin-2 signal in the correspondingly numbered poles. The percentage of spindles with supernumerary centrosomes is reported to the right as mean ± S.E.M. ($n = 2$; $^*p < 0.05$; unpaired t-test; approximately 70 spindles were analyzed per condition). In (**b**) cells were immunostained with centrin-2 and the percentage of interphase cells with more than 4 centrioles was reported as mean ± S.E.M. ($n = 3$; $^*p < 0.05$; unpaired t-test; approximately 100 cells were analyzed per condition). In **c** cells were stained with anti-cep170 (green) and anti-centrin-2 (red) Abs. DAPI staining (blue) was used to visualize DNA. Representative images of different siCDKL5 phenotypes are shown on the left. The percentage of cells with the indicated phenotypes is reported to the right as mean ± S.E.M ($n = 2$; $^*p < 0.05$; unpaired t-test; approximately 200 cells were analyzed per condition). n.s. = not significant. Scale bar, 10 µm.

analyzed factors, we found only HIPK2 to be absent from the midbody in a high percentage of siCDKL5 cells compared with the siCtr cells (Fig. 6c and Supplementary Figure S6). HIPK2 contributes to cytokinesis through the phosphorylation of extrachromosomal histone H2B at S14 at the midbody[21]. Thus, using a phospho-specific Ab we analyzed the presence of phosphorylated H2B-S14 at the midbody in cells silenced for CDKL5. Consistently with the delocalization of HIPK2, we did not detect any phosphorylation of H2B-S14 at the midbody in a high percentage of CDKL5-depleted cells (Fig. 6d) suggesting that CDKL5 contributes to cytokinesis by regulating HIPK2/H2B activity at the midbody.

The most evident phenotype we have observed in the CDKL5 depleted cells is spindle multipolarity, which we linked to polyploidization and centrosome accumulation. Moreover, we observed a cytokinesis failure that is known to depend on HIPK2/H2B activities at the midbody. Thus, we hypothesized that loss of HIPK2 and H2B-S14 phosphorylation at the midbody might trigger a cascade of events starting from cytokinesis failure leading to centrosome accumulation and the formation of multipolar spindles. We thus asked whether spindle multipolarity in siCDKL5 HeLa cells could be rescued by the expression of a phosphomimetic H2B-S14D derivative, which was previously shown to be capable of overcoming cytokinesis failure in HIPK2-defective cells[21]. As shown in Fig. 6e, the expression of H2B-S14D significantly reduced the number of cells with multipolar spindles in siCDKL5 cells indicating that CDKL5 contributes to cytokinesis through HIPK2-mediated H2B phosphorylation.

Discussion

In the last ten years genetic lesions in *CDKL5* have been found in patients with neurologic disorders characterized by the early onset of often intractable seizures, intellectual disability, and impaired motor control[2]. Given the huge

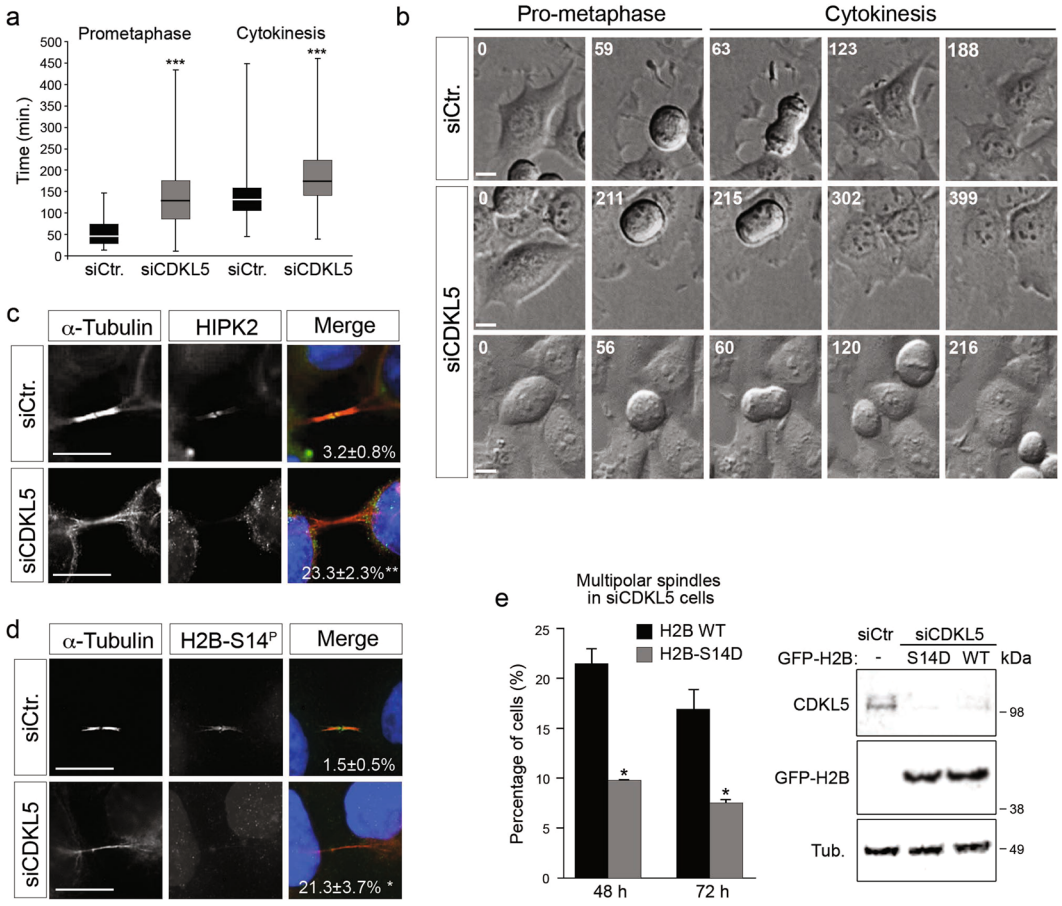

Figure 6. CDKL5 depletion is associated with cytokinesis failure and impaired HIPK2/H2B activity. (**a**) Indicated HeLa cells were analyzed 60 h post-silencing by time-lapse videomicroscopy. The duration of prometaphase and cytokinesis is reported in box plot graphs (***$p < 0.001$, unpaired *t* test). (**b**) Still images related to Supplementary Movies S1, S2 and S3, respectively upper, middle and lower panels. Representative still images of siCDKL5 cells with very long cytokinesis time (middle panels) and of siCDKL5 cells that fail cytokinesis and form binucleated cell (lower panels) are showed. Time is indicated in minutes. Scale bar, 10 µm. (**c**, **d**) Midbody localization of HIPK2 (**c**) and H2B phosphorylated at S14 (**d**; H2B-S14^P) was analyzed in the indicated HeLa cells 60 h post-silencing by staining with Abs against α–tubulin (red) and HIPK2/ H2B-S14^P (green) and with DAPI (blue). The percentage of cells with HIPK2/ H2B-S14^P negative midbodies is indicated for each condition (n = 2; mean ± S.E.M., *$p < 0.05$; **$p < 0.01$ unpaired t-test; approximately 80 midbodies were analyzed per condition). Scale bar, 10 µm. (**e**) Graph showing percentage of multipolar spindles in siCDKL5 cells expressing GFP-H2B WT or GFP-H2B-S14D 48 and 72 h after siRNA transfection (n = 2; *$p < 0.05$; unpaired t-test; approximately 80 cells were analyzed per condition). WB showing CDKL5 and GFP-H2B protein levels 72 h after siRNA transfection is reported.

repercussion of *CDKL5* mutations on brain functions, most studies have so far focused on the role of this kinase in neurons and very few pieces of information are yet available regarding its role in proliferating cells. Few data have suggested that CDKL5 is involved in cell proliferation[11,12], but the subcellular localization and the function of this kinase during the cell cycle are still missing.

Here we present evidence that CDKL5 contributes to faithful cell division. Indeed, we found that the acute ablation of CDKL5 leads to multipolar spindle formation and cytokinesis failure in HeLa and in MRC-5 cells. The increase in the duration of prometaphase and the presence of micronucleated cells suggest that chromosome segregation occurs with reduced fidelity in these cells and that genome instability might be linked to CDKL5 dysfunctions. Therefore, it might be relevant to investigate further genome stability in *Cdkl5*-null or defective backgrounds.

In accordance with a role of CDKL5 in cell division, we observed that its subcellular localization is highly dynamic throughout mitosis and cytokinesis. Indeed, we found an accumulation of CDKL5 at the centrosome from prophase to anaphase and at the midbody in cytokinesis. Among the various midbody factors that we analyzed, only HIPK2 was absent from the midbody in CDKL5 depleted cells. The concomitant reduction of phosphorylated H2B at the midbody and the capacity of the phospho-mimetic H2B-S14D to rescue multipolarity in CDKL5 deficient cells suggest a causative link between the midbody defects and the aberrant mitotic spindles. This is reinforced by the increased number of centrosomes that appear to arise through accumulation rather

than through centrosome duplication defects and by the observation that multipolarity appears to be strictly associated with polyploidy after CDKL5 depletion in the diploid MRC-5 cells (Supplementary Figure S3d and e). Even if further studies are warranted to explore the precise mechanism through which CDKL5 depletion leads to the midbody deprivation of HIPK2, our results highlight a novel function of CDKL5 in cytokinesis through the regulation of HIPK2/H2B at the midbody.

At this point, we cannot ruled out that CDKL5 has additional roles in early mitotic stages (prometaphase and metaphase). Indeed, the longer prometaphase time (Fig. 6a,b) and the higher frequency of chromosome bridges and micronuclei compared to the reduced number of binucleated cells (Fig. 4c) that we observed in siCDKL5 cells suggest that CDKL5 depletion might also induce defects in chromosome alignment and/or segregation. Such defects cannot only be linked to midbody alterations.

Conversely, we do not observe any apparent structural centrosome defects in CDKL5 deficient cells. However, this does not preclude the existence of centrosome-associated CDKL5 functions that may emerge from further studies. Interestingly, it is to note that the large group of proteins that have been functionally linked to the centrosome includes MeCP2[29], the main cause of Rett syndrome and an interactor and *in vitro* substrate of CDKL5[30,31]. Whether a cross-talk between CDKL5 and MeCP2 exists at the centrosome still remains to be understood. Of note, the reduced MT nucleation capacity of centrosomes in MeCP2 deficient cells, but not in cells silenced for CDKL5, indicate that the two proteins have at least some separate functions in this organelle[29].

Previous loss- and gain-of-function studies in SH-SY5Y neuroblastoma cells suggested that CDKL5 inhibits cell proliferation[11]. In agreement, in the developing mouse brain, genetic inactivation of *Cdkl5* increases BrdU and Ki67 positivity[12]. Even if we observed an increased positivity for phosphorylated H3-S10 in our CDKL5-depleted cells, we did not find any increase in cell proliferation (data not shown), suggesting that the phospho-H3 positivity might be due to a prolonged cell division time. Our results, showing a role of CDKL5 in cell division, suggest that the influence of CDKL5 on cell proliferation might be linked to its effects on genome stability. This would be in agreement with the observation made in neuroblastoma patients, in which high expression of CDKL5 correlates with an increased overall survival[11]. However, the action of CDKL5 in tumorigenicity is definitively more complex since, at variance with neuroblastomas, in glioblastomas, CDKL5 was shown to be required for tumor cell survival and increased CDKL5 expression was found to be associated with reduced overall survival[32]. Future studies will be essential to investigate the role of CDKL5 in tumorigenesis.

Although defects in CDKL5 have mainly been associated with a neurological disease we consider likely that its influence on cell cycle progression may be of relevance also in the pathology. In fact, it is well known that the precise control of the cell cycle critically regulates neurogenesis, neuronal differentiation and migration[33] and defects in neuronal progenitor proliferation and differentiation seem to be a convergence point in many neurodevelopmental disorders[34]. Of interest, defects in centrosomal proteins are known to impinge on neuronal migration and axon formation[35]. We thus speculate that the defects in radial neuronal migration and axon specification that have previously been associated with CDKL5 knock-down may be linked to a function of CDKL5 at this organelle[6,9]. Altogether, a further understanding of the precise role of CDKL5 in cell cycle progression and at the centrosome might be relevant to recognize the origin of some features of the human pathology associated with CDKL5.

Materials and Methods

Ethics Statement. Protocols and use of animals were approved by the Animal Ethics Committee of the University of Insubria and in accordance with the guidelines released by the Italian Ministry of Health. Adult mice were euthanized by cervical dislocation.

Plasmids. pGFP-CDKL5, expressing the 107 kDa hCDKL5 isoform has been described elsewhere[36]. pCAGGS-CDKL5-ires-GFP, expressing a siRNA resistant form of CDKL5, was cloned by inserting an EcoRI-EcoRV digested PCR product containing the murine CDKL5 cDNA (NP_0010795) into pCAGGS-ires-GFP digested with EcoRI and SmaI. siRNA resistant CDKL5 contains three nucleotide changes in the third position of codons 25–27 (ggagttgra = > ggcggagtt). pBosH2B-GFP and pBosH2BS14D-GFP have been described in Rinaldo *et al.*[21].

Antibodies. Antibodies (Abs) against the following proteins were used: β-actin (Sigma-Aldrich, St Louis, MO, USA, A5441), α-tubulin (Sigma-Aldrich, T6074), β-tubulin (Sigma-Aldrich, C4585), γ-tubulin (Sigma-Aldrich, T5326), CDKL5 (polyclonal, Sigma-Aldrich, HPA002847; monoclonal Santa Cruz, clone D-12, sc-376314), AKT (Cell Signaling, 4685), Aurora kinase A (Sigma-Aldrich, A1231, clone 35C1), GFP (Roche Diagnostics Ltd, 1814460), PLK-1 (Santa Cruz, sc-17783), phospho-H3-S10 (Abcam, ab14955), H2SB14-P (Cell Signaling, 6959); centrin-2 (Santa Cruz, sc-27793), Cep170 (ThermoFisher Scientific, 41-3200) and HIPK2 (rabbit polyclonal[21]); MgcRacGAP1 (Abcam, ab2270), MKLP1 (Santa Cruz; sc-22793); PRC1 (Santa Cruz, Sc-8356); spastin (Santa Cruz, Sc-53443), CREST centromere protein (Antibodies Inc., 15-234-0001). HRP-conjugated goat anti-mouse or anti-rabbit secondary Abs for immunoblotting were purchased from Thermo Fisher Scientific. DAPI and secondary Alexa Fluor anti-rabbit, anti-mouse, anti-human, and anti-goat Abs for immunofluorescence were obtained from Life Technologies while FITC- or TRITC-conjugated Abs were from Jackson Immuno Research Lab.

Cell cultures, transfections and RNA interference. Human cervix adenocarcinoma HeLa cells, the monkey SV-40-transformed kidney COS7 cells, and human fetal lung fibroblasts MRC-5 cells were maintained in DMEM (Dulbecco's modified Eagle's medium; Sigma-Aldrich) supplemented with 10% FBS, L-glutamine, 100 units/ml penicillin, and 100 μg/ml streptomycin at 37 °C with 5% CO_2. Rat adrenal gland pherochromocytoma PC12 cells were maintained in RPMI (Gibco, Thermo Fisher Scientific) supplemented with FBS, L-glutamine, penicillin, and streptomycin as above; these cells were seeded on poly-D-lysine coated coverslips.

For transfection, cells were cultured in 6- or 12-well dishes and transfected with plasmids using Lipofectamine™ 2000 (Life Technologies) following the manufacturer's protocol. Cells were collected or fixed 24 h post-transfection. For siRNA transfection, 20 nM siRNA oligonucleotides targeting CDKL5 or control GL2 siRNA targeting the luciferase gene (shCDKL5#1: CUAUGGAGUUGUACUUAAAUU; shCDKL5#2: GCAGAGUCGGCACAGCUAUUU; siCtr. 5′CGUACGCGGAAUACUUCGAUU3′) were transfected into HeLa or MRC-5 cells using Lipofectamine™ RNAiMAX (Life Technologies).

For CDKL5 rescue experiments, a siRNA resistant pCAGGS-CDKL5-ires-GFP vector was transfected 60 h after CDKL5 silencing and cells analyzed after another 24 h. For H2B-GFP or H2B-S14D expression, encoding vectors were transfected 24 h after CDKL5 silencing and cells were analyzed 24 and 48 h post-transfection.

Primary neuronal cultures. Primary hippocampal cultures were prepared from embryonic day 17 (E17) CD1 mouse embryos, considering the day of the vaginal plug as E0, as described previously[7] and plated on poly-L-lysine coated plates (densities: $2{,}5 \times 10^3/cm^2$).

Neurosphere preparation. Neurospheres were prepared as previously described[37]. Briefly, E15.5 embryos were individually dissected in PBS and the neocortex was transferred in Dulbecco's Modified Eagle Medium/F12 (DMEM) and dissociated by extensive enzymatic digestion with Papaine (Sigma-Aldrich). Cells were grown in medium containing DMEM/F12, 0.66% glucose, L-glutamine 1%, Pen/Strep 1%, 4 μg/mL of heparin, hormone mix with the addition of either 20 ng/mL epidermal growth factor (EGF) and 10 ng/mL basic fibroblast growth factor (bFGF). In such conditions, cells spontaneously formed neurospheres. Neurospheres were then dissociated into single-cell cultures and plated on matrigel-coated coverslips (BD Bioscience).

Centrosomal fractionation. Centrosome fractionation was performed as previously described[29]. Briefly, exponentially growing cells were treated with 10 μg/ml nocodazole and 5 μg/ml cytochalasin B (both from Sigma-Aldrich) for 90 min, followed by hypotonic lysis. Centrosomes were harvested by centrifugation onto a 20% Ficoll cushion and further purified by centrifugation through a discontinuous (70%, 50% and 40%) sucrose gradient. Fractions of 0.3 ml were collected and analyzed by WB.

Western blotting (WB) and immunoprecipitation (IP). Cells were lysed with lysis buffer (50 mM Tris-HCl pH 7.5, 150 mM NaCl, 1% Triton X-100, 1 mM EDTA, 1 mM DTT) with addition of protease inhibitor cocktail (Sigma-Aldrich) and PhosSTOP (Roche Diagnostics). After 30 min on ice, the lysates were clarified by centrifugation and the supernatants collected. Samples were separated by either 10% or 8% SDS-PAGE, transferred to nitrocellulose membranes, and blocked in 5% non-fat milk in TBS (20 mM Tris-HCl, pH 7.5, 150 mM NaCl) with 0.2% Tween-20 (T-TBS). Blots were incubated with primary Abs overnight at 4 °C, washed in T-TBS, and incubated with appropriate secondary Abs for 1 h at room temperature. After extensive washes, blots were developed with either West PICO Chemiluminescence kit (Pierce) or with ECL Prime Western Blotting Detection Reagent (GE Healthcare).

Immunofluorescence (IF). Cells were grown on poly-L-lysine coated coverslips and fixed in ice-cold methanol or 2% formaldehyde, washed three times in phosphate buffered saline (PBS), permeabilized in 0.25% Triton X-100 in PBS for 10 min and then blocked in 5% bovine serum albumin (BSA) in PBS for 1 h before the required primary Abs were applied. For the staining of γ-tubulin and centrosome associated proteins, cells were permeabilized before fixation in PHEM (60 mM Pipes, 25 mM Hepes, 10 mM EGTA, and 2 mM $MgCl_2$) with 0.5% Triton X-100 for 2 min and then fixed in 4% paraformaldehyde.

Microscopy on fixed samples. For Figs 1, 2a,b,c, 3a,e and 4b,f and Supplementary Figures S2 and S3a, preparations were examined under a NikonEclipse Ni upright microscope equipped with a 100X (1.35 NA) oil immersion objective and a Nikon DIGITAL SIGHT DS-U1 CCD camera. Images were acquired using the NIS-Elements BR 4.13.04 software. For Supplementary Fig. S1a and S1, microscopy analysis was performed using a Olympus U-RFL-T microscope equipped with a 100X (1.35 NA) oil immersion objective and a Rriga R1 CCD camera (QImaging). Images were acquired using Ocular 1.0 software. For Supplementary Figure S4, microscopy was performed using a confocal laser-scanning microscope (model TCS SP8; Leica) with a 63X NA 1.2 oil immersion objective (Leica). Images were acquired using LAS-AF Lite software. For the Figs 3b, 4c and 6c,d and Supplementary S5, preparations were examined under an Olympus Vanox microscope equipped with a 100X (1.35 NA) oil immersion objective and a Tucsen tch-1.4ice CCD camera (Tucsen photonics co., LTD). Images were acquired using Isocapture 4.1.3 software (Tucsen photonics co., LTD). For Fig. 5a, microscopy was performed using a Nikon Eclipse 90i microscope equipped with a oil immersion Plan Fluor 100x objective (N.A. 1.3; Nikon) and a Qicam Fast 1394 CCD camera (QImaging). Image acquisition, deconvolution and Extended Depth of Focus on z-serial optical sections were performed using Nis-Elements HC 4.2 (Nikon); Images shown were Maximum Intensity Projections from z-stacks.

Midbody purification. HeLa cells were enriched in telophase by treatment with nocodazole (100 ng/ml) for 4 h followed by mitotic shake-off. Nocodazole was washed out and the collected cells incubated for 80 min to reach telophase. Midbodies were isolated as described by Kuriyama *et al.*[38] and extracted in extraction buffer (50 mM Tris-HCl pH 7.4, 150 mM NaCl, 0.1% SDS, 0.5% NP40, 5 mM EDTA) supplemented with protease- (Sigma-Aldrich) and phosphatase-inhibitors (Roche, Diagnostiics). Total cell extracts (TCE) from asynchronous and telophase enriched cells were analyzed in parallel.

Live-cell imaging. Cells were seeded in 8-well slides (80826, ibiTreat) and observed under an Eclipse Ti inverted microscope (Nikon) using a 40x objective (Plan Fluor, N.A. 0.60, DIC, Nikon). During the observation, cells were kept in a microscope stage incubator at 37 °C and 5% CO_2. DIC images were acquired by using a DS-Qi1Mc camera. Image and video processing were performed with NIS-Elements AR 3.22.

Statistics. For statistical analysis we assessed the normality distribution of data using the Shapiro-Wilk normality test: student's *t* test or parametric ANOVA followed by Dunnet's *post hoc* test was applied to determine the significance of quantitative experiments when the data distribution was normal. In other cases we used non-parametric Kruskal Wallis with Dunn's *post hoc* test.

References

1. Montini, E. *et al*. Identification and characterization of a novel serine-threonine kinase gene from the Xp22 region. *Genomics.* **51**, 427–433 (1998).
2. Kilstrup-Nielsen, C. *et al*. What we know and would like to know about CDKL5 and its involvement in epileptic encephalopathy. *Neural Plast.* **2012**, 728267 (2012).
3. Wang, I. T. *et al*. Loss of CDKL5 disrupts kinome profile and event-related potentials leading to autistic-like phenotypes in mice. *Proc Natl Acad Sci USA* **109**, 21516–21521 (2012).
4. Amendola, E. *et al*. Mapping pathological phenotypes in a mouse model of CDKL5 disorder. *PLoS One.* **9**, e91613 (2014).
5. Rusconi, L. *et al*. CDKL5 expression is modulated during neuronal development and its subcellular distribution is tightly regulated by the C-terminal tail. *J Biol Chem.* **283**, 30101–30111 (2008).
6. Chen, Q. *et al*. CDKL5, a protein associated with Rett syndrome, regulates neuronal morphogenesis via Rac1 signaling. *J Neurosci.* **30**, 12777–12786 (2010).
7. Rusconi, L., Kilstrup-Nielsen, C. & Landsberger, N. Extrasynaptic N-methyl-D-aspartate (NMDA) receptor stimulation induces cytoplasmic translocation of the CDKL5 kinase and its proteasomal degradation. *J Biol Chem.* **286**, 36550–36558 (2011).
8. La Montanara, P. *et al*. Synaptic synthesis, dephosphorylation and degradation: a novel paradigm for a developmentally regulated NMDA-dependent control of CDKL5. *J Biol Chem.* **290**, 4512–4527 (2015).
9. Ricciardi, S. *et al*. CDKL5 ensures excitatory synapse stability by reinforcing NGL-1-PSD95 interaction in the postsynaptic compartment and is impaired in patient iPSC-derived neurons. *Nat Cell Biol.* **14**, 911–923 (2012).
10. Nawaz, M. S. *et al*. CDKL5 and Shootin1 interact and concur in regulating neuronal polarization. *Plos ONE.* **11**, e0148634 (2016).
11. Valli, E. *et al*. CDKL5, a novel MYCN-repressed gene, blocks cell cycle and promotes differentiation of neuronal cells. Biochim Biophys Acta. 18, 1173–1185.
12. Fuchs, C. *et al*. Loss of CDKl5 impairs survival and dendritic growth of newborn neurons by altering AKT/GSK-3b signaling. *Neurobiol Dis.* **70**, 53–68 (2014).
13. Ricciardi, S. *et al*. CDKL5 influences RNA splicing activity by its association to the nuclear speckle molecular machinery. *Hum Mol Genet.* **18**, 4590–4602 (2009).
14. Gönczy, P. Towards a molecular architecture of centriole assembly. *Nat Rev Mol Biol Cell* **13**, 425–435 (2012).
15. Doxsey, S., McCollum, D. & Theurkauf, W. Centrosomes in cellular regulation. *Annu Rev Cell Dev Biol.* **21**, 411–434 (2005).
16. Nigg, E. A. & Raff, J. W. Centrioles, centrosomes, and cilia in health and disease. *Cell.* **139**, 663–678 (2009).
17. Ganem, N. J., Godinho, S. A. & Pellman, D. A mechanism linking extra centrosomes to chromosomal instability. *Nature.* **460**, 278–282 (2009).
18. Vitre, B. D. & Cleveland, D. W. Centrosomes, chromosome instability (CIN) and aneuploidy. *Curr Opin Cell Biol.* **6**, 809–815 (2012).
19. D'Avino, P. P., Giansanti, M. G. & Petronczki, M. Cytokinesis in animal cells. *Cold Spring Harb Perspect Biol.* **7**, a015834 (2015).
20. Bracaglia, G. *et al*. Methyl-CpG-binding protein 2 is phosphorylated by homeodomain-interacting protein kinase 2 and contributes to apoptosis. *EMBO Rep.* **10**, 1327–1333 (2009).
21. Rinaldo, C. *et al*. HIPK2 controls cytokinesis and prevents tetraploidization by phosphorylating histone H2B at the midbody. *Mol Cell.* **47**, 87–98 (2012).
22. Hu, C. K., Coughlin, M. & Mitchison, T. J. Midbody assembly and its regulation during cytokinesis. *Mol Biol Cell.* **23**, 1024–1034 (2012).
23. Maiato, H. & Logarinho, E. Mitotic spindle multipolarity without centrosome amplification. *Nat Cell Biol.* **16**, 386–394 (2014).
24. Nigg, E. A. Origins and consequences of centrosome aberrations in human cancers. *Int J Cancer* **119**, 2717–2723 (2006).
25. Guarguaglini, G. *et al*. The forkhead-associated domain protein Cep170 interacts with Polo-like kinase 1 and serves as a marker for mature centrioles. *Mol Biol Cell.* **16**, 1095–1107 (2005).
26. Duensing, A., Ghanem, L., Steinman, R. A., Liu, Y. & Duensing, S. p21 (Waf1/Cip1) deficiency stimulates centriole overduplication. *Cell Cycle.* **5**, 2899–2902 (2006).
27. Elia, N., Sougrat, R., Spurlin, T. A., Hurley, J. H. & Lippincott-Schwartz, J. Dynamics of endosomal sorting complex required for transport (ESCRT) machinery during cytokinesis and its role in abscission. *Proc Natl Acad Sci USA* **108**, 4846–4851 (2011).
28. Connell, J. W., Lindon, C., Luzio, J. P. & Reid, E. Spastin couples microtubule severing to membrane traffic in completion of cytokinesis and secretion. *Traffic.* **10**, 42–56 (2009).
29. Bergo, A. *et al*. Methyl-CpG binding protein 2 (MeCP2) localizes at the centrosome and is required for proper mitotic spindle organization. *J Biol Chem.* **290**, 3223–3237 (2015).
30. Mari, F. *et al*. CDKL5 belongs to the same molecular pathway of MeCP2 and it is responsible for the early-onset seizure variant of Rett syndrome. *Hum Mol Genetics* **14**, 1935–1946 (2005).
31. Bertani, I. *et al*. Functional consequences of mutations in CDKL5, an X-linked gene involved in infantile spasms and mental retardation. *J Biol Chem.* **281**, 32048–32056 (2006).
32. Varghese, R. T. *et al*. (2016). Survival kinase genes present prognostic significance in glioblastoma. *Oncotarget.* **7**, 20140–20151 (2012).
33. Jiang, X. & Nardelli, J. Cellular and molecular introduction to brain development. *Neurobiol Dis.* **2016**, 3–17 (2016).
34. Ernst, C. Proliferation and differentiation deficits are major convergence point for neurodevelopmental disorders. *Trends Neurosci.* **39**, 290–299 (2016).
35. Higginbotham, H. R. & Gleeson, J. G. The centrosome in neuronal development. *Trends Neurosci.* **30**, 276–283 (2007).
36. Williamson, S. L. *et al*. A novel transcript of cyclin-dependent kinase-like 5 (CDKL5) has an alternative C-terminus and is the predominant transcript in brain. *Hum Genet.* **131**, 187–200 (2012).
37. Bedogni, F. *et al*. Defects during Mecp2 null embryonic cortex development precede the onset of overt neurological symptoms. *Cereb Cortex.* **26**, 2517–2529 (2016).
38. Kuriyama, R., Keryer, G. & Borisy, G. G. The mitotic spindle of Chinese hamster ovary cells isolated in taxol-containing medium. *J Cell Sci.* **66**, 265–275 (1984).

Acknowledgements

Live cell imaging experiments were performed at the Nikon Reference Centre, CNR Institute of Molecular Biology and Pathology; we acknowledge Dr. Giulia Guarguaglini and Dr. Patrizia Lavia for support. We thank Dr. Giulia Guarguaglini, Dr. Francesca Degrassi and Dr. Manuela Ferrara for the help in cep-170 and CREST staining experiments. We thank the parents' associations Albero di Greta and ProRett Ricerca for their continuous support. This work was supported by grants from Italian Association for Cancer Research (AIRC) to SS (IG #14592) and to CR (IG #17739), Italian Foundation for Cancer Research (FIRC) to DV, Telethon (GGP10032) to NL and SS, Lejeune Foundation to NL, EU Initial Training Network program (no. 238242 "DisChrom") to CKN, and from Albero di Greta to NL and CKN.

Author Contributions

Designed the experiments: I.B., C.R. and C.K.N.; Conducted the experiments: C.C., D.V., I.B., F.M., A.B. and L.M.; Analyzed the data: C.C., D.V.,. I.B., F.M., A.B., L.M., S.S., N.L., C.R. and C.K.N.; Contributed reagents, materials: M.T. and M.F.; Wrote the manuscript: S.S., N.L., C.R. and C.K.N. All authors reviewed the manuscript. C.R. and C.K.N. jointly supervised this work as co-last authors.

Additional Information

Supplementary information accompanies this paper at doi:10.1038/s41598-017-05875-z

Competing Interests: The authors declare that they have no competing interests.

Publisher's note: Springer Nature remains neutral with regard to jurisdictional claims in published maps and institutional affiliations.